Photocapacitor systems for generation and storage of electrical energy

Espen Hestenes Eika

Master Thesis in Nano Science

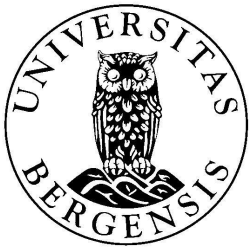

University of Bergen, Norway
Department of Physics and Technology
2015

Abstract

In this project, the combining of photovoltaic cells and supercapacitors into a single, photocapacitor system, was studied. A complete photocapacitor system of commercial components was put together, and characterized. The components were first characterized on their own, and then as a part of the complete system. Some of characterization techniques normally used for individual components was observed to break down during testing on the complete photocapacitor system, giving inconclusive measurements. The mechanisms for charging and discharging of such a system was surmised, and compared to the experimental data. The comparison between the proposed model and the data showed a strong relation for the current and voltage responses during charging and discharging. The efficiency of the photovoltaic cell was determined, and through the charging curve, the efficiency in energy storage for the photocapacitor system. This efficiency was found to be 44.3% for the electricity-to-stored-energy conversion. A variety of electrochemical photovoltaic and supercapacitor electrodes were fabricated, and combined to form two-electrode photocapacitor devices. These devices were then characterized using the same methods as was used for the commercial components system. From the testing, a conflicting functionality requirement between the energy generating and energy storing parts of the system was observed. This proved to strongly limit the performance of the devices. The effects of shunt and series resistances of the complete photocapacitor system were also investigated, and related to the quality of the individual components in the fabricated devices.

Contents

List of Figures

List of Tables

Abbreviations

AM - Air Mass
CE - Counter Electrode
CV - Cyclic Voltammetry
DR - Depletion Region
DSSC - Dye-Sensitized Solar Cell
E_c - Energy of conduction band
E_f - Fermi level
E_{redox} - Redox potential
E_v - Energy of valence band
EDLC - Electrochemical Double-Layer Capacitor
FF - Fill Factor
I_{sc} - Short-Circuit Current
IHP - Inner Helmholtz Plane
ITO - Indium Tin Oxide
IVC - IV Characterization
MWNT - Multi-Walled Nanotube
N-type - Semiconductor material doped with donor atoms
OC - Open-Circuit
OHP - Outer Helmholtz Plane
P-type - Semiconductor material doped with acceptor atoms
PV - Photovoltaic
PVDF - Poly(vinylidene fluoride)
R_s - Series Resistance
R_sh - Shunt Resistance
SC - Short-Circuit
SEM - Scanning Electron Microscope
STC - Standard Test Conditions
V_{oc} - Open-Circuit Voltage

Acknowledgement

First of, I want to express my sincere gratitude to my supervisor, Prof. Lars Egil Helseth, for the support and guidance throughout this project. I would also like to thank Guo Xiaodong for the assistance with the SEM imaging.

There are many people that I'd like to thank. Sondre Eliasson, Anders Huseboe, Sveinung Føllesdal, Sondre Heimdal, and the rest of the Pi-Happy guys and girls. Without you, these last few years would not have been the same.
Miriam, Simon, Sofia, Joakim and Snorre, my new and old siblings.
My parents, Solveig and Kjetil, for life.
Yngve Trulsen should also get a mentioning.

And last, but definitely not least, I want to express my deepest gratitude to Ida Sævrøy Mulvik. For your patience and understanding. For your support and motivation. For your strict attitude and critical eye. To you I want to dedicated this thesis. Thank you.

- Espen Hestenes Eika

Chapter 1

Introduction

1.1 Energy demands in the world

The industrialized world is dependent on the consumption of fossil fuels, like oil and natural gas, to operate. The total energy supply in the world was in 2012 at 13 371 Mtoe[1], where oil, natural gas and coal constituted over 81%. In the future however, this share will have to be significantly reduced. [22] [2, p.7]

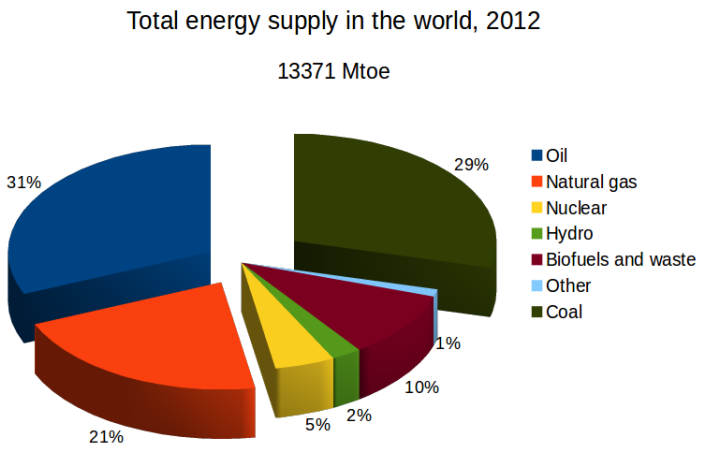

Figure 1.1: Distribution of total primary energy supply in the world, 2012. [2]

[1]tonne of oil equivalent, energy generated by burning 1 metric ton of oil, same as 11.63 megawatt hours (MWh) [1]

Fossil fuels originate from organic matter that has been compressed and transformed in the Earth's crust, over millions of years. [21] The huge advantages of the fossil fuels lie in their high energy density and the ease by which they may be transported, and their low cost of production. The discovery and utilization of these sources of energy have been major catalysts for extensive industrial, national and economic development, and rapid technological advancements. An example of this rapid advancement is the history of aviation. In 1903 the first powered flight took place, by the Wright brothers, and in the following century the technology went through major improvements. The phrase that the world has become a smaller place, is realized by the fact that the fossil fuels have made it possible to transport people and goods throughout the world, in a fraction of the time it would have taken in previous times. [22, 47]

There are some major drawbacks with these types of energy sources, however. Looking past their environmental impacts with emission of CO_2 and pollution in the atmosphere, there is the major concern of their limited and rapidly decreasing supply. It is predicted that the peak of oil production has already passed and that peak of gas is soon to follow[2]. These predictions are reinforced by the high, and increasing, pricing of petroleum products. [22].

With the decrease in oil availability, there has been an increase in the interest and development of energy production methods based on renewable sources of energy. Among these types of sources, there are solar radiation, wind-, wave- and hydro-power, geothermal heat, and nuclear power. To extract the energy from these sources, there are a variety of ways. The heat from nuclear fission, absorbed solar radiation, or geothermal hot-spots can be used to drive a heat engine for generation of electrical energy, or simply for domestic heating. The force in wind, waves or water can be used to generate electrical energy through induction, and the solar radiation can also be directly converted to electrical energy in solar cells. This is done by taking advantage of the photovoltaic effect, when electrons are exited into the conduction band of a semiconducting material. [21] Since many of these energy sources either come directly or indirectly from the sun, their potential is truly great, with perhaps the possibility of totally eliminating the dependence on fossil fuels. The solar radiation that gets absorbed by the Earth is sufficient to power the human energy needs in the world almost 9000 times over. If we were to capture and utilize just a fraction of this abundance of radiation, the energy requirements would largely be covered, and the current level of living could be

[2] 2007 for the oil-peak, 2024 for the natural-gas peak [21, p.272]

maintained. Many of these technologies, however, are not yet at a level of efficiency high enough, or with a good enough method for large-scale production, to be able to compete with fossil fuels. To do so the cost of production and installation per watt (W) of generated energy needs to come down. A goal of reaching 1 USD/W is set, but to get to this point further development and research is needed. [23, 27]

A serious downside with energy production from renewable sources of energy is that many of these sources are severely influenced by environmental factors. These can be factors like the weather, the seasons, or simply the time of the day. Alas, the problems with these types of technologies are not necessarily that their peak efficiency is not good enough, but rather that the efficiency is not constant. The problem with an unsteady supply of energy is perhaps one of the biggest concerns for the replacement of fossil fuels. Unlike fossil fuels, that can adjust the energy production according to needs, most renewable sources provide an unsteady supply of energy. The need to be able to store the produced energy is therefore apparent. They need to capture the energy when available, even if it is not needed at that exact moment. [23]

1.2 Energy storage

The need to store the generated energy is obvious, but the choice of method is not. There are primarily two different approaches to energy storage, batteries and capacitors, with variations.

Batteries work by converting and storing electrical energy as chemical energy. This is done by applying an electrical current across two electrodes, consisting of two different, reactable chemicals. This electrical current is applied in such a way, that if the reaction equation for the chemicals spontaneously goes towards the product, then the current will drive the reaction the other way, towards the reactants. This way, the energy is stored in the reactants, with a high reaction potential, and when the electrodes are connected there will be a positive electrode potential between the two. [16]

Capacitors do not store the energy as chemical energy, but rather by positioning opposite electrical charges near each other. These charges are placed near enough to be attracted by each other, through Coulomb forces, but still conductively insulated, so they are unable to fully meet. This separation is achieved by placing the charges on two opposing, conductive plates that are separated by an insulator, also called a dielectric material. The attraction between the charges on the plates

creates an electrical field that holds the energy as an electrostatic potential. [30]

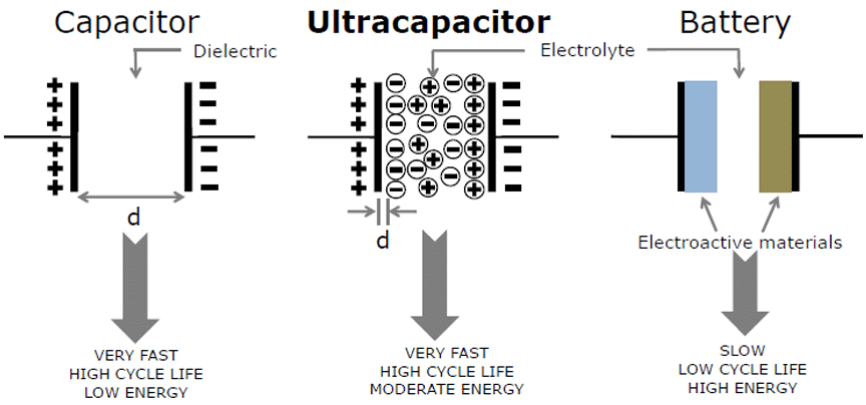

Figure 1.2: Comparison between a capacitor, an ultracapacitor (supercapacitor) and a battery. [42]

When it comes to the choice between storing energy in a battery or in a capacitor, both options got their strengths and weaknesses. Some of the most important properties to consider are the amount of energy the device can store, and how effectively this stored energy can be utilized. Another important point is the lifetime of the device. By lifetime, it is meant how the energy storing capability changes over time, with repeated cycles of dis- and recharging. Of less, but still not negligible importance, is the size and weight of the devices and how easy they are to produce, in terms of cost and quantity. A Ragone plot can be seen below in figure 1.3, where different energy storing devices are compared.

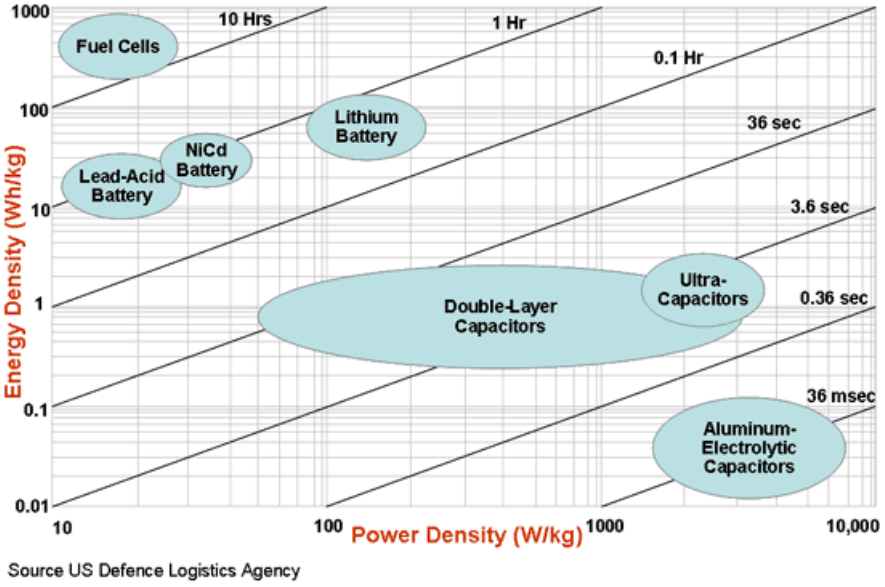

Figure 1.3: Ragone Plot. Compares different types of energy storage devices, in terms of energy and power density. [3]

The strength of batteries lies in their high energy density, which is the amount of energy that can be stored, compared to its physical size and weight. The energy density of batteries is much larger than even the best supercapacitors, i.e., the capacitors that can store the most energy. A downside, however, is that batteries got a poorer power density than the capacitors, which is a measure of how fast the unit can be discharged, and how fast it can be recharged. Since batteries store the energy as chemical energy, the utilization of this energy is dependent on the reaction rate by which the reactants become products and release the energy. Capacitors are not dependent on such a conversion. The energy is held between the free charge carriers, and all that is needed is to establish an external, conductive circuit between the two plates, allowing the charges to meet. [16, 30, 44]

Another downside with batteries is that their lifetime is severely limited. After just a limited number[3] of discharge/recharge cycles, a battery has deteriorated irreversibly and can no longer store energy. This can easily be seen by just looking at today's smart phones; after just a year of usage, their energy storing capabilities are drastically diminished and they typically have to be recharged daily. While

[3]Best cases up to a 1000 cycles, for a Lithium polymer battery [44]

batteries dominate over capacitors in terms of total energy storage, when it comes to lifetime, the capacitors are much better. There has been reports of supercapacitors with electrodes based on nano-structured carbon, that have a lifetime of up to 10^5 cycles. This could contribute to years and years of consecutive dis- and recharging, without notable deterioration in the storage capability. And while this in truth is the more extreme cases, there are several other examples of capacitors having lifetime cycles in the $10^3 - 10^4$ range, which is still tangent or better than even the best batteries. [44]

The importance of size and weight is dependent on the intended usage. In a device that is meant to be mobile, it is important that the weight and size is held down to make it less cumbersome. A downside with increased mobility, however, is that by choosing smaller components, the overall performance might suffer. In a stationary device, where size and weight are of less importance, the choosing of individual components with optimal performance could get higher focus. To choose between a battery or a capacitor regarding size and weight would be difficult, as the choice would be more dependent on their energy storage capabilities and efficiency, and lifetime.

In short, they both got their strengths and weaknesses. Batteries can hold a large amount of energy, but with a limited utilization power, and severely limited lifetime. Capacitors can hold much less energy, but makes up for it in how fast the stored energy can be used, and in their extensive lifetime. The choice between the two would largely come down to their usage. If a slow, energy demanding usage is the case (e.g., computers, mobile phones), a battery would probably be the best choice, given that there is an opportunity to replace the old batteries when their lifetime comes to an end. If the usage do not necessarily demands much energy, but rather high power, and the ability to function extended periods of time without supervision, than a capacitor would probably be the better choice. In the context of adding storage capabilities alongside energy production, it should also be considered for what period of time the energy needs to be stored. If a generator of electrical energy do not generate excessive amounts of energy in between the periods the energy is needed, even the limited storing capabilities of a capacitor might be sufficient. [34, 44]

Whether the choice falls between using a battery or capacitor alongside an energy generating unit, there still remains the general problem of wiring together individual components to function. While a capacitor can be directly connected to the energy generating unit, this is not the same for a battery. A battery typically requires a charging circuit, that controls when the it is fully charged. With external wiring between components, a potential loss in efficiency is created. This is both

a loss in electrical efficiency, because the wiring and connection points contribute to unwanted electrical resistance, but also a loss in spatial efficiency because the overall system is larger. In some devices these losses could be sufferable. In other devices, such as sensors, the allotted space can be limited and therefore size becomes of critical importance. Optimizing the performance efficiency in such a device needs to take into account that by choosing smaller and lighter components, to get a tiny device, the optimal functionality of individual parts may be compromised. From this, we can see that there is an interest in trying to create an electrical component that merges both the ability of energy generation and the ability to store energy into a single component. [30]

1.3 Photocapacitor - The target device of this project

The concept of a single component that can both generate and store electrical energy, is a powerful one. One such component would be the photocapacitor, which converts electromagnetic radiation into electrical energy through the photovoltaic effect, and then, by eliciting similar methods and properties of storage found in a supercapacitor, stores the converted energy. The goals of this thesis are the design, fabrication and characterization of photocapacitors.

The benefits of a photocapacitor are many. In addition to the aforementioned reduction in electrical resistance, the size of the system could also be reduced. In a system made up of individual components, like a commercial solar cell and a commercial supercapacitor, the individual parts might be designed and manufactured by individual companies, and their match in terms of spatial form may create dead space in between the components. By designing functional parts that are made to fit together, this dead space is eliminated, at least between the energy-generating and -storing parts of a system.

One usage where such a component might contribute greatly is in the field of wireless sensors. Being wireless, it could mean that the sensors only take the readings, which then have to be downloaded manually later. It could also mean that they will be able to transfer the recorded data wirelessly, to a receiver. Such a transfer is typically quite a power-demanding process, and would greatly benefit from a capacitor that can deliver energy with a high power. The longevity of capacitors is also a benefit, making the sensor able to run consecutive transfers for a long time, before needing to be replaced. [34, 44]

When I say that the goal of this thesis is the creation of photocapacitors, it

would be more accurate to say that I will seek to elaborate upon its design. The reason for this, is that the creation of such devices has been reported. In 2010, Lo et al. at the University of Wisconsin-Madison, USA, were among the first to succeed in creating a photocapacitor, that could hold a significant amount of charge for over 24 hours. [33]

In the process of designing and manufacturing photocapacitors, the more specific goals are to strive for similar performances as seen in a system consisting of individual parts. This include the storage capability and lifetime expectancy as that of a commercial supercapacitor, as well as the efficiency in converting light into electrical energy as a commercial solar cell. A goal would also be to reduce the resistive losses in the device, through an elimination of excess circuitry. A variety of methods for photovoltaic cells and supercapacitor units are tested, to establish which combinations are best suited for such a device. This is coupled with still trying to minimize the size and loss in efficiency, as these are some of the potential strengths of a photocapacitor. Figure 1.4 below shows a diagram of the basic design for a photocapacitor.

Another part of the project, is to study the working mechanisms of a photocapacitor system. This includes how the system is charged and discharged, and at what efficiency. This was something that was poorly explained in the Lo et al. paper.

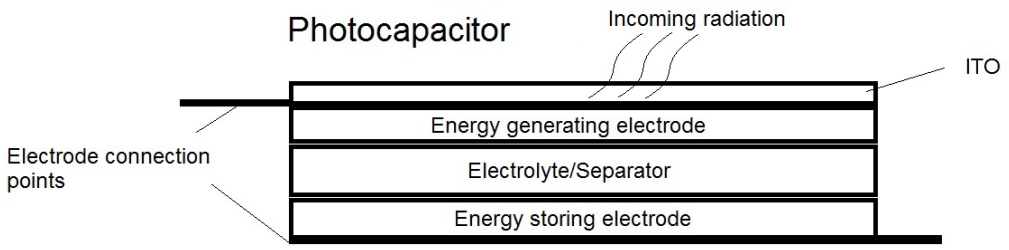

Figure 1.4: Basic design for photocapacitor. Transparent Indium Tin Oxide (ITO) on one electrode to allow radiation to reach the energy generation electrode. The electrolyte doubles as a separator to separate the two electrodes from each other.

Chapter 2

Theory

In this chapter, the detailed working principles of both supercapacitors and photovoltaic cells will be explained. In the first section supercapacitors will be covered, and photovoltaic cells in the second section. How to characterize each type of device will also be covered at the end of their respective sections. In the third section, the photocapacitor system will be looked at.

2.1 Supercapacitors

Capacitors have the ability to store electrical energy, similar to batteries. The way the energy is stored, however, is different. A battery works through chemical reactions, where the energy is converted between being electrical and chemical, depending in the reaction potential. These reactions enables batteries to both store and create electrical energy, given sufficient reactants. Capacitors are not able to create electrical energy, since there is no chemical reactions (ideally), but they are able to store it as an electrostatic potential. This is done by conductively and spatially separating charge carriers with opposing charge. By doing so the charges are not able to recombine, while still being attracted to each other through their electrical fields lines. It is in this way the electrostatic potential is created. Since capacitors do not need to convert the electrical energy, they got a much higher power density than batteries, not being limited by the speed of the chemical reaction, and are able to charge and discharge much quicker. [30, 48]

2.1.1 Electrochemical Double-Layer Capacitors

How much energy a capacitor can store, is primarily determined by two factors. The first of these factors are how high the voltage between the separated charges can become before the insulating material separating them breaks down and creates a conducting pathway. The second factor is the capacitors capacitance. This is defined as electrical charge per electrical voltage, and given by;

$$C = \frac{Q}{V} \tag{2.1}$$

Here C is capacitance, Q is charge and V is voltage. From (2.1) it can be seen that more charge per unit of voltage gives a higher capacitance. The capacitance is to a large degree dependent on the geometry and permittivity of the capacitor. This includes how the components that make up the capacitor are shaped, and how they are put together. This dependence can be showed by taking the relation between electrical field strength, and surface charge;

$$E = \frac{\sigma}{\epsilon}, \quad \sigma = \frac{Q}{A}, \quad \epsilon = \epsilon_r \cdot \epsilon_0 \tag{2.2}$$

Here E is the electric field, σ is the charge density, A is the surface area, and ϵ is the relative permittivity of the medium the electric field is going through. ϵ is defined as the permittivity of vacuum times the permittivity in the specific medium. Also of interest is the relation between an uniform electrical field and voltage;

$$V = E \cdot x \tag{2.3}$$

Here x is the distance from an initial point where the voltage is defined as zero. By inserting equations (2.2) into equation (2.3) we get;

$$V = \frac{Qx}{\epsilon A} \tag{2.4}$$

Finally, inserting equation (2.4) into equation (2.1) gives:

$$C = \frac{\epsilon A}{d} \tag{2.5}$$

Here x has been substituted for d, which is the distance between the charges, i.e. the width of the separator. From this we can indeed see that the capacitance is dependent on the spatial configuration of the capacitor. A large specific surface area, a high relative permittivity, and a small separation will give a higher capacitance. [30, 31]

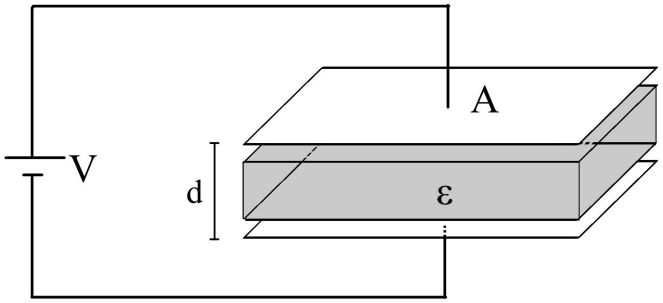

Figure 2.1: Diagram of a conventional parallel plate capacito with a dielectric separator.

A conventional parallel plate capacitor usually have two conducting plates facing each other, and an insulating dielectric material that separates the plates. The conducting plates are usually some form of metal foil, separated by a solid-state dry separator material. In figure 2.1 above, a parallel plate capacitor is shown. On the left there is a vacuum between the two plates, hence ϵ_0, and on the right a material with permittivity ϵ. An example of the latter is one where a thin film of the plastic polypropylene is used as the separator. Reported parameters sets the relative permittivity as 2.2, and the minimum commercial thickness of the separator as 2.4 μm [9]. Using equation (2.5) and assuming a surface area of $1m^2$, gives a capacitance of; [30]

$$C = \frac{\epsilon_r \epsilon_0 A}{d} = \frac{2.2 \cdot 8.854 \cdot 10^{-12} F m^{-1} \cdot 1m^2}{2.4 \cdot 10^{-6} m} = 8.1 \mu F \tag{2.6}$$

From this we can see that the capacitance of commercial parallel plate capacitors lies in the range of nF to μF, depending on the surface area.

To improve the capacitance, one obvious approach would be to reduce the thickness of the separator, consequently reducing the distance d. This is paired with increasing surface area by making long strips of the conducting foils, which are then rolled up into compact cylinders. Though the capacitance will increase, the physical size of the components will quickly become a limiting factor. The construction and make-up of a supercapacitor is similar in many ways to conventional capacitors. They both have two electrodes that are insulated and separated

from each other, and the energy is still (mainly) stored as an electrostatic potential. There are, however, some major differences between the two that strongly influence how they function.

The first difference is found at the surface of the electrodes. The electrodes of supercapacitors are coated in a nano-porous materials, like nano-carbon. This results in a much higher specific surface area, in the range of $10^3 : 1$, compared to a flat, non-textured surface. Since the electrical charges are held at the surface, this increase allows even more charge to be present at approximately the same volume or weight. It should, however, be mentioned that this procedure is not limited to supercapacitors. Newer models of conventional capacitors usually also has this feature, to increase the capacitance and energy storage. [30, 44]

The second difference is what really sets supercapacitors apart from conventional capacitors. Instead of using a dry, solid-state dielectric material as the separator, an electrolyte is used. This makes a major difference in how the capacitor functions. When a voltage is applied across the electrodes in contact with the electrolyte, the free charge carriers will start to move. Given that there is no external circuits the charge carriers can move through, they will start to accumulate at the surface of the electrodes. Depending on the direction of the applied voltage, the negatively electrons will gather at one electrode, and the positive holes at the other electrode. These charge carriers will have electric fields associated with them that gets stronger as they build up in the electrodes. The electric fields will then permeate into the electrolyte, and start interacting with the ions in the solution. This interaction will make the ions start drifting. The charge carriers on each electrode will attract ions of opposite charge, toward their respective electrode. This gathering at the electrodes can be seen in figure 2.2 below, where a simplified diagram of a supercapacitor is shown.

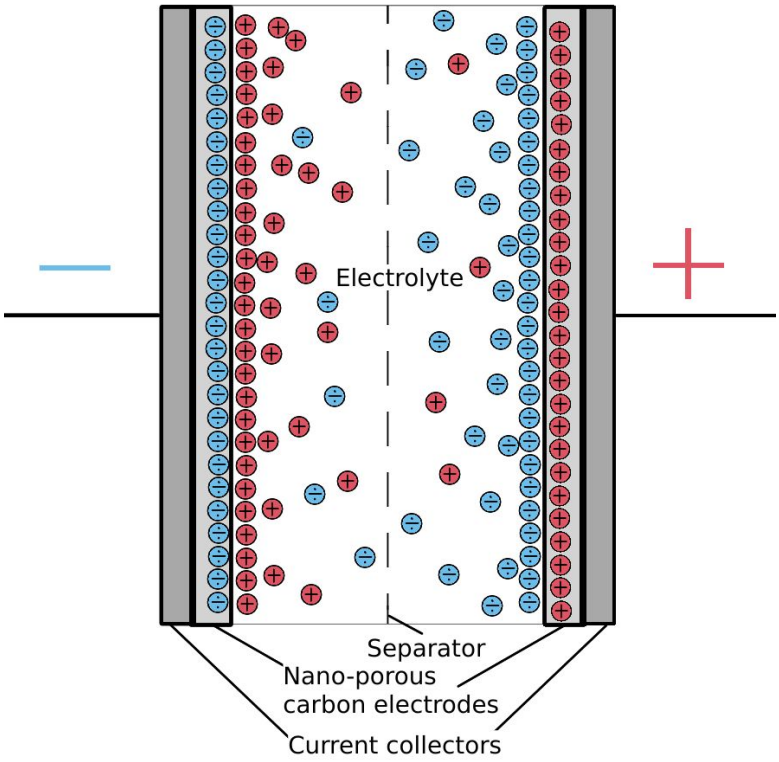

Figure 2.2: Simplified diagram of a supercapacitor. [6]

The movement of the ions in the electric field can be described as a current density, given by the following equation; [7, 48]

$$\overrightarrow{J}_{drift} = q\overrightarrow{E}n\mu_n \tag{2.7}$$

Here J_{drift} is the current density due to drift, q is the charge of the ion in solution, n is the ion concentration, and μ is the mobility of the ions. The ions nearest their respective electrode will quickly arrive at the surface of the electrode. The first ones to arrive will arrange themselves in a single compact layer on the surface of the electrode. The ions in this first layer will be attracted quite strongly. This first layer will also to a large degree shield the electrical field lines coming from the charge carriers in the electrode from the other ions in the solution. The first layer is however unable to completely shield all the field lines, so subsequent layers of ions will also form, but that got a lower concentration of ions, and with a weaker

attraction. Besides the drift current, there will also be (at least) one other current present. The other current of interest is the diffusion current. This current is a product of Fick's law of diffusion. Fick's law relate the diffusion movement of particles in a medium, due to there being a concentration gradient of the particles. The diffusion movement happens in the direction to even out this gradient. After separation of the ion-pairs, a concentration gradient is created. This concentration gradient will induce a diffusion from the electrodes, where the concentration is high, to the bulk of the solution where the ion concentration is lower. Since we are here speaking of ions, particles with a charge, their movement can also be expressed as a current density; [7, 15, 32]

$$\overrightarrow{J}_{diffusion} = -qD\nabla n(\overrightarrow{r}) \tag{2.8}$$

Here $J_{diffusion}$ is the diffusion current density, D is the diffusion coefficient, and $\nabla n(\overrightarrow{r})$ is the change in ion concentration at position r in the electrolyte. The negative sign indicates the movement from high to low concentration. This current will move in the opposite direction as the drift current, and we get a net current density as sum of the two; [7]

$$\overrightarrow{J} = q\overrightarrow{E}n\mu_n - qD\nabla n(\overrightarrow{r}) \tag{2.9}$$

Sometime after the voltage over the electrodes is applied, the current densities will enter a steady-state, where they exactly cancel each other out and the net current density will be zero. At this point the capacitor has reached its maximum potential for energy storage, given the applied voltage. By now inspecting the ions at the electrodes, we will see the first single layer of ions with a very high concentration, and then subsequent layers with exponentially decreasing concentration as the distance from the electrode increase. This type of capacitor is called an electrochemical double layer capacitor (EDLC). It gets is name for the two layers of ions that form; the first one at the surface of the electrode by the free charge carriers, and the second one in the electrolyte by the ions with opposite charge. [7, 15]

2.1.2 The Electrochemical Double-Layer and the Gouy-Chapman Diffuse Layer

If we look closer at the electrode-electrolyte interface, we will see that there are several parts to an EDLC. First, if the electrolyte is aqueous, the ions in the solution will usually be hydrated. This means that the molecules of the solvent has formed a single layer, or shell, around them. When the electrodes are put in

contact with the electrolyte, this same type of layer of solvent molecules is also formed in their surface. The solvent is often water, which because its conformation got a net dipole moment. This dipole moment interact with the electric fields of the ions and the charged electrodes, and gives the molecules an ordered orientation and structure, which binds them strongly to the surfaces. When a voltage is applied over the electrodes and the ions start drifting towards the electrodes, these layers will mostly persist even as the ions is adsorbed on the surface of the electrodes. The result is a first, thin layer of solvent molecules, followed by a second layer, which consists of the hydrated ions. These layers can be seen in figure 2.3 below. [7,15,48]

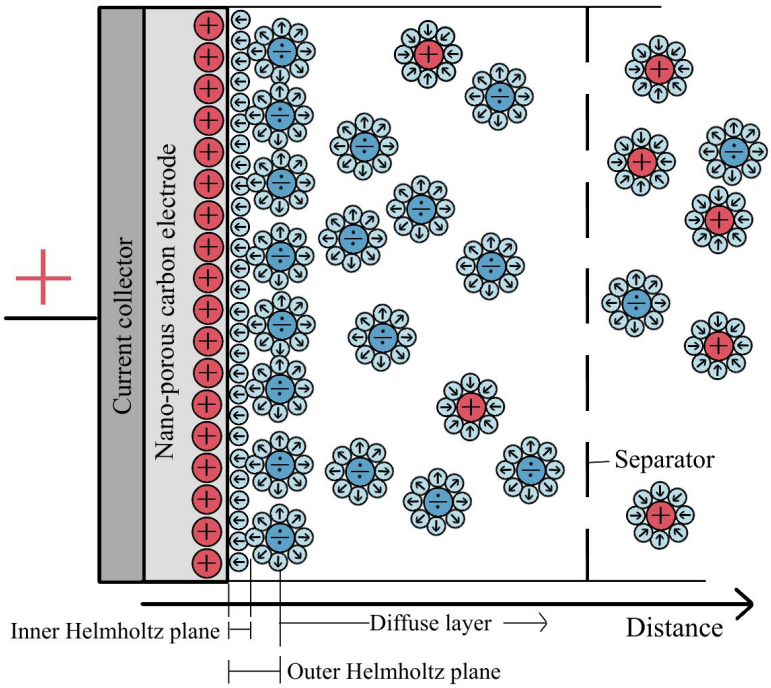

Figure 2.3: Electrochemical Double-Layer, with the Inner- and Outer Helmholtz planes, and the Diffuse layer marked.

The layer of solvent molecules is called the Inner Helmholtz plane (IHP). This plane is placed at the thickness of the solvent molecules diameter from the surface of the electrode, approximating a spherical shape. The second layer is called the

Outer Helmholtz plane (OHP), or sometimes known as the Stern Layer. This plane runs through the center of the first layer of adsorbed ions. The distances from the surface layer of free charge carriers in the electrode, and the IHP and OHP is of crucial importance for the capacitance. The high capacitance values found in an EDLC can be understood by a look at equation (2.5). The distance between the separated charges can be set as the distance between the electrode surface and the OHP. [7, 15, 48]

In some cases there are ions that have adsorbed directly onto the surface of the electrode, without being hydrated. If the electrode contains certain reactive metals or oxides, redox reactions can occur. These reactions are fast faradic reactions where there is only a charge transfer, and no bonding to the electrode materials. The transferred charges will contribute to capacitance, which is called pseudocapacitance. This type of capacitance have a higher specific capacitance than EDLC, but a much shorter lifetime. [15, 44]

Moving beyond the OHP there is the diffuse layer, known as a Gouy-Chapman Layer. As mentioned, this is the result of incomplete shielding from the ions in the OHP. The concentration of ions in this layer is much lower, and drops rapidly as the distance from the electrode surface increase. This is due to that fact that fewer and fewer field lines remain unshielded. While the ions in the OHP to a large extent remains fixed, this does not hold true for the weaker bound ions in the diffuse layer. At a certain distance from the electrode surface there is a plane known as the Slipping Plane. This plane marks the boundary between the fixed and mobile ions. How far into the bulk of the solution the diffuse layer stretches, i.e. how fast the ion concentration drops, is mainly determined by the concentration of ions in, and the temperature of, the electrolyte. The relation between ion concentration and separation from the surface of the electrolyte, in one dimension, is given by; [7, 14]

$$n_1(x) = n_1(x = 0) \cdot e^{-x/d} \tag{2.10}$$

Here $n_1(x)$ is the number density of ions at distance x from the surface, and d is the Debye length. The Debye length is a characteristic length constant of the system, and marks a distance where the electrostatic potential has dropped about 2.7 times compared to the potential at the electrode surface. The value of the

Debye length is approximated by; [7]

$$d = \sqrt{\frac{\epsilon_r \epsilon_0 k_B T}{q^2 n_0}} \tag{2.11}$$

Here ϵ_r is the relative permittivity of the solution, ϵ_0 is the permittivity in vacuum, k_B is the Boltzmann constant, T is absolute temperature of the electrolyte, q is the elementary charge, and n_0 is the ion number density in the bulk of the electrolyte, where no external field or force is applied. From equation (2.11) we can see that a high ion concentration and a low temperature will give a shorter Debye length. This will in return give a shorter diffuse layer. The total capacitance and electrostatic potential in a supercapacitor is a sum of both the ions in the OHP and in the diffuse layer. This means that a shorter diffuse layer will give a higher capacitance, and a supercapacitor that can store a larger amount of energy. [7, 44]

Looking at the typical distances from the surface of the electrodes in these types of planes, it is understandable how the capacitance in supercapacitors can get so high. The distance to the Outer Helmholtz plane with an aqueous electrolytes, is typically in the range of 0.8-1.3 nm. The Debye length, depending greatly on the ionic strength of the electrolyte, is typically between 1-10 nm. This is paired with the stability of the solvent plane. The solvent molecules in this plane do typically have a very high relative permittivity. Distilled water for instance has a relative permittivity of 80. This high relative permittivity allows the layer of solvent molecules to withstand extremely high electric fields without overloading. [14, 15, 30]

Comparing equation (2.6) for a parallel plate capacitor, with a similar calculation with the parameters for a typical supercapacitor, a good indication of the difference in specific capacitance between the two can be seen. For a supercapacitor using activated carbon, the most common electrode material, and an appropriate electrolyte, the specific capacitance is in the range of 150-355 F per gram of active material. This corresponds to about 0.15-0.36 F/m^2, assuming $1000m^2$/g for activated carbon. From this we can see that there are several orders of magnitude difference between the specific capacitance of a supercapacitor and a conventional parallel plate capacitor. [44]

2.1.3 Total capacitance

The calculation for total capacitance in a supercapacitor differs a bit from a conventional capacitor. In a conventional capacitor where the electric field runs between the two electrodes, the calculation is straight forward according to equation (2.1). In a supercapacitor however, with its two electrodes and an electrolyte, this is in fact two capacitors in series. [30, 48]

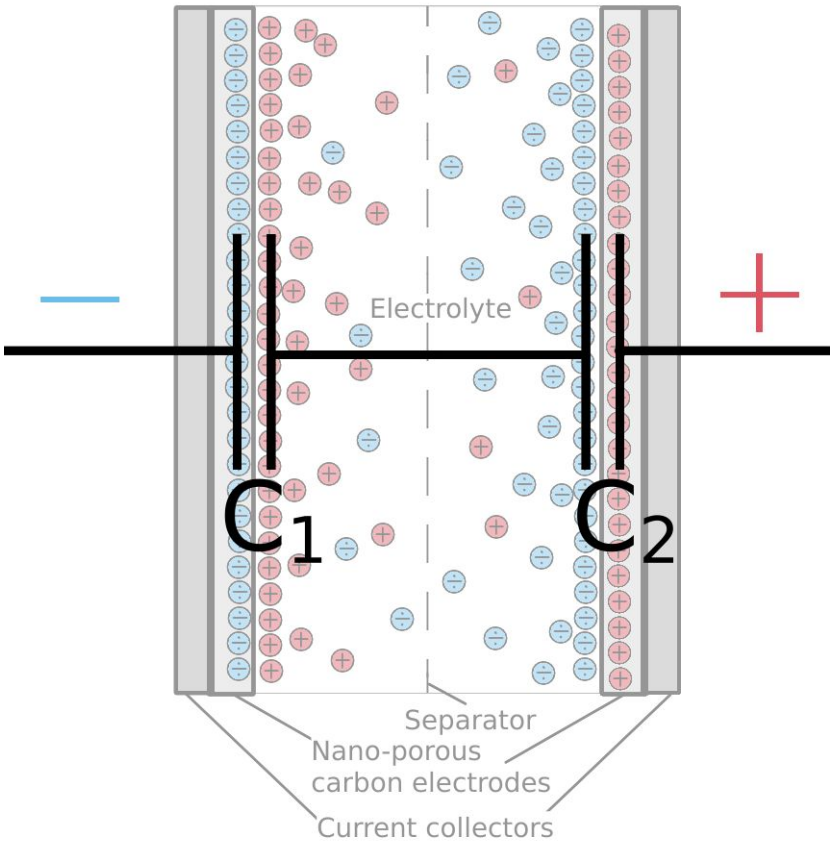

Figure 2.4: Equivalent circuit representation superimposed on a diagram of a charged supercapacitor

These are the two sets of electrochemical double- and diffuse-layers formed at each electrode. Figure 2.4 above shows an equivalent circuit representation for the

two capacitors, superimposed on a diagram of a charged supercapacitor. The total capacitance in the device is accordingly;

$$\frac{1}{C_{total}} = \frac{1}{C_1} + \frac{1}{C_2} \tag{2.12}$$

where C_1 and C_2 is the capacitance at each of the two electrodes. If we were to calculate the capacitance of a supercapacitor using equation (2.1), it is the total capacitance we would have found. If the two electrodes are made the same, i.e. a symmetric SC, and by assuming they have the same capacitance, this simplifies to;

$$C_{total} = \frac{C}{2} \tag{2.13}$$

From this we can see that the total capacitance of a symmetric supercapacitor is exactly half of the capacitance at each electrode. If the two capacitances are not equal, the total capacitance is limited towards the lower of the two. In a SC where there is a big difference in the two capacitances, $C_1 \ll C_2$, the total capacitance can be approximated as being the same as the lowest, $C_{total} \approx C_1$. [44, 48]

2.1.4 Important parameters in a supercapacitor

How well a supercapacitor performs is determined by a number of factors. The most important of these factors are mentioned and explained below.

2.1.4.1 Electrolyte Stability Window

One of the most important factors for how much energy a supercapacitor can store, is the range of the stability window of the electrolyte. Since supercapacitors uses electrolytes, there is a greater limitation on the voltage that can be applied between the electrodes than with a capacitors that use a dielectric. If a voltage above the stability window is applied, unwanted redox reactions will start to occur. The products from these reactions could potentially destroy the desired properties of the electrolyte, and subsequently destroy the energy storing capabilities. The range of the stability window depends greatly on the solvent in the electrolyte. There are primarily two different types of electrolytes, aqueous and organic. Aqueous electrolytes got the lowest stability windows, of about 0.7-0.8 V for a symmetric supercapacitor. Organic electrolytes got a stability window of about 2.7 V. These voltages are not as high as the theoretic limits, but due to uncertainties like uneven potential over the two electrodes, and presence of impurities, they are lowered.

Organic electrolytes are particularly sensitive to impurities, like in the form of water molecules. E.g. an extremely pure acetonitrile with a glassy carbon electrode got a stability window of 5.9 V. This stability window however starts dropping fast with just trace amounts of water. [15]

The importance of striving for a higher stability window is easily shown through the equation for total energy in an ideal capacitor;

$$E = \frac{1}{2}CV^2 \tag{2.14}$$

As can be seen from the equation, the total energy is proportional to the square of the voltage. Just a small increase in the stability window will greatly increase the total energy. [44]

2.1.4.2 Porosity

The electrodes in a supercapacitor are made of highly porous materials, to increase the specific surface area. However, a high specific surface area is not the only important factor regarding porosity. The dimensions, layout and size distribution of the pores are also of importance. When the pores decrease in size, a larger percentage of the atoms in the materials will be at the surface. This will increase the specific surface area, and subsequently increase the capacitance of a SC. This increase in capacitance will however only go on to a certain point. At some point making the pores smaller will actually lower the capacitance, even though the specific surface area will still increase. The main reason for this is that the pores are now too small for the ions in the electrolyte solution. If the pores are smaller than the ions, the ions will no longer be able to permeate and "wet" the pores. If the pores are not able to be wetted, their large surface area cannot be utilized. If the pores are to large, however, there are more volume to "spare" after the first layer of ions has adsorbed onto the surface. Based on this, an optimal pore size should exist. This optimal pore size will be individual for each supercapacitor, since it will be depend on the specific electrolyte used. The optimal pore size will typically also differ between the cathode and the anode, as the cations and anions in an electrolyte solution is usually of different sizes. [25, 44]

The distribution of pore sizes are also important. Ideally, the distribution of sizes should be centred at, and with a high concentration of, the ideal pore size. Large divergence from this point will result in a less than ideal capacitor. The layout of the pore networks, combined with the distribution of pore sizes, will also influence how well the SC can be charged and discharged. This is based on the

fact that the ions in the electrolyte needs to be able to permeate into the pores, filling all the potential adsorption sites. This filling could be hindered if the layout of the pores promote early clogging. How well filling occurs is also influenced by the mobility of the ions and the viscosity if the electrolyte. [25, 44]

To maximize the capacitance in a SC, the creation of asymmetric electrodes could be important. As there is an asymmetry between the two ions in an ion-pair, using the same type of electrode at both the cathode and anode could likely give difference capacitance. By considering equation (2.12), it could therefore be argued that each individual electrode should be designed for the specific ion intended to be used, not just the ion-pair.

2.1.4.3 Mobility and viscosity of ions and solvent

The mobility and viscosity of the electrolyte impacts more than just the filling of the supercapacitor. It also influence the frequency of charge/discharge cycles, and the series resistance of the device, as well as the total energy the supercapacitor can store. The electrolytes viscosity can be thought of as its "thickness", its reluctance to flow when an external force is applied. There are several parameters that determine the viscosity of a liquid, with the temperature being one of the most important. In a liquid, the viscosity is lowered with an increasing temperature. In relation to electrolytes, a higher viscosity is typically associated with a higher electrical resistance, increasing the equal series resistance of the supercapacitor, which will lower the maximum efficiency of the device. This can be understood by the reduced mobility of ions in solution, the current mediators. With a low viscosity the electrolyte flows more readily, with increased mobility of the ions. This allows easier wetting and emptying of the pores during charge/recharge cycles, allowing for a higher operating frequency. However, a low viscosity might also play an indirect role in reducing the performance of a supercapacitor. As can be seen from equation (2.10) and (2.11), the length of the diffuse layer is a function of temperature. With increasing temperature the viscosity will decrease, while the length of the diffuse layer will increase, which will lower the capacitance and total energy storage. [4, 5, 7]

2.1.4.4 Inert electrode materials

One last point to touch upon, is the demand for the electrode materials to be inert. This might not be of as immediate importance for the performance of the

supercapacitor as the other parameters mentioned above, but it plays a vital role to the lifetime of the device. With energy storage through electrochemical double-layers, it is important that the opposing charges in the electrode and electrolyte do not get to meet and react. If they met, and electron transfer occurred, irreversible redox reactions could take place between the electrolyte and electrode material, which would permanently damage the electrode. This damage would reduce the amount of sites for ions to adsorb onto the electrode surface, as well as creating unwanted conducting pathways. To limit these types of reactions, a deliberate choice of electrode materials, substrate/current collector, and electrolyte needs to be taken. They need to be as inert towards each other as possible, while still taking into account the different parameters mentioned above. For electrode materials, this is typically some derivative of carbon. For the type of electrolyte there are several options, given that they remain non-reactive within the operation voltage, i.e. their stability window. The choice of substrate/current collector is to a large degree dependent on the electrolyte, as some electrolytes can be quite corrosive, corroding the substrate if they were to make contact. In an ideal supercapacitor no irreversible reactions will occur. With a good choice of materials, and correct operation, a close approximation can be seen, where SC operate to upwards 10^5 charge/discharge cycles, without significant loss in energy storing capabilities. [41, 44]

2.1.5 Characterization of supercapacitors

In the characterization and analyzation of both supercapacitors and photovoltaic cells there is one type of test, and the curve it gives, that is virtually indispensable. This is the I-V measurement, and it gives the relation between the current and voltage going through and over the tested cell, respectively. If this type of measurement is done on either a supercapacitor or a photovoltaic cell, they will each produce a curve that is characteristic to the type of device tested. From these curves most of the important parameters can be calculated. In the following section the characteristic I-V curve of supercapacitors will be presented.

For characterizing supercapacitor one of the most useful I-V measurement techniques is the cyclic voltammetry (CV). In CV the supercapacitor is repeatedly charged and discharged, usually in a potentiodynamic measurement. In a potentiodynamic measurement the voltage is changed at a controlled pace, while measuring the current. By plotting the measured current and voltage in an I-V curve, the capacitance and total stored energy can be found. From the I-V curve the quality of the supercapacitor can be assessed, as well as the type of capacitance, whether

it is from an electrochemical double-layer, or from pseudocapacitance. [36, 48]

How the capacitance can be found from an I-V curve is easily shown. Capacitance is related to charge and voltage in the following way;

$$Q = CV \tag{2.15}$$

The charge is also related to current;

$$I = \frac{dq}{dt} \tag{2.16}$$

By inserting equation (2.15) into equation (2.16), and assuming that the capacitance is time-independent, we get;

$$I = C \cdot \frac{dV}{dt} \tag{2.17}$$

When performing a CV, one of the important set parameters is the scan rate, v, which is defined as change in voltage per unit of time;

$$v = \frac{dV}{dt} \tag{2.18}$$

From this the capacitance can be found by comparing the current running through the cell to the scan rate;

$$C = \frac{I}{v} \tag{2.19}$$

This procedure can be thought of as measuring the time it takes for the supercapacitor to completely "fill up" with electrical charge, and how much time it needs to deplete itself again, for the given voltage range. Comparing two different supercapacitors at the same current, a longer charging/discharging time for one signifies a higher capacitance. When presenting the capacitance it is often done by giving a specific capacitance, C_s, which gives the capacitance per weight unit of active electrode material. [36]

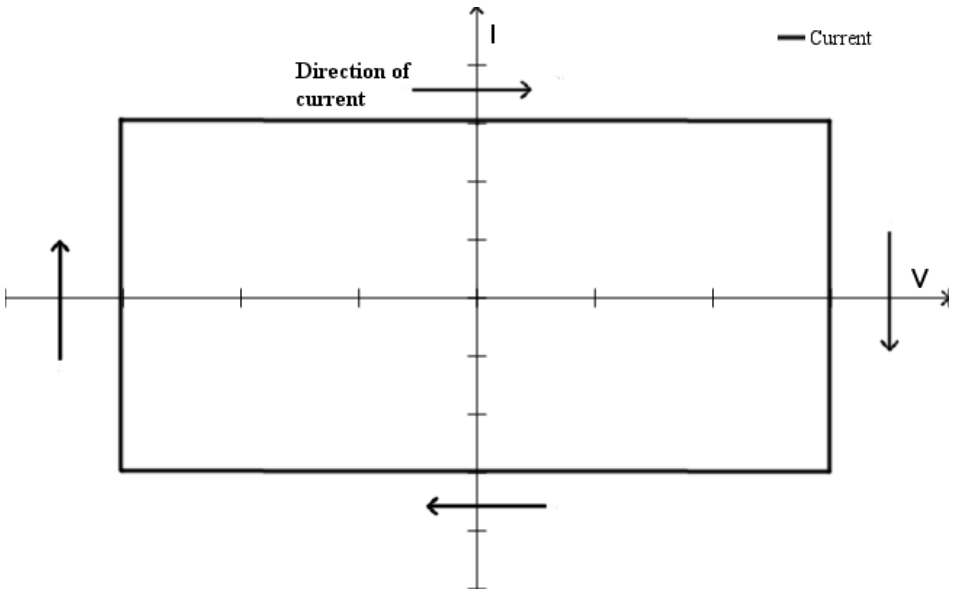

Figure 2.5: I-V curve if an ideal supercapacitor

In an ideal supercapacitor, the I-V curve of supercapacitor gives a square box for the charge and discharge cycles. Such a curve is shown above in figure 2.5. The constant current at increasing voltage means that the capacitance is constant. In a real supercapacitor the I-V curve is more rounded, owing to resistive losses in the device and other effects. One such effect is if the curve has sudden peaks, often at about the same voltage at both the forward and backward part of the cycle. These peaks usually represents redox reactions, and are called redox peaks. One reason for these peaks is if the supercapacitor has components in its electrodes that can contribute to pseudocapacitance. Other, unwanted reasons for such peaks could be the breakdown of the electrolyte or the substrate/charge collectors. Examples of such non-ideal curves are shown in figure 2.6 below. [48]

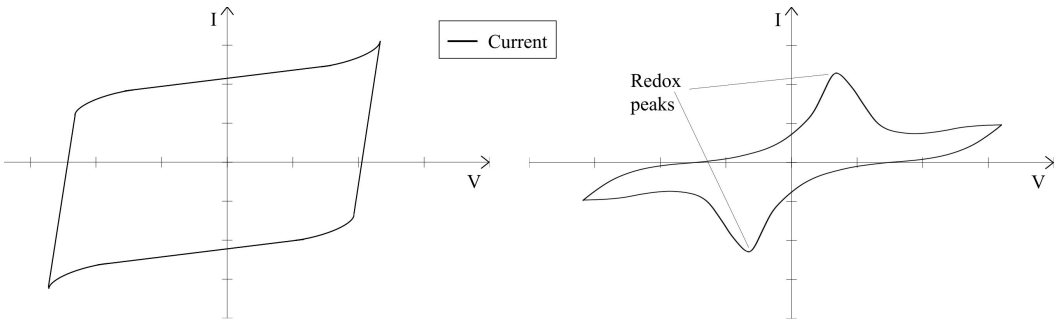

Figure 2.6: Left: I-V curve if non-ideal supercapacitors, rounding of the square curve. Right: I-V curve with redox peaks.

Deviations from the square curve can also be a product of the capacitance not being a constant, but rather a function of the voltage. One way to view this is by looking at the graph where a galvanostatic measurement of a charge-/discharge-cycle is taken. By plotting the curve of the voltage as a function of time, the changing capacitance becomes apparent. For in ideal supercapacitor, such a plot would look like a triangle wave. In a non-ideal supercapacitor however, these curves will be rounded, sometimes resembling "ocean waves". A diagram of the two plots is presented below in figure 2.7. [48]

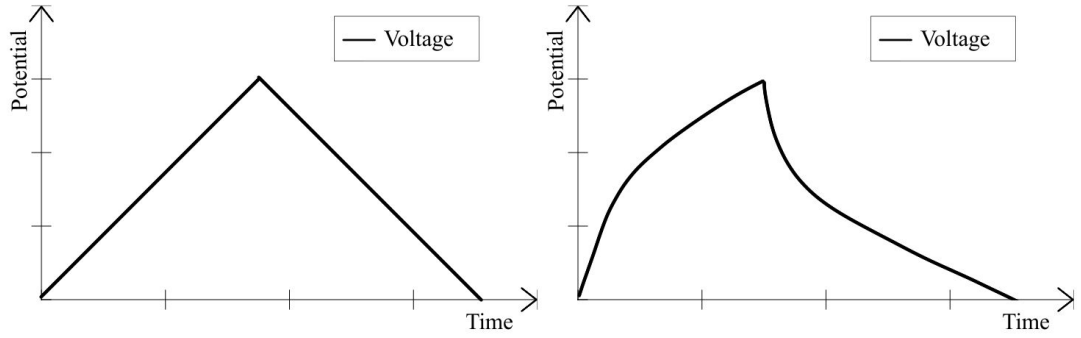

Figure 2.7: Galvanostatic charge and discharge curves for supercapacitor. Left: Ideal. Right: Non-ideal.

When presenting the parameters for a capacitor, the norm is to only give the capacitance and the voltage stability window. One problem with this practice, is that it assumes that the capacitance remain constant at all voltages. If this is not the case, calculations for capacitance and total energy will be wrong. This is typical for asymmetric capacitors, i.e. the two electrodes do not have the same capacitance. This is more often the case with supercapacitors, with capacitance in the form of electrochemical double-layers and/or pseudocapacitance, than with traditional parallel plate capacitor. As shown above in figure 2.7 the charge-discharge curve is no longer a linear function, but are either concave or convex. If the capacitance was calculated from curves where the starting and ending voltages where the same, with the same discharge time, the capacitance and stored energy would be different between the concave, linear and convex curves. These problems were mentioned by Yang et al., and they proposed an alternative method for the characterization of supercapacitors. [48]

In the alternative method it is the energy stored in the device that is of interest, rather than the capacitance. This energy is found through a potentiodynamic measurement, and calculated with the equation below;

$$E_t = \int P\mathrm{d}t = \int IV\mathrm{d}t = \frac{1}{v}\int IV\mathrm{d}V \tag{2.20}$$

Here E_t is the energy stored in the device, V is the voltage, v the scan rate, and I is the current. The area enclosed by the integral is the instantaneous power. One benefit of such a characterization method is that the performance of the supercapacitor in terms of energy storage would be more accurate. The integration limits can be set as the actual working voltages, giving the actual, utilizable energy stored. An effective capacitance, C_{eff}, can also be calculated. This is found through the relation between total energy, capacitance, and voltage over the cell; [48]

$$E_t = \frac{1}{2}C_{eff}V^2 \tag{2.21}$$

2.2 Photovoltaic cells

Solar cells are also known as photovoltaic cells, because they function through the photovoltaic effect. This is when electrons in the valence band of a semiconductive

materials gets excited into the conduction band, leaving behind a positive hole. These charges, the positive hole and the negative electrons, are free charge carriers that can mediate electrical current. In the following sections it will be explained how this effect can be utilized to create devices that can produce electrical energy. [13]

2.2.1 PN-junctions and Solid-state Solar Cells

To better understand how solar cells work, we start by look at the energy band structure of the materials that make up the cell. More specifically we take a closer look at the band structure of the semiconductor materials. These have an energy barrier between the highest energy of the valence band, E_v, and the lowest energy of the conduction band, E_c. This barrier is known as the energy gap, E_g. If energy corresponding to E_g or higher is transferred to the material, electrons can be excited. Semiconductors differ from conductors and insulators in this regard. In conductors the valence and conduction bands are continual, merging into each other. In insulators there is also a band gap, but which is very large, effectively eliminating the possibility of exiting electrons into the conduction band. For solar cells made of semiconductive materials, the energy needed to excite electrons comes from incident photons with wavelengths short enough to have the required energy. [10, 13]

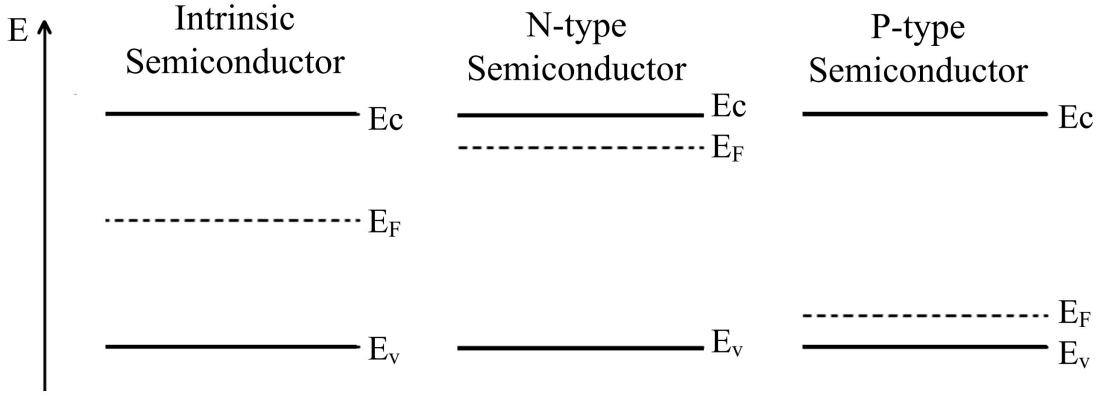

Figure 2.8: Energy band diagram of Fermi levels of intrinsic, N-type and P-type semiconductors.

Every electron in an atoms orbital has a specific energy, and because of Paulis exclusion principal no two electrons in an atom can have the exact same energy. The probability for an electron to have a certain energy, is given by the Fermi–Dirac distribution. The Fermi level, E_f, is a point on this distribution where there is a 50% chance for the electron to occupy that energy state. In a semiconductor, where no modifications have been made i.e. no doping, the Fermi level is usually located at the half way point between the valence band and the conduction band. However, if the semiconductor has been doped with either donor or acceptor atoms, the location of the Fermi level will have shifted. A donor atom is usually an atom with 5 electrons in the outer valence orbital. The 5th electron is more loosely bound, and is easily excited. An acceptor atom is usually an atom with 3 electrons in the outer valence orbital. To form a more stable configuration, a 4th electron is easily absorbed. If the doping is in the form of donor atoms, more loosely bound electrons have been introduced to the semiconductor. This results in there being more free electrons in the conduction band than normally, and the Fermi level lies higher, towards the conduction band. This type of semiconductor is called a N-type semiconductor. If the doping is in the form of acceptor atoms, the opposite has happened. There are now atoms with more "holes" to be filled, and they start binding the free electrons. This reduces the electrons available to be excited to the conduction band, consequently shifting the Fermi level down towards the valence band. This type of semiconductors is called a P-type semiconductor. The energy bands of intrinsic, N-type and P-type semiconductors are shown above, in figure 2.8. It is often both a N-type and a P-type semiconductor in junction with each other that make up the functional parts of a solar cell. [11, 13, 46]

Often in the literature both the N- and P-type semiconductors are made from the same type of solid-state semiconductor, doped with donor and acceptor atoms, respectively. The heavily researched mono- or crystalline silicone solar cells are examples of this. Because of the focus on these types of solar cells, most of the relevant terminologies used to explain their functioning are made with such solid-state solar cells in mind. However, in this thesis it is of more relevance to talk about the joining of either a N-type or a P-type solid-state material, with an electrolyte. Luckily the working principals between the two are very much the same, with just a few alterations. Therefore, to get a qualitative understanding, the first part of the further reading will be about the workings of a standard solid-state N-P type semiconductor solar cell. Afterwards, the few alterations needed for the joining of a solid-state semiconductor and an electrolyte will be given. [11, 13]

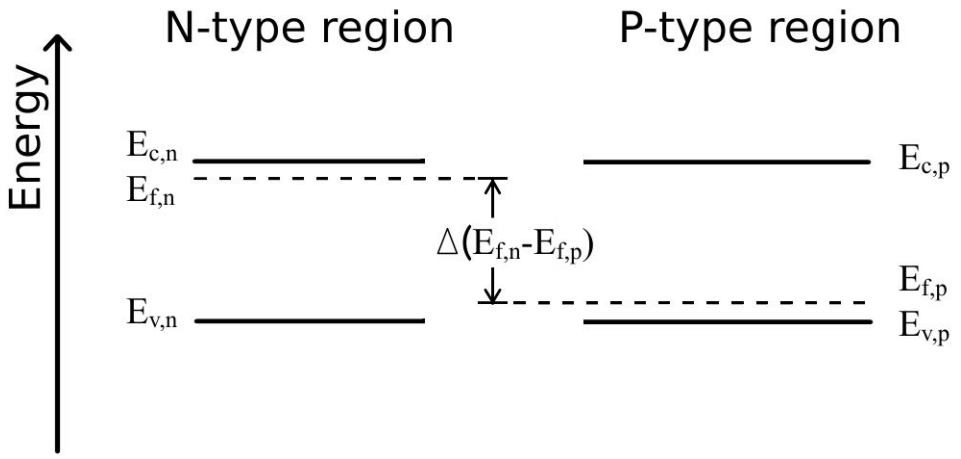

Figure 2.9: Energy band diagram of N-type and P-type semiconductors. Conduction band, valence bands and Fermi levels of the N- and P-type semiconductors, before joining them together.

The location of the Fermi levels become important when two dissimilar materials are joined together. A difference in Fermi levels between two materials indicate an electric potential. Such a difference is shown in figure 2.9. However, according to Gauss' law, there is no potential difference on the inside of a conductive material in equilibrium. This can be understood as at a certain time after the two materials are joined together, a rearrangement of the charges in the materials have occurred. This rearrangement takes form as a drift current driven by the electrostatic potential, as described in equation (2.7). Also, similar to the situation for supercapacitors under the formation of an electrochemical double-layer, a concentration gradient for the different charges starts forming, and a diffusion current is created. This gives a diffusion current going in the opposite direction, as described in equation (2.8). These currents will keep on running until a balance is struck, and the system is in equilibrium. If we now look at the band structures of these two materials, we will see how they have changed to achieve this equilibrium. These changes are shown in figure 2.10 below. [10, 13]

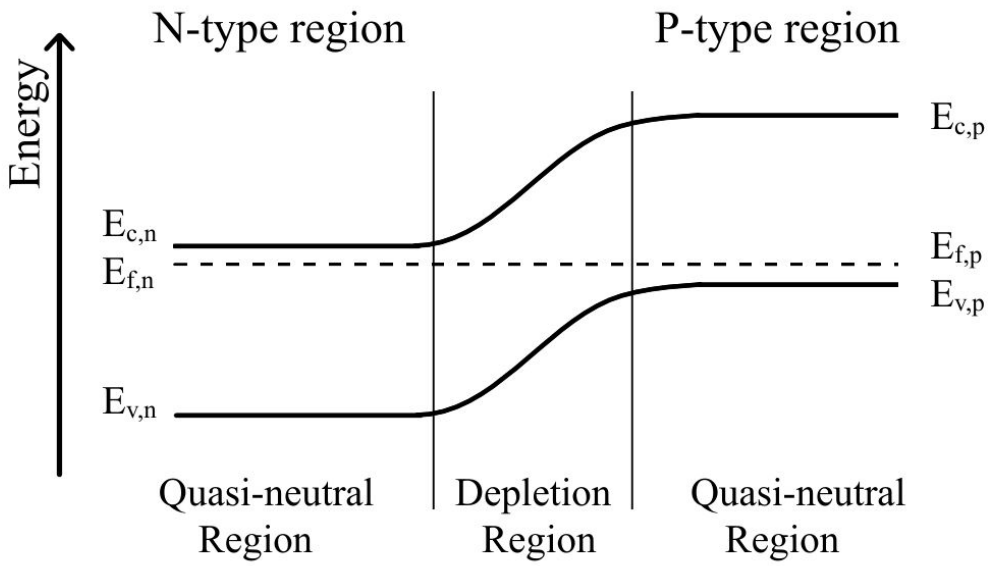

Figure 2.10: Energy band diagram of a N-type and P-type semiconductor junction, with depletion regions and quasi neutral regions marked. These are the bands at equilibrium, with no externally applied voltage.

In equilibrium the Fermi levels remains the same in the two materials. Thus, the position of the conduction and valence bands for the two materials in relation to the Fermi level in the bulk of the material, i.e. far away from the junction, shall be the same as the relation for the uncombined materials. Because of this the valence and conduction bands have been shifted, to make the Fermi levels line up. The energy gap between the valence and conduction band for each of the joining materials remain the same. Secondly, the valence and the conduction bands between the two materials have met up with each other, respectively, forming continual bands. This is a result of the continuity equation, for the charges and energies. To achieve this continuity, the bands have undergone something called band bending, which is the result of the rearrangement of the charges in the materials. These charges are mainly the free charge carriers, the electrons and the holes, as the other charges like the doping atoms, are stronger bound. At the junction between the two materials, as good as all the free charge carriers have been transported away by the initial potential difference. This region is called the Depletion Region (DR), and stretches into the joining materials at each side of the junction. How far this region stretches into each side varies, being in the order

of angstrom to nm, and is determined by the concentration of the strongly bound donor and acceptor atoms at each side. The concentration of donor and acceptor atoms at each side of the junction is known as the doping profiles. The doping profile also determines the shape of the bended bands. The region outside of the DR is known as the quasi-neutral region, and is named so because there is no net electric field. [10, 11]

Far away from the junction, after the Fermi levels are lined up, if the energy levels of the valence and conduction bands for the two material are at different levels, then this corresponds to a potential difference. This potential difference is called the built-in potential, and are present at all junctions between dissimilar materials. Unlike an applied electric potential from an external voltage source this potential is not readily available to be measured. This potential can be understood by looking at the remaining charges in the DR. These charges primarily consist of the stronger bound donor and acceptor atoms. At the N-type side the donor atoms are bound, which are now positive ions, and at the P-type side the acceptor atoms are bound, which are now negative ions. Since the positive ions are at the N-type side, the electrical field formed between the charges runs from the N-type to the P-type sides. It is this built-in potential that is responsible for maintaining the drift part of the new drift-diffusion balance between the charges, and depleting the free carriers from the DR. The built-in potential will also separate all new electron-hole pairs that gets introduced to the regions where the potential exist. In relation to the band diagram, the free charge carriers will separate in such a way that the electrons will move downwards to the lower of the E_c bands, from the P- to the N-type side, while the holes travel upwards to the higher of the E_v bands, from the N- to the P-type side. The electrons on the P-type side, and the holes on the N-type side, are known as minority carriers. The holes on the P-type side, and the electrons in the N-type side, are known as majority carriers. [10, 11]

What has been described above is a basic diode. The current that runs through the diode is given by the diode equation;

$$I = I_0(e^{\frac{qV}{k_bT}} - 1) \tag{2.22}$$

Here I is the current, I_0 is the dark saturation current, V is an external voltage applied over the diode, q the electric charge, k_B the Boltzmann constant and T the absolute temperature. The dark saturation current, also known as the reverse leakage current, is the current that runs through the cell when it is in complete darkness. This current comes from minority carriers that diffuse from the bulk of the material to the DR, where they are swept across the junction by the built-

in potential. When the externally applied voltage over the cell reaches a certain value, the current running through the cell start increasing exponentially, as can be seen from (2.22). When such a voltage is applied, with a positive value, the cell is said to be under forward bias. If the applied voltage has a negative value, the cell is under reverse bias. Under reverse bias there is no current except the reverse leakage current, until a certain negative voltage known as the breakdown voltage is applied. The diode equation above is the equation for an ideal diode. For a real diode an ideality factor, m, is usually added. This gives; [13]

$$I = I_0(e^{\frac{qV}{m \cdot k_b T}} - 1) \tag{2.23}$$

In these equations there is only the applied voltage that makes the current run through the cell. For real diodes this is not always the case, as is the case for solar cells where the incoming light hitting the cell induces a current. An equation for a photovoltaic cell can be devised by taking equation (2.23), and expanding it. This expansion comes in the form of adding the light-generated current, I_{ph}; [13]

$$I = I_0(e^{\frac{qV}{m \cdot k_b T}} - 1) - I_{ph} \tag{2.24}$$

The origin for this light-generated current can be explained by the absorption of photons and creation of electron-hole pairs. When photons with sufficiently short wavelength, corresponding to the energy given by the Planck-Einstein relation below, the photons can be absorbed and electrons excited into the conduction band, leaving a hole being. [10]

$$E = hc/\lambda \tag{2.25}$$

Where the photons are absorbed and consequently where the electron-hole pairs are created is of critical importance for the light-generated current. For a solar cell to work, the minority carrier of the newly created electron-hole pair has to be able to reach the DR, where it can be swept across the junction by the built-in potential. As soon as the electron-hole pairs are created, a race between the two most likely outcomes start. The first outcome is that the minority carrier of the pair manage to reach the DR and is swept across. The second outcome is that too long time passes before it manages to reaches the DR, and the electron and the hole recombine. Since the DR is typically quite short, most of the electron-hole pairs created are in the quasi-neutral region where there is no electrical field. This means that approximately all of the particles movement is caused by diffusion.

How fast the electron-hole pairs recombine is given by the recombination lifetime of the minority carrier, τ. By combining the diffusion coefficient and recombination lifetime of each of the minority carriers, we get two critically important parameters, namely the Diffusion Length of the electrons and holes, respectively; [10, 12]

$$L_n = \sqrt{D_n \cdot \tau_n} \tag{2.26a}$$
$$L_p = \sqrt{D_p \cdot \tau_p} \tag{2.26b}$$

These parameters have the unit of length. In a working solar cell the electron-hole pairs have to be created within a few diffusion lengths of the DR to be able to reach this zone, and be swept across the junction. If the pairs are created much further away than this, they will recombine before reaching the DR. The diffusion length might vary greatly between different materials. Single crystalline silicon cells have a reported diffusion length of 50-1200 μm, poly crystalline silicon cells a length of 4-30 μm, while in GaAs thin-film cells the diffusion length is just a few micrometers, around 1-3 μm. The total current that runs in the cell is the sum of both the electrons and the holes that crosses the junction. [11, 19, 37, 39]

$$I_{total} = I_p + I_n \tag{2.27}$$

These are the fundamental working principals of a photovoltaic solar cell, which is primarily meant for solar cells where there are two solid-state, doped semiconductor meeting in a junction. Above it was mentioned that in this thesis there is a bigger interest in solar cells made with semiconductor/electrolyte junctions. The next section is about the alterations to the theory that needs to be made to accommodate this.

2.2.2 Electrochemical Solar Cells

In the solid-state junction, the Fermi level of the two joining materials are at different energies, and ultimately gives rise to the in-built potential. In an electrolyte, there is no Fermi-level. However, there is an analogous level, the redox potential, E_{redox}. This the affinity a specific species has for electrons, giving how easily it is reduced. In a redox pair, it will give the probability for an electron to be in the reductant or the oxidant, i.e. the reaction balance between the two species.

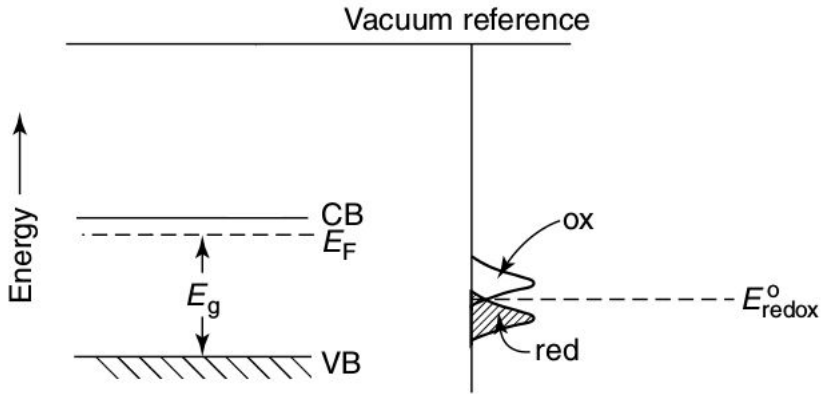

Figure 2.11: Energy band diagram of N-type semiconductor in contact with electrolyte. Shows the Fermi level for the semiconductor, and the redox potential for the electrolyte. Edited from [38]

A comparison between the Fermi level and the redox potential is shown above in figure 2.11. When a semiconductor and an electrolyte with Fermi level and redox potential at different energies are joined together, a similar reaction to the joining of two dissimilar solid-state semiconductors starts to occur. At first the difference in Fermi level and redox potential signifies an electric potential, and electric current starts running in accordance with the direction of the potential, until an equilibrium is reached. Near the junction a distinct charge distribution will have occurred, similar to the depletion region, which will make the energy bands between the two materials meet up. How this charge distributed is achieved is similar to how it is achieved in solid-state PN-junctions, but not exactly the same. On the semiconductor side, the charge distribution will have happened in the same way, with the free charge carriers having been swept away, leaving the more immobile ions behind. On the electrolyte side, the charge distribution will have happened by the formation of an electrochemical double-layer, with the adjoining diffuse layer, at the junction. To make the energy bands meet up, band bending will have occurred, but only on the semiconductor side. For describing the nature of the band bending, a few definitions can be made, by focusing on the movement of the electrons. If the electrons are transported from the electrolyte into the semiconductor, an accumulation layer will have formed. The increase concentration of free electrons near the junctions on the semiconductor side will cause the energy bands to bend downwards from the bulk, giving N-type semiconductor characteristics. Alternatively, if the electrons were transported from the

semiconductor into the electrolyte, a depletion layer will have formed. In this, the decrease concentration of electrons in the semiconductor will cause the energy bands to bend upward from the bulk, giving P-type semiconductor characteristics. With extreme potential differences, the electron concentration can be depleted below the intrinsic concentration in the bulk of the semiconductor. This will cause P-type semiconductor characteristics near the junction, and N-type characteristics in the bulk. All these different charge distributions are shown below in figure 2.12, along with the flat band distribution. In semiconductor in this figure is a N-type. [17, 20, 38]

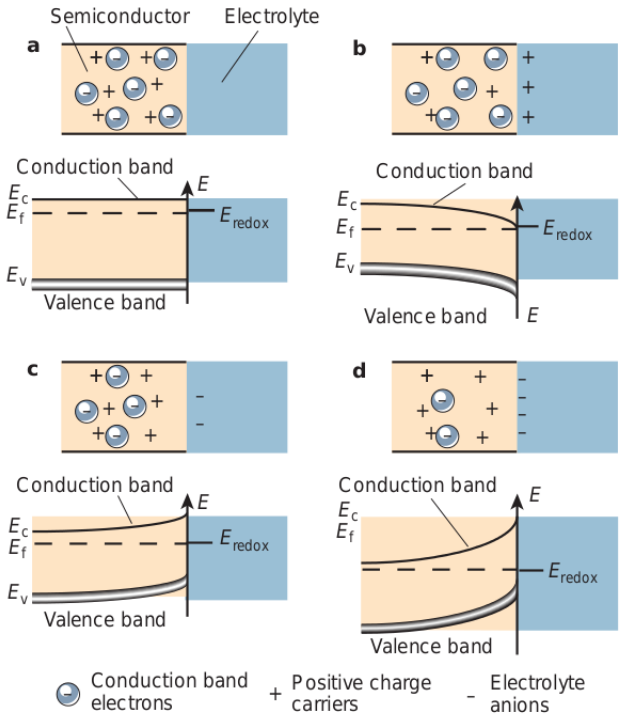

Figure 2.12: Energy band diagram of a N-type semiconductors in contact with an electrolyte. Potential differences between Fermi level and redox potential gives various charge distributions: a) Flat band distribution. No potential difference, and no band bending. b) Accumulation layer. High electron concentration in semiconductor causes downward band bending. c) Depletion layer. Low electron concentration in semiconductor causes upward band bending. d) Extreme depletion layer. Electron concentration below intrinsic level in semiconductor causes extreme upward band bending. [20]

In an electrochemical solar cell, the working mechanics are much the same as for a solid-state solar cell. Electron-hole pairs are created in the semiconductor, and diffuse towards the junction. When they get there, they either oxidise or reduce the species in the redox pair, depending on the minority carrier being holes or electrons, respectively. Which charge carrier that is moved across the junction is determined by the direction of the band bending. Electrons move downwards along band from the bulk, while holes move upwards. The other free charge carrier is transported into the bulk of the material. For a current to continuously be able to run, a counter electrode (CE) is needed, that is connected to the semiconductor through an external circuit. The reduced or oxidised species in the electrolyte can migrate towards the CE, and there be oxidised or reduces back to their original state, respectively. A diagram of this cycle is shown below, in figure 2.13. [20, 35]

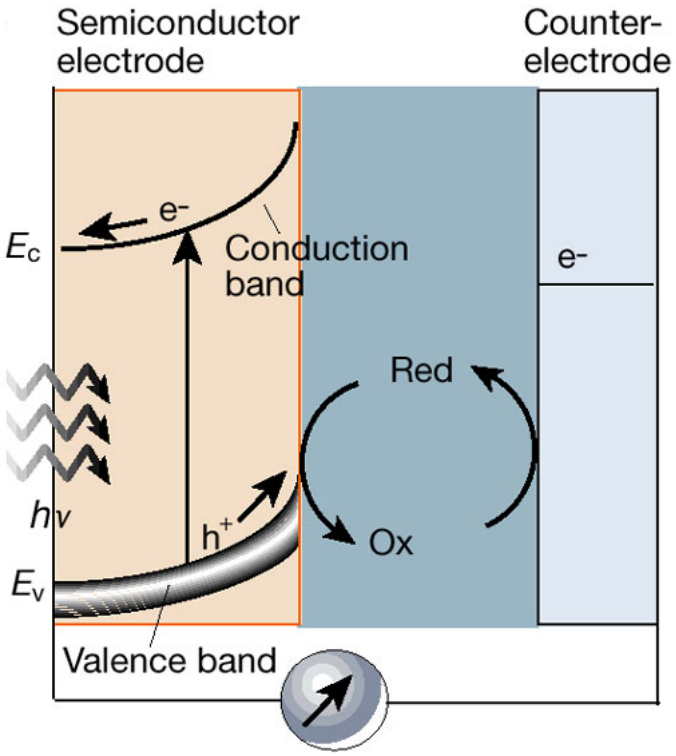

Figure 2.13: Circuit diagram of a complete electrochemical photovoltaic cell. Edited from [20]

2.2.3 Important parameters in a photovoltaic cell

To describe and to characterize how well a photovoltaic cell works, there are primarily 4 parameters that are of interest. These are the cells short-circuit current, I_{sc}, open-circuit voltage, V_{oc}, the fill-factor (FF), and efficiency, η. It is through these 4 parameters that virtually all commercial photovoltaic cells are described, and they give a satisfactory overview of the cells performance. The easiest way to find and calculate these parameters are with an I-V curve. Figure 2.14 gives an overview of such a curve, with the important parameters marked. [12, 13]

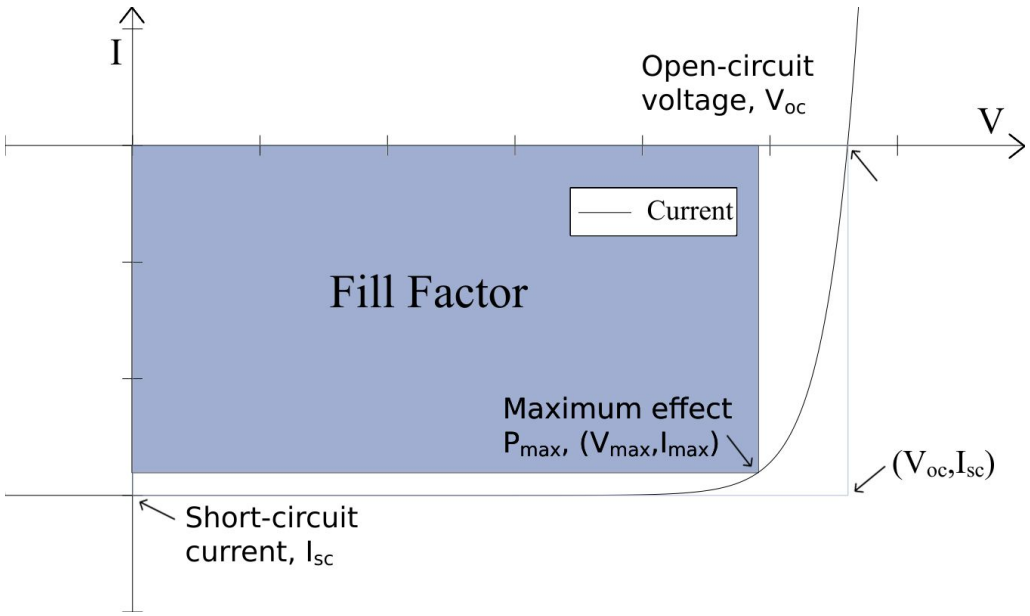

Figure 2.14: I-V curve of a typical photovoltaic cell under illumination, with approximate standard test conditions.

2.2.3.1 Short-Circuit Current

The short-circuit current is the current that runs through the cell when the two terminals of the cell are short-circuited, i.e. connected together by an external circuit with no resistance. For practical purposes this is the current measured when the voltage over the cell is zero. The short-circuit current is the sum of both the

dark saturation current and the light generated current. Since the dark saturation current is typically quite small, the light generated current can be approximated as the short-circuit current. The height of the short-circuit current is primarily a function of the number of electrons and holes that pass over the junction in the cell. This means that some of the determining factors is the cross sectional area the charges move through, their diffusion length, and the electron-hole pair generation rate. A higher value in all of these three will give a higher short-circuit current. For the generation rate of the electron-hole pairs, the intensity of the incident light is important. This is reasonable as light with higher intensity have more photons that can get absorbed by the semiconductor, and produce more electron-hole pairs. [12, 13]

2.2.3.2 Open-Circuit Voltage

The open-circuit voltage is the voltage over the cell when the two terminals are not connected by any external circuit. When measuring, this is the voltage when the current running through the cell is zero. The open-circuit voltage has a strong relation to the built-in potential of the cell, and have many of the same determining factors. One of these are the temperature, which through the Fermi-Dirac distribution influence at what energies the electrons in the materials are distributed at. For a doped solid-state solar cell the doping profile would also be quite determining, as it sets the relation between the Fermi levels of the joining materials, which again determines the built-in potential. For a solid semiconductor/electrolyte solar cell this built-in potential, and consequently the open-circuit voltage, is more determined by the (possible) intrinsic Fermi level of the semiconductor and the redox potential of the ion-pairs in the electrolyte. [12, 40]

2.2.3.3 Maximum Power and Fill Factor

The power of the photovoltaic cell can be expressed as the product of the current running through and the voltage over the cell, given by;

$$P = I \cdot V \tag{2.28}$$

At some point between the I_{sc} and V_{oc} in an I-V curve, the power will reach a maximum. The current and voltage at this point of the curve is designated I_{max} and V_{max}, respectively. From this we can get what is called the fill factor, which

is given by;

$$\text{FillFactor} = \frac{I_{max} \cdot V_{max}}{I_{sc} \cdot V_{oc}} \tag{2.29}$$

The fill factor is a measure of the "squareness" of an I-V curve for a solar cell, and gives an indication of the quality of the cell. As can be seen from equation (2.22), in an ideal diode or solar cell the voltage should increase exponentially. Given the range of the voltage and current in a solar cell, and the abruptness at which the current starts to increase, this can be approximated as if the current increase as a step function. This gives that the enclosed area from an ideal solar cell curve is the product of I_{sc} and V_{oc}, as can be seen in equation (2.29).

Deviations from the ideal square curve are usually from resistive losses in the device. These come in two main types, shunt and series resistances losses. The series resistance is the ohmic resistance of all parts in series with the main component, here the solar cell. The current that runs through these resistances will be the same that runs through the solar cell. This means that to limit the energy loss, these resistances should be as low as possible. The shunt resistances is the resistance in circuits that runs in parallel with the main component. These often comes from unwanted connection points that bypass the main circuit. Since these circuits are in parallel, a certain fraction of the total current will go through each. How much is inversely proportional to the resistance in each of the circuits. This means that to limit the energy loss caused by shunt resistances, these resistances should be as high as possible. [12, 13]

2.2.3.4 Efficiency

The efficiency of a solar cell is perhaps the most presented parameter of solar cells performance, especially for commercial uses. The efficiency is the fraction of the generated electrical power to the total power of the incident light. It is calculated by dividing the maximum power of the cell, with the power of the incident light absorbed the cell;

$$\eta = \frac{I_{max} \cdot V_{max}}{P_s} \tag{2.30}$$

Or alternatively expressed by I_{sc}, V_{oc} and the FF;

$$\eta = \frac{FF \cdot I_{sc} \cdot V_{oc}}{P_s} \tag{2.31}$$

Here η is the efficiency and P_s is the power of the incident light.

The efficiencies given for varies solar cells are usually the efficiencies at peak performance under ideal standard test conditions (STC). Some of these standard conditions are that the intensity of the light should be at $1000W/m^2$, with an air mass of 1.5 (AM1.5), and the temperature at $25°C$. Air mass is a factor that gives a quantified measure of the attenuation by the atmosphere of the incident light hitting earth. It is defined as the fraction of the length of the optical light path to the sun at a specific position, to the length of the optical light path when the sun is directly ahead. This fraction can be expressed as a angle of elevation from top position, and AM1.5 is equal to the sun being at a 42° elevation. [37]

Below in table 2.1, typical FF and efficiency for varies types of solar cell materials are listed. These are performance characteristics at STC.

Table 2.1: Solar cells performance characteristics, at STC. [37]

Cell Type:	Fill Factor:	Efficiency (%):
Crystalline Si	82.8	24.7
Crystalline GaAs	87.1	25.1
Poly-Si	79.5	19.8
a-Si	74.1	12.7
$CuInGaSe_2$	77.0	18.4
CdTe	74.5	16.4

Since these efficiencies are usually only given at ideal conditions, the actual performance of the cells at other conditions may vary greatly, potentially yielding much lower efficiencies. [12, 13, 40]

2.2.4 Characterization of photovoltaic cells

To characterize a photovoltaic cell, the first step would be to perform an I-V measurement while the cell is under controlled illumination. This measurement is often done as potentiodynamic measurement, where the voltage is changed at a controlled pace, the scan rate, while the current is measured. The controlled voltage usually starts at 0 V, recording the I_{sc}. The voltage is then increased steadily, and goes on until the recorded current intersects the V-axis. This gives the V_{oc}. From the data points between I_{sc} and V_{oc} an I-V curve can be plotted. From these data points the point of maximum efficiency can also be found, and the fill factor and efficiency calculated.

For evaluating the quality of the photovoltaic cell, the plotted I-V curve can be related to an expanded version of equation (2.24). In this equation the shunt and series resistances are included, and gives a better understanding of deviations from the ideal curve; [40]

$$I = I_0\Big[exp(\frac{q(V - I \cdot R_s)}{mk_BT}) - 1\Big] - I_{ph} + \frac{V - I \cdot R_s}{R_{sh}} \tag{2.32}$$

Here R_s is the series resistance, and R_{sh} the shunt resistance. By looking at the exponential term in the equation we can see that the series resistance will influence the voltage over the cell. This will affect how the current rises towards the V_{oc} point with increasing voltage. A high series resistance will give a slower rise, and a less ideal curve. The shunt resistance will primarily influence the area close to the short-circuit current. A low shunt resistance will allow current to move through alternative pathways. This will to a larger degree cancel out the light generated current, as is seen in the last two terms on the right side of the equation. Because of this, the shunt resistance should ideally be infinite. In figure 2.15 below the equivalent circuit diagram for the photovoltaic cell is shown. [40]

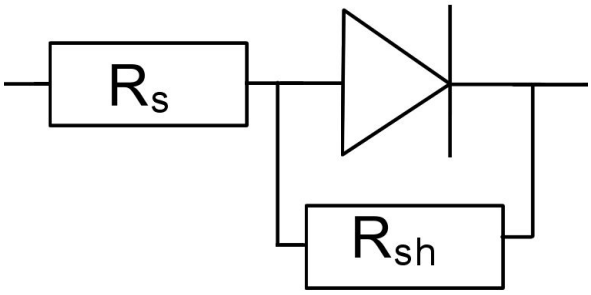

Figure 2.15: Equivalent circuit diagram for the photovoltaic cell, with shunt and series resistances.

During the testing there are some parameters that can easily be varied, which will give a more complete characterization of the system. Among these are the illumination intensity, and the scan rate. The varied illumination intensity can give a relation between the intensity and the light generated current. The change in scan rate can give an indication on the impedance of the system. [28]

The impedance relate what electrical resistance the current in the system will meet, with changing voltages. Different electrical components, like ohmic resistances, capacitors, and inductors, will affect the current differently. In most equivalent circuit diagrams of real electrical system, like a solar cell, all of these different components will be present, in one degree of of another. E.g. in a solar cell system, there will be a small capacitance between the charges separated by the junction. The shunt and series resistances in the solar cell system will also contribute to the impedance. The impedance value is heavily influenced by the rate of which the voltage is changed, and each type of components is affected differently. By doing measurements on the solar cell at differing scan rates, the size and contribution to the total impedance for each of these components can be deduced. [10, 29]

2.3 Photocapacitor systems

In this last section, the complete photocapacitor system will be looked at. This includes what what parts are required to make a well functioning photocapacitor. The charging and discharging mechanisms of the system will also be covered.

2.3.1 Requirements for a functioning photocapacitor system

In principal, the photocapacitor system is just two distinct electrical components working in conjunction with each other. This means that to have a functioning supercapacitor, each individual component just needs to perform its function.

For the photovoltaic components, this means generating electron-hole pairs when irradiated by electromagnetic radiation. These then needs to be separated by a barrier, so that recombination can only happen by going through an external circuit. This movement of charges produces an electrical current. [10]

For the supercapacitor component, this means positioning two opposing electrical charges close to each other, but still not touching. This creates an electrical potential. To place the charges in these positions, an electrical current is used. Most of energy expended in moving these charges is stored in the electrical potential. The stored energy can be acceded by presenting an alternative circuit through which the charges can recombine. [30]

To have a functioning photocapacitor system on its own, may not be that difficult. To have a photocapacitor system that is performing at the limits of

its individual components, may be more difficult. To have this, the performance of one of the component must not come at the cost of the performance of the other. In a system containing individual, commercial, components, this is easy to achieve. In a fabricated, single device photocapacitor, however, this becomes more challenging.

2.3.2 Charging and discharging mechanisms of a photocapacitor system

To describe the charging and discharging mechanisms of a photocapacitor system, a circuit diagram can be created. Such a diagram is shown in 2.16 below. In the diagram the photovoltaic parts and the supercapacitor parts are represented as individual components, connected in series. The photovoltaic component is a solid-state, PN-junction solar cell. The diagram shows the circuit during charging.

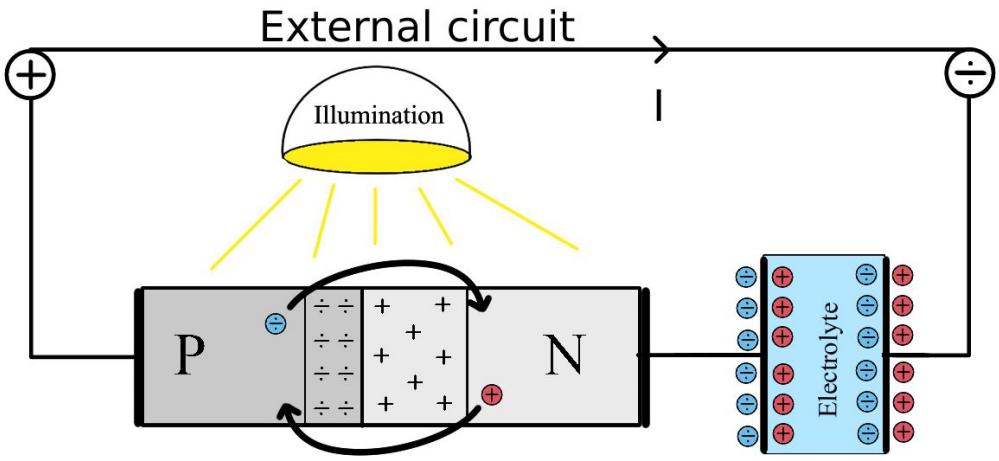

Figure 2.16: Diagram of photocapacitor system.

2.3.2.1 Charging the commercial photocapacitor system

When the solar cell is illuminated, the light induced current is generated. It is a result of the photo excited electron-hole pairs that diffuse and drift across the

PN-junction. This current goes in the opposite direction to the current that would run if the solar cell diode was under forward bias. To keep a continual current flowing, the two terminals of the system needs to be connected to each other. Depending on the built-in potential of the PN-junction, V_{PV}, the resistances in the circuit, and the dark-saturation current, there will be a certain voltage over the solar cell. The current that runs through the circuit after the two terminals are connected together will gradually charge the supercapacitor. This charging will continue until the voltage that builds up over the supercapacitor, V_C, is equal to the voltage over the solar cell, but in the opposite direction. When measuring the open-circuit voltage over the complete system, the value should be zero since the voltages over the two components almost completely cancels each other out. The last voltage drop to make the total potential zero comes from the series resistance in the circuit. This means that the two photovoltaic parameters, I_{sc} and V_{oc}, it is the V_{oc} that is the determining factor for how much energy can be stored in the supercapacitor of a photocapacitor system. [10, 30]

2.3.2.2 Discharging the commercial photocapacitor system

To discharge the system, the light needs to be turned off, and the terminals connected. When the light is turned off there is no more light-generated current, and the solar cells is in effect a diode. The lead direction of the diode is in the opposite direction to the current that charged the supercapacitor. This means that when the supercapacitor is to be discharged, the discharging current will run in the lead direction of the diode, and through the closed circuit. Because of this, it might seem that the complete discharge of the supercapacitor should not be a problem. There is one issue, however. This issue is caused by the diode, and will greatly limit the speed and degree of which the supercapacitor can be discharged. In a diode, the current allowed to flow through is heavily influenced by the applied voltages over it. This relation is shown in equation (2.32), where the shunt and series resistance for the diode (solar cell) is also included;

$$I = I_0\Big[exp(\frac{q(V - I \cdot R_s)}{mk_BT}) - 1\Big] - I_{ph} + \frac{V - I \cdot R_s}{R_{sh}} \tag{2.33}$$

In the simple, ideal diode equation, V is the applied voltage over the diode. In a non-ideal system, there will be resistive losses in the circuit, that reduce the effective voltage over the diode. In this system, during the discharge, the applied voltage comes from the electrostatic potential in the supercapacitor, and the resistive losses, R_s, is the series resistance in the whole circuit. From this

equation, an explicit expression for the discharge current can be devised.

To start of we can assume that there is no illumination and that the shunt resistance is sufficiently large, eliminating the last two terms on the right side of the equation. This gives

$$I = I_0\Big[exp(\frac{q(V_C - I \cdot R_s)}{mk_BT}) - 1\Big] \tag{2.34}$$

If the current through the diode is very small, this expression can be approximated to

$$I \approx I_0 \cdot \frac{q(V_C - I \cdot R_s)}{mk_BT} \tag{2.35}$$

By further rearranging equation (2.35), the explicit expression for the discharge current is found

$$I = I_0 \cdot \frac{qV_C}{mk_BT} \cdot \frac{1}{1 + \frac{qR_sI_0}{mk_BT}} \tag{2.36}$$

From this equation, a few very important relations can be noted. The first is how the voltage over the supercapacitor affects the current. With a higher voltage, a higher current will run through the diode. As the supercapacitor discharges, this voltage will drop, and subsequently the current also drops. This could means that if the initial V_C was very large, the discharge could also happen very quickly in the start, but then quickly slow down more and more. The validity of this proposed mechanism has to be considered though, as the approximations used for equation (2.36) has a very limited range. The second relation is how the series resistance affects the current. With increasing series resistance, the total current would get lower and lower. This means that if the complete photocapacitor system was connected to an external circuit, with a certain resistive load, R_L, the discharge of the supercapacitor would happen slower and slower with increasing R_L, and then slow down even further as V_C decreased. In a discharge of an actual photocapacitor, these relations put together would mean that the current and the discharge would practically come to a stand-still, before the supercapacitor is completely emptied of charge. One last think to consider validity of equation

Chapter 3

Method

In this chapter the procedures used to fabricate photocapacitor devices will be explained. How the devices were tested and characterization will also be covered. The instruments, chemicals and computer programs that were used in the fabrication and characterization are presented in summary tables in the appendix.

3.1 Fabrication of a photocapacitor

A complete photocapacitor consists of many different components, and several of these share the same fabrication procedures. In the following sections the general steps are presented and explained, with the specifics for each type of electrode with regards to components and ratios, afterwards.

3.1.1 Preparing the indium tin oxide glass slides

1. The indium tin oxide (ITO) glass slides are cleaned. They are placed in a solution of ethanol and sonicated for a few minutes. Afterwards the slides are removed from the solution, rinsed with a bit more ethanol and placed in a drying rack for glass slides.

2. Checking for conductive side. The glass slides are only coated with ITO on one side, and which side this is needs to be established. This is easily done by using a multimeter and checking the resistance across the edges of the

slide. On the ITO side the resistance will typically be in the range of 10-100 Ω, while on the non-coated side in the range of 10^6 Ω.

3. The last step is masking up the sides of the glass slide. This primarily serves two purposes. The first purpose is to mask up areas that needs to be uncoated in the electrode material. These areas are left bare for the connection of clamps and external wires for characterization. The second purpose is to serve as thickness limiters for the applied layer. The masking is done with some sort of regular tape, like scotch tape or electrical tape, the latter can be seen in figure 3.1 below. This figure shows both the unmasked and masked ITO-slide, where one edge of the slide is left unmasked. This tape had a thickness of about 0.15 mm.

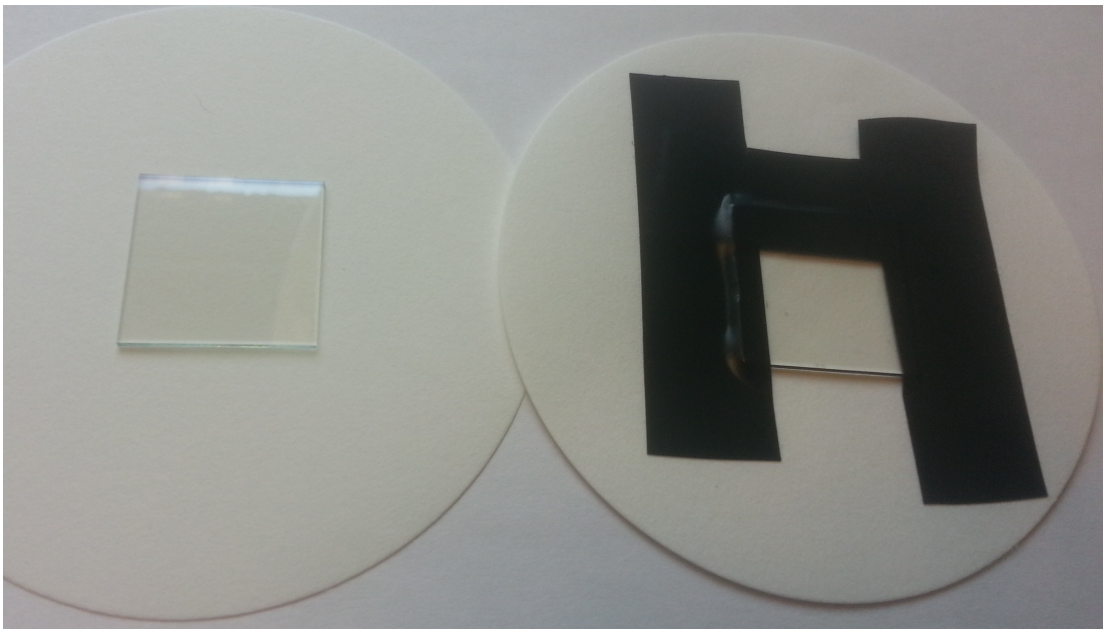

Figure 3.1: Unmasked (left) and masked (right) ITO-slide. Tape thickness of 0.15 mm.

3.1.2 Applying electrode material to ITO glass slides

1. Measure out the right amount of the primary, nanostructured electrode material, and the polymer binder used. Measurements are done by weight percent

(wt%) of total weight, from dry powders, with a precise scale.

2. Mix the measured components together.

   The following steps should be performed under a fume hood, as an organic solvent is used:

3. Dissolve the polymer in the mixture with tetrahydrofuran.

4. The solution needs to be sonicated for about 10 minutes to break up agglomerations of the nanoparticles. This should ideally be done in a closable glass container. This is to limit the evaporation of the volatile solvent, and also in preparation for the next step. [18]

5. Before applying the solution to the slides, the solution needs to be stirred vigorously to ensure homogeneous distribution of the nanoparticles. Also, the amount of solvent should be regulated to give the right consistency of the solution. The consistency should be that of a light paste, that can be spread easily. This is most easily achieved by using a bit more solvent in step 3, and then letting it evaporate while sonicating and stirring till the right consistency is reached.

6. Using a stirring rod, apply a small amount of the paste on one of the edges of the unmasked part of the glass slide. Then, using a razor blade, drag the paste across the remainder of the unmasked parts of the slide. The edge farthest away from the unmasked opening of the slide is usually chosen, to allow excess paste to be swept away easily. The elevated, masked parts serves as limiters and height guides for the applied layer. However, be aware that if the height of the masking tape is too low, or the paste too thick, the applied paste will not spread evenly, but rather be dragged of completely.

7. After the paste has been applied, let the slide remain under the fume hood for a few hours, to allow the solvent to completely evaporate.

8. When the applied layer has dried, the masking can be removed.

3.1.3 Fabrication of supercapacitor carbon electrode

For the construction of the carbon electrodes two different types of solutions were made.

The first solution contained nanostructured carbon spheres and binding polymer. The carbon spheres were at sub 50 nm in size. The binding polymer was

Poly(vinylidene fluoride) (PVDF). They were mixed at a ratio of about 60 wt% carbon nanospheres to 40 wt% of PVDF, in powdered form.

The second solution contained the same as the first, with the addition of a small amount multiwalled carbon nanotubes (MWNTs). The MWNTs were primarily added to increase conductivity. The amount added should however be limited, as they have great tendency to agglomerate into large grains. These grains are quite difficult to break up, even with extensive sonication. The MWNTs used had an outer diamater of 6-9 nm, and a length of 5 μm. The ratio of substances in this mixture was 5 wt% MWNTs, 55 wt% carbon nanosphere, and 40 wt% PVDF, in powdered form.

3.1.4 Fabrication of photovoltaic silicone electrode

The photovoltaic electrode made of silicon was made in a similar way to how the first carbon-electrode was made. It only contained the primary electrode material, nanostructured silicon spheres, and PVDF. The nanostructured silicon spheres used were at sub 100 nm in size. The solution was mixed at a ratio of 70 wt% silicon nanospheres to 30 wt% PVDF.

3.1.5 Fabrication of dye-sensitized solar cell

The making of a dye-sensitized solar cell is a bit different from the making of the previously mentioned electrodes. The procedures given below is based on the procedure presented by Takechi et al., with a different electrolyte used. [45]

1. Measure up 3.5g of nanostructured titanium(IV) oxide in powder form.
2. Add 15 ml of ethanol to suspend the powder.
3. Sonicate for at least 30 min to break up agglomerations of the nanoparticles.
4. Add titanium(IV) tetraisopropoxide to the solution, and mix until the solution is homogeneous.
5. The solution should have a paste-like consistency. It is applied to an ITO glass slide in similar manner as described in step 6 of section 3.1.2 above.
6. Let the applied layer dry some, then remove the masking on the slide.

7. Heat the glass slide for 10 min at 150°C to temper the surface and evaporate the remainder of the solvent. Remove from the heat.

8. Make the dye mixture. Mix eosin Y in ethanol to a concentration of 1 mM, to a total volume of about 50 mL.

9. Apply dye to the glass slide. The length of exposure determines the degree of filling of the titaniumoxide complex. An adequate degree of filling is achieved after 10 minutes, but to ensure a filling as complete as possible, keep the slide submerged in the dye solution for 24 hours. The dye solution can be heated slightly to promote filling. This will however accelerate the evaporation of the ethanol in the dye solution if not kept on a closed/covered container.

10. After the dyeing is complete, the glass slide is first rinsed with distilled/deionized water, and then with ethanol. The uncoated parts of the slide is cleaned clear of dye with cotton swabs and ethanol.

3.1.6 The electrolyte solutions

Regarding the electrolytes used, two different types were made. The first one was an aqueous iodine/iodide electrolyte, I^-/I_3^-, which is the most standard electrolyte used with DSSCs. The second one was an aqueous solution of lithium hexafluorophosphate, $LiPF_6$. This as an electrolyte typically used in commercial batteries, but also the one used by Lo et al. in their 2010 photocapacitor paper. [33]

The procedure for making the iodine/iodide electrolyte used was presented by Johnson et al. [26]. It is made by mixing 0.127g of 0.05M iodine (I_2) in 10 mL of ethylene glycol, and then adding 0.83 g of 0.5 M potassium iodide (KI). The potassium iodide was mixed from powder form with water, to a 0.5 M solution.

The lithium hexafluorophosphate solution was made by mixing 0.76 g of $LiPF_6$ powder with 10 mL of deionized water. This gives an electrolyte solution of 0.5M $LiPF_6$.

3.1.7 Final assembly

When both the photovoltaic and supercapacitor electrodes are made, and the electrolyte solutions mixed, the final photocapacitor device can be assembled.

1. Place both the two electrodes side up on the assembly table, and apply a small amount of the chosen electrolyte on each with a syringe. This is to pre-wet the electrode materials, to ensure a more complete wetting.

2. When this is done, place a separator on the carbon electrode. A CultureWell^{TM} Multiwell Chambered Coverslip, cut to size, is used. The opening in the separator should only be in the area where the glass slide is coated in the electrode material. The remainder of the separator should be large enough to cover the uncoated areas, to prevent shortening the cell. One edge is excepted from this, as it is the edge where clamps for external circuiting are to be connected.

3. Fill the opening in the separator with more electrolyte until it is completely full.

4. Lift the photovoltaic electrode up, and flip it around as it is placed on top off the separator. Make sure that the uncoated parts are not placed over the opening in the separator, same as was done for the supercapacitor electrode. Also, leave one edge uncovered by the separator, on the opposite side of the uncovered edge on the supercapacitor electrode. In a side-view, the complete cell could resemble the shape of a Z, where the two edges are where the clamp are attached. Make sure that the opening in the separator, between the two electrodes, are completely filled with electrolyte, with no air bubbles.

5. Carefully slide the combined cell to the edge of the table, until one edge of the longest side sticks out. Add a binder clip to the exposed edge, while making sure to apply downward pressure to holt the parts together. Turn the cell around, and attach a second binder clip on the opposite side. Make sure that the metal parts of the binder clips do not touch any conductive part of the cell.

6. Inspect the cell to make sure the chamber inside is still properly filled with electrolyte. If this is not the case, move the binder clips slightly downwards along the edge until a small gap appears. Inject more electrolyte through this gap with a syringe, and move the binder clips back to the original position.

7. Wipe away the excess electrolyte that got squeezed out when the electrodes were combined.

3.2 Characterization

After the photocapacitors were fabricated and assembled, both they and a photocapacitor system of commercial components needed to be characterized. How this characterization was performed is explained in the following sections.

3.2.1 Characterization set-up

To characterize the commercial and fabricated supercapacitor, an optic rig system was constructed, with several key features.

The first of these features was the mounting and focusing of a light source. The light was produced from a 150 W Halogen light bulb in Thorlabs' OSL1-EC. A data sheet for this light source can be found at [8]. From the light source the light was sent through a fibre optic cable, was attached to the rig, and the light sent through a lens. This lens served to focus the light, and illuminate the sample uniformly. The light from the fibre optic cable needed to be focused enough to give a power upwards of 100 mW/cm^2, the standard testing condition for photovoltaic cells. To test at conditions of lower power, the light intensity was adjusted at the light source, keeping the lens fixed.

On the other end of the light source and focusing lens, is a mounting stage for the samples to be tested. The first part of this stage is a mounting block, where the samples are fixed vertically by clips. This mounting block is attached to a metal rail, making it easy to both attach and remove samples, and to fix them in the right position.

Between the lens and the mounting stage the light path is tapered, ending in an aperture. Aperture is in the form of a 15.5 mm long tube with a diameter of 11.6 mm. When testing, the sample is positioned flush with the aperture, which gives a controlled area of light exposure on the photovoltaic cell. The aperture tube can also be easily removed, and a 'Thorlabs PM100D - Digital Handheld Optical Power and Energy Meter Console', with a 'Thorlabs S302C - Thermal power sensor' probe, can be attached. With this instrument the power of the incident light can be measured, and calibrated to the right intensity. The light path of these two possible set-ups, in terms of dimensions, are about the same. This makes the measured power a good approximation of the power of the incident light hitting the sample to be tested.

Lastly, the whole rig is enclosed in a black box. This is to prevent unwanted illumination of the samples from the surroundings. A schematic drawing of the setup is shown below, as well as pictures.

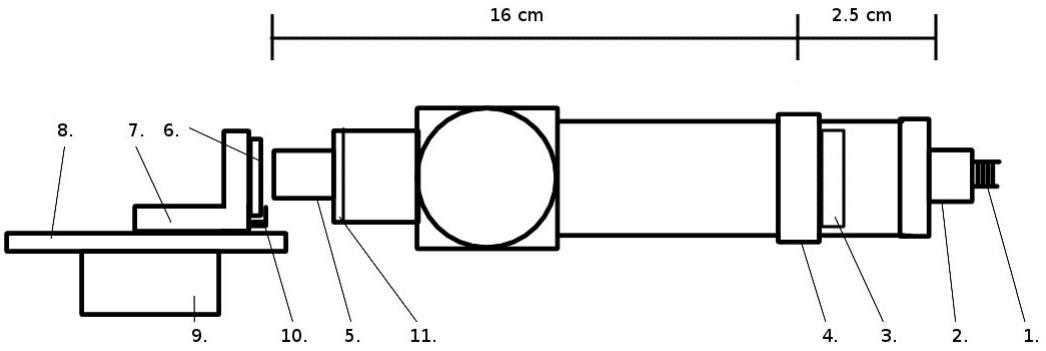

Figure 3.2: Schematic drawing of the light rig system. 1. Fibre optic cable 2. Fibre optic cable holder 3. Optic lens, Thorlabs AC254-030-A-ML 4. Lens holder 5. Aperture tube 6. Sample 7. Sample mounting stage 8. Mounting stage rail 9. Mounting rail support 10. Sample clamps 11. Tube reducer. The tube reducer can be removed, and the optical power probe attached.

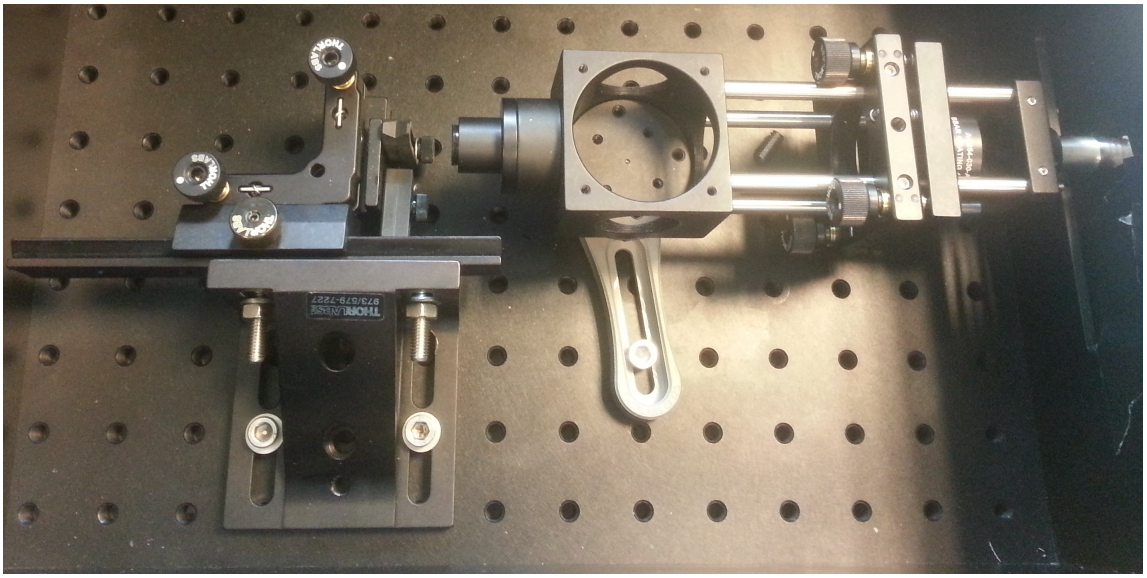

Figure 3.3: Photo of the light rig system.

3.2.2 Characterization procedures

For the major part of the characterization, the computer program EC-lab was used, in junction with a potentiostat. In this program, two measuring techniques were primarily utilized, the 'Cyclic Voltammetry - CV' and the 'I-V characterization - IVC' techniques. Another computer program was also used, name Logger Pro, where differential voltage was measured.

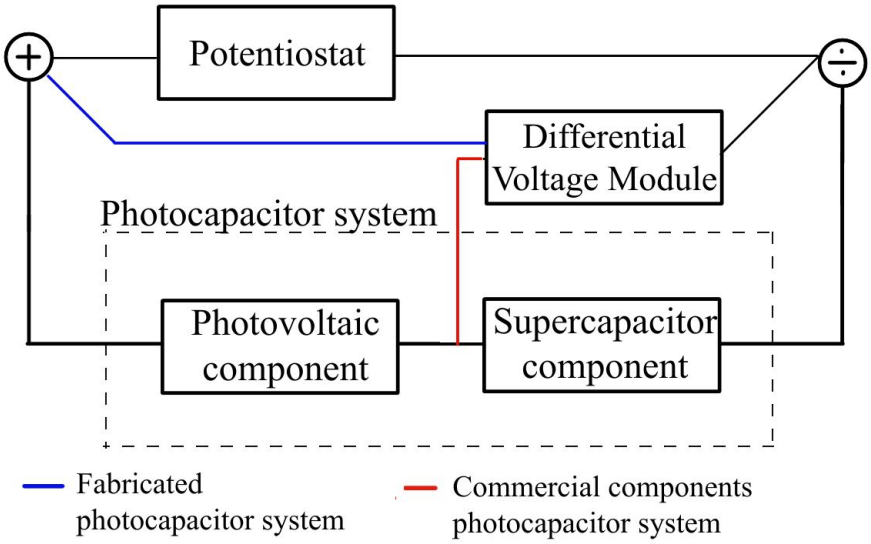

Figure 3.4: Diagram showing the circuit of the characterization setup. The differential voltage module is connected differently for between the fabricated and the commercial component systems.

In figure 3.4 above, a diagram of the characterization circuit is shown. In this diagram we see how the potentiostat is connected to the photocapacitor system, which consists of the photovoltaic and supercapacitor components. The diagram also shows that the differential voltage module is connected differently between the fabricated photocapacitors, and the commercial components systems. In the former, the module is connected in the same way as the potentiostat. In the latter, the module is connected over the supercapacitor component.

3.2.2.1 Cyclic Voltammetry - CV

The cyclic voltammetry technique is especially useful for determining the capacitance of a capacitor/super capacitor, as was mentioned in section 2.1.5. It works by cycling, or 'sweeping', the voltage between two set values, forming a triangular wave, while measuring the current. This triangular wave can be seen in figure 3.5 below, which shows a screenshot from the EC-Lab program.

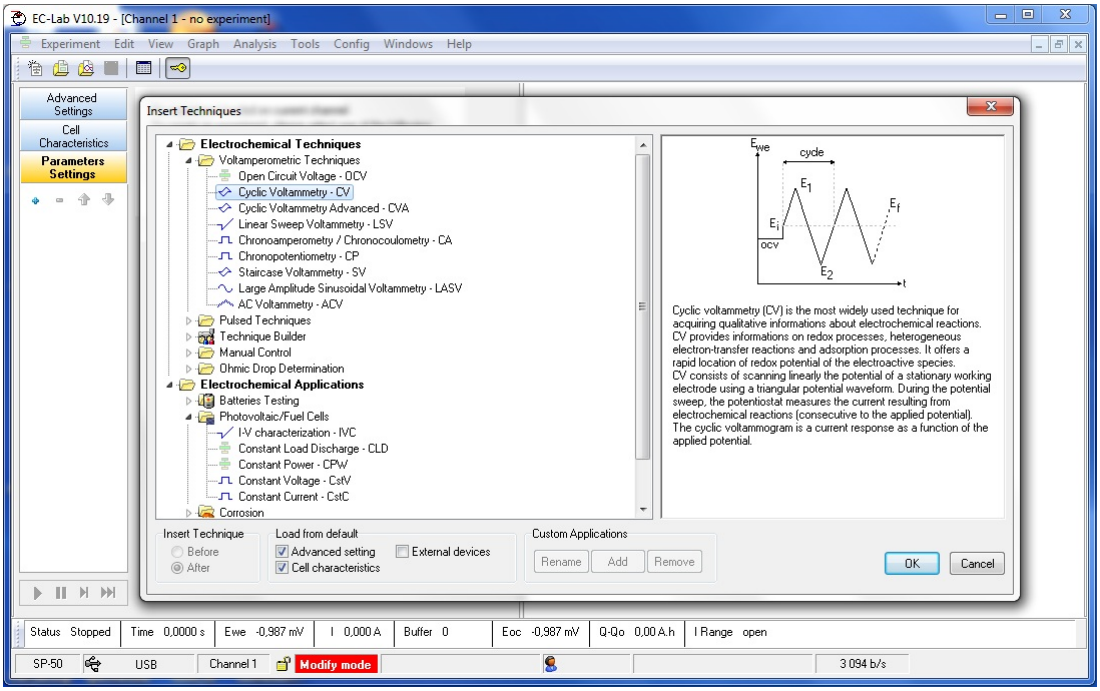

Figure 3.5: Screenshot from the EC-Lab program, showing the CV technique option.

When performing this technique there are a few important set-parameters, three in particular. The first is the range between the two set values for the potential sweeping. These values are typically set symmetrical with the zero potential axis, and should exceed the range of the stability window of the supercapacitor. The second important set-parameter is the speed at which the potential is changed, i.e. the scan rate. The scan rate is directly related to how large the measured current gets while testing. Differing scan rates also give information to how well the supercapacitor performs at various charge/discharge frequencies. The third parameter is the number of scanning cycles. This is the number of complete sweeping periods performed. By testing the supercapacitor through several cycles, information about the stability of the device can be acquired, and the lifetime can be derived.

When testing the photocapacitors and commercial supercapacitor, a series of tests were performed at varying scan rates. These scan rates were set at 5, 10, 20, 30, 50, and 100 mV/s. The range of the potential sweeps were set at $\pm$ 0.5

V. The range was set at this potential because the open-circuit voltage of a single photovoltaic cell rarely goes much higher.

3.2.2.2 I-V characterization - IVC

While the cyclic voltammetry technique can be used to characterize supercapacitors, the I-V characterization technique is meant for characterizing photovoltaic cells. It works through a similar scan rate, changing the potential at a certain rate, while measuring the current. Unlike the CV, the potential sweep is only done in one direction, instead of cycling between two set values. This is seen in figure 3.6 below. The sweeping starts at zero voltage, i.e. the short-circuit current of a photovoltaic cell. The voltage is then increased, sweeping in the positive direction along the V-axis. It goes on until the measured current starts increasing and intersects the V-axis, i.e. the open-circuit voltage. The current measurement between these two points are then used to calculate the maximum power, fill factor and efficiency.

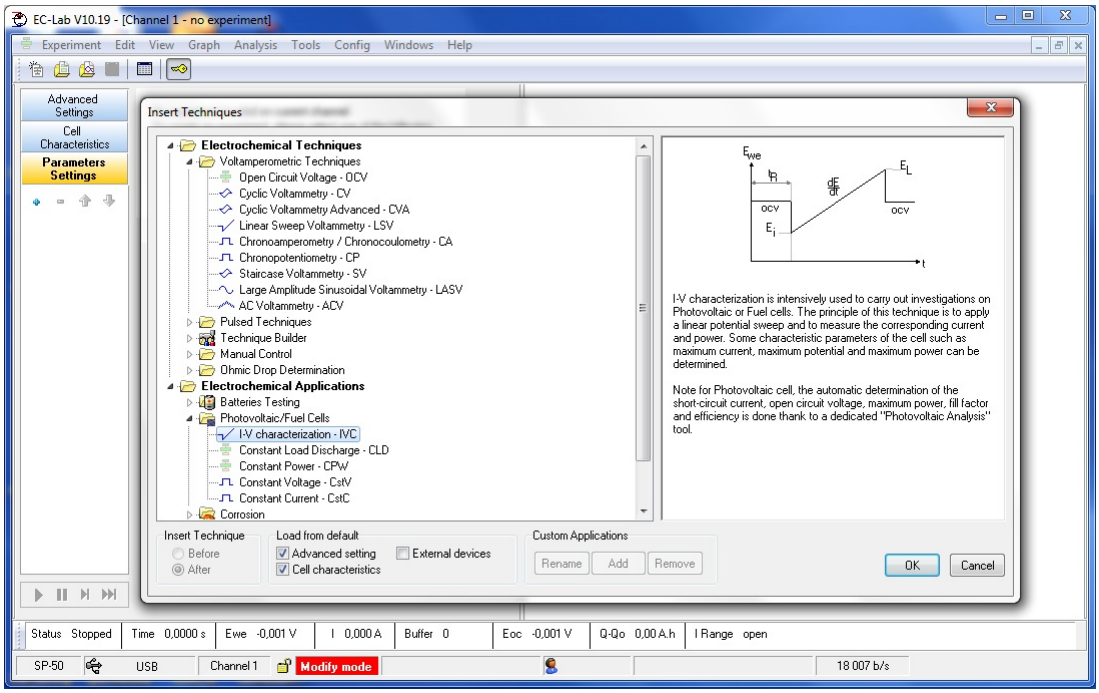

Figure 3.6: Screenshot from the EC-Lab program, showing the IVC technique option.

Two of the most important parameters when using this technique is the scan rate, and the power of the incident light illumination the photovoltaic cell. While the scan rate can be controlled by the program, the power of the incident light can not. This is rather controlled by the external light source. Consequently, when testing for performance at varying light conditions, the power of the light needs to be calibrated by the external optical power probe for each condition.

When testing the photocapacitors and commercial solar cells, both the scan rates and the power of the incident light was varied. The scan rates were the same ones used during the CV technique. The power of the incident light was primarily set at 100 mW/cm^2, but with some measurements at lower intensities as well.

3.2.2.3 Differential Voltage Measurement

With the Logger Pro program, the differential voltage between two terminals could be recorded as a function of time. This was used to measure the charging and discharging of the photocapacitor systems. The voltage measuring was achieved by using a Differential Voltage Module, that was connected to a 'LabQuest mini' usb-hub from Vernier. The module had two probes that could be connected to the photocapacitor circuits. Before connection, the voltage between the probes has to be zeroed in the program, as there typically was a small initial bias. In the program the measurement time, and measuring frequency could be set. In figure 3.7 below a sceenshot from the program presented, showing the zeroing of the bias.

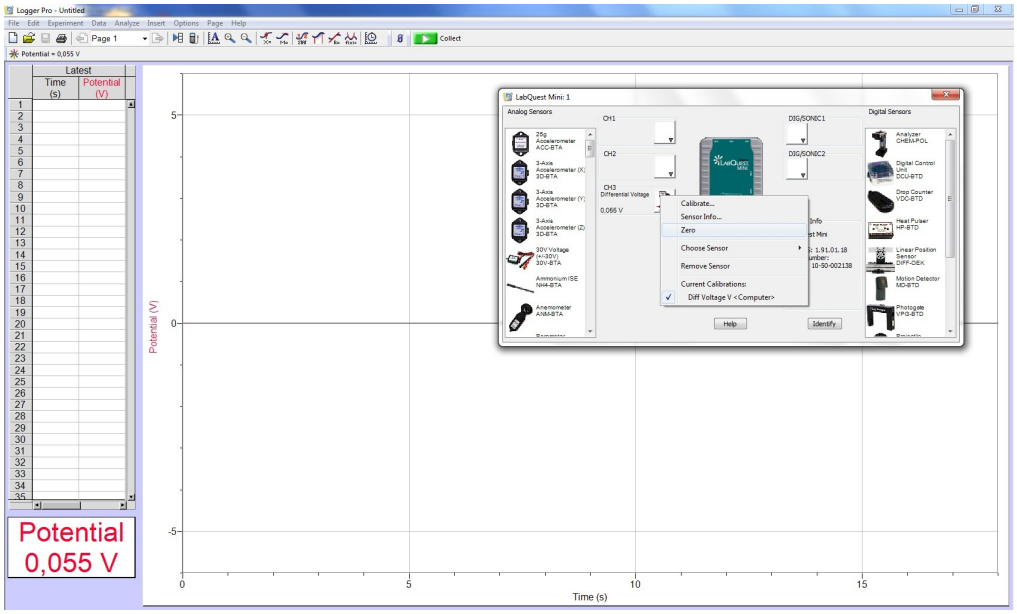

Figure 3.7: Screenshot from the Logger Pro program, showing the zeroing of the voltage bias.

Chapter 4

Results

In this chapter, the main results from the characterization and testing are presented. The results are divided into distinct sections, as the characterization was done in several parts with different components and parameters in focus. In each of these sections the data from both the fabricated units and the commercial components are presented. The data is primarily presented in the form of measurement graphs, with tables showing the calculated parameters. The results are commented on briefly, reserving the major part of the discussion for the next chapter.

The first section focuses on supercapacitors, and the calculated capacitance. The second section focuses on photovoltaic cells, and their V_{oc}, I_{sc}, fill factor and efficiency. The third section is about the complete photocapacitor system, either in the form of a single, fabricated device, or a setup of commercial components.

4.1 Supercapacitor measurements

By characterizing the supercapacitors on their own, a better insight in their individual performances were achieved. This included their specific capacitance, but also the degree of non-ideal behaviour like ohmic resistance and redox reactions. These performances would indicate an upper bound on the expected performed on a complete photocapacitor system.

4.1.1 Commercial supercapacitor

In the setup of commercial components, a 1 farad supercapacitor was used. The supercapacitor was tested using cyclic voltammetry with a sweep range of [-0.5V,0.5V], 5 cycles, and scan rates of 5, 10, 20, 30, 50, and 100 mV/s, respectively. In figure 4.1 below the graph of the CV measurement at 20 mV/s is shown.

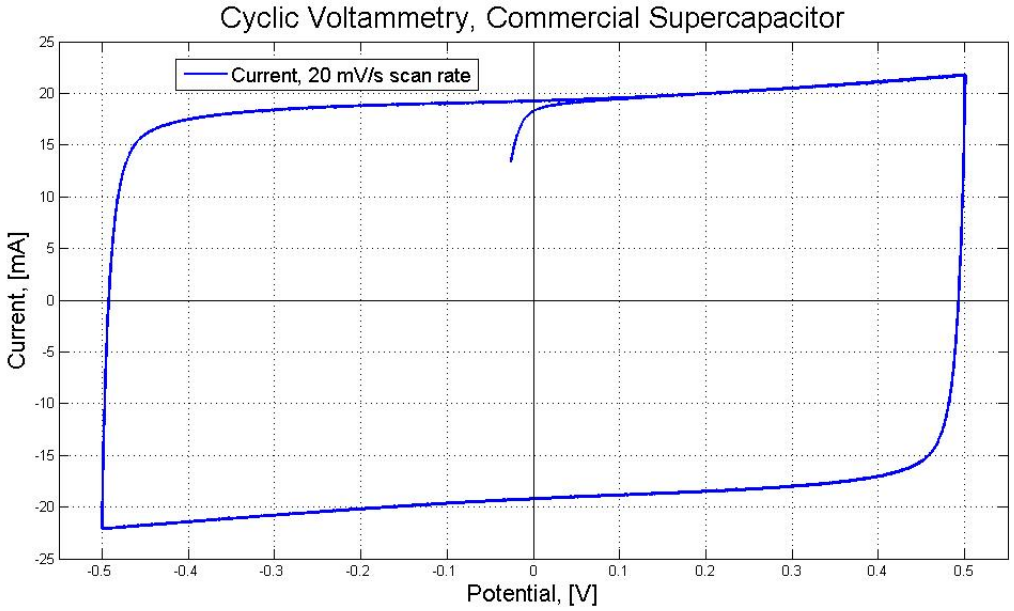

Figure 4.1: CV-graph of a commercial 1 farad supercapacitor, 20 mV/s scan rate.

The most noticeable feature from the figure is the squareness of the curve. With only a very slight slant, and some rounding of the curve where the sweeping voltage changes direction, the graph is a close approximation to an ideal SC.

With the method described in section 2.1.5, the effective capacitance of the supercapacitor was calculated. This was done by first finding the area of the hysteresis for the power, from the CV-curve. The areas was found using the 'trapz' function in MATLab. Knowing the scan rate, this area could then be related to the total energy stored in the supercapacitor by using equation (2.20). With the total stored energy, and equation (2.21), the effective capacitance could be estimated. The effective capacitance was calculated for each cycle. These calculations were

then averaged, and the standard deviation calculated, using the 'mean' and 'std' functions in MATLab, respectively. In table 4.1 below the calculated effective capacitance at various scan rates are presented.

Table 4.1: Effective capacitance of commercial supercapacitor

Commercial Supercapacitor	**Scan Rates, [mV/s]**					
	5	**10**	**20**	**30**	**50**	**100**
Effective Capacitance, [F]	1.018 ± 0.002	0.9738 ± 0.0004	0.9238 ± 0.0002	0.8908 ± 0.0002	0.8412 ± 0.0003	0.750 ± 0.001

In the table, it can be seen that the calculated capacitance is the same as the listed value of 1 F, within 10% tolerance, for the lower scan rates. When the scan rates increase, this value decrease some.

4.1.2 Fabricated supercapacitor electrodes

There were made two different types of supercapacitor electrodes. The first type consisted of just nano-textured carbon spheres, supported by Poly(vinylidene fluoride) on an ITO glass slide. The second type also consisted of nano-textured carbon spheres, but with a small amount of multi-walled nanotubes (MWNTs) added. These were also supported by Poly(vinylidene fluoride) on an ITO glass slide. There were also mixed two different types of electrolytes, I^-/I_3^-- and $LiPF_6$, both in distilled water. In figures 4.2 and 4.3 below, camera pictures and SEM images of the two types of supercapacitor electrodes are shown, respectively.

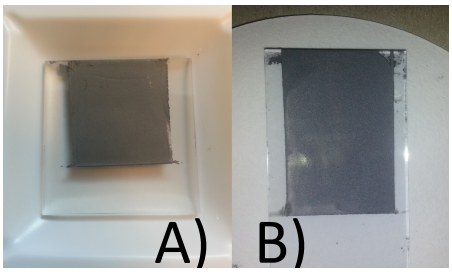

Figure 4.2: Pictures of the supercapacitor electrodes. A) Nano-carbon electrode B) Nano-carbon w/ MWNTs electrode

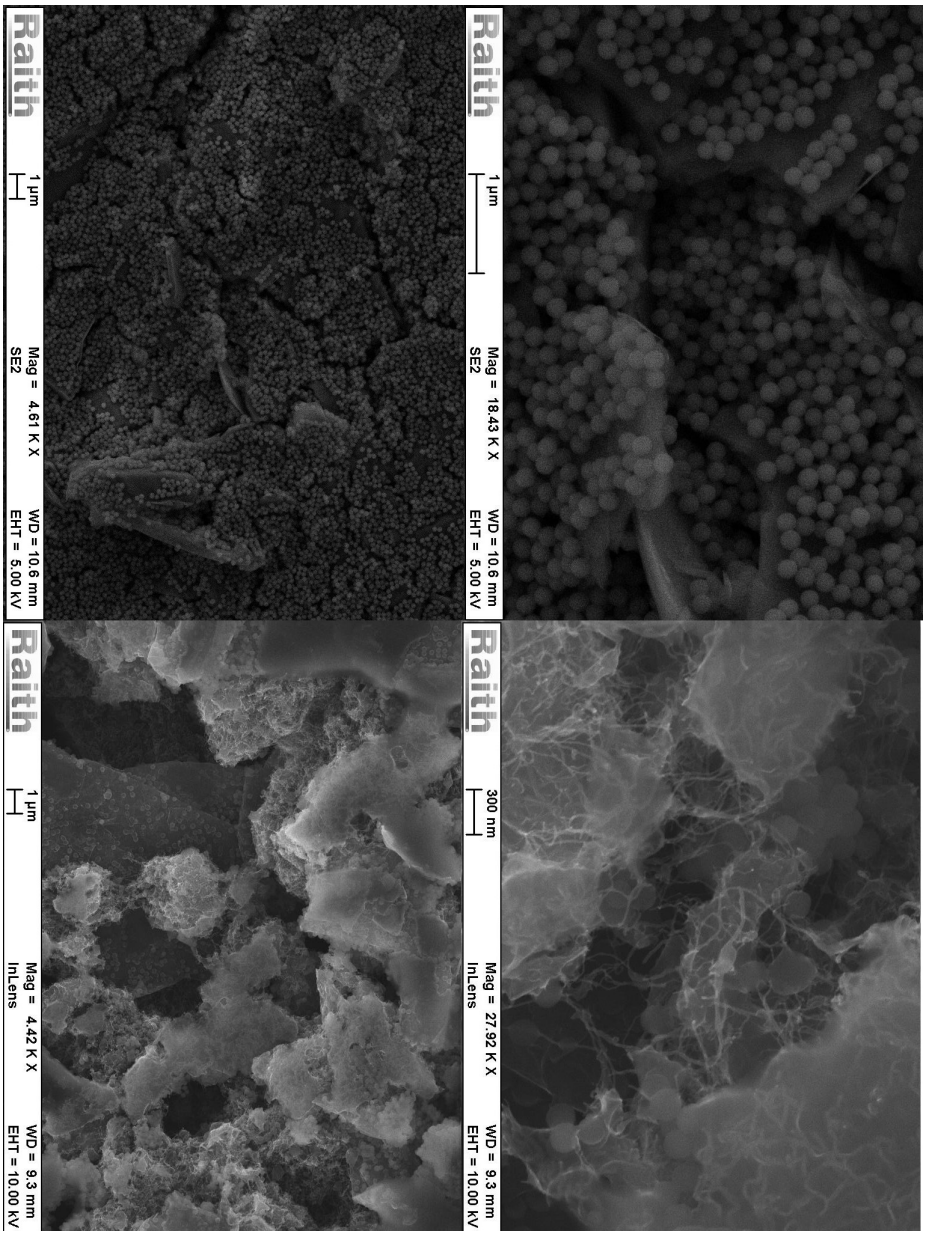

Figure 4.3: SEM images of the two supercapacitor electrodes. Two top images: pure nano-carbon. Two bottom images: nano-carbon w/ MWNTs.

The supercapacitor electrodes and the electrolytes where combined to form complete supercapacitor devices. In each of these devices both of the two electrodes had the exact same composition of carbon coating. From the two types of supercapacitor electrodes, and the two types of electrolytes, a total of four unique setups could be made. A diagram of the fabricated supercapacitors is shown below in figure 4.4

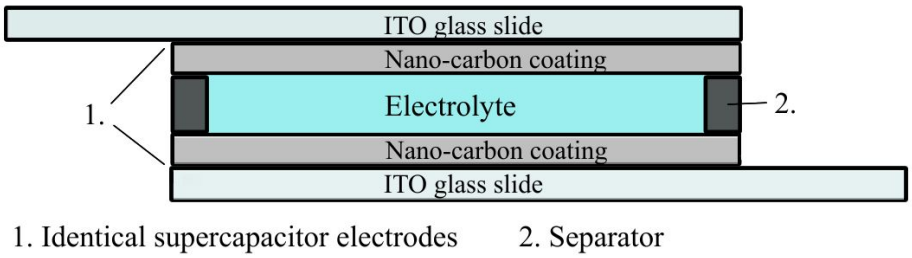

Figure 4.4: Diagram of the fabricated supercapacitors. Both of the electrodes had the same type of nano-carbon coating.

These supercapacitors where then all tested using cyclic voltammetry with the same testing parameters as the commercial supercapacitor. Below in figures 4.5-4.8 the CV-graphs from the measurements at 20 mV/s for all four supercapacitors types are presented.

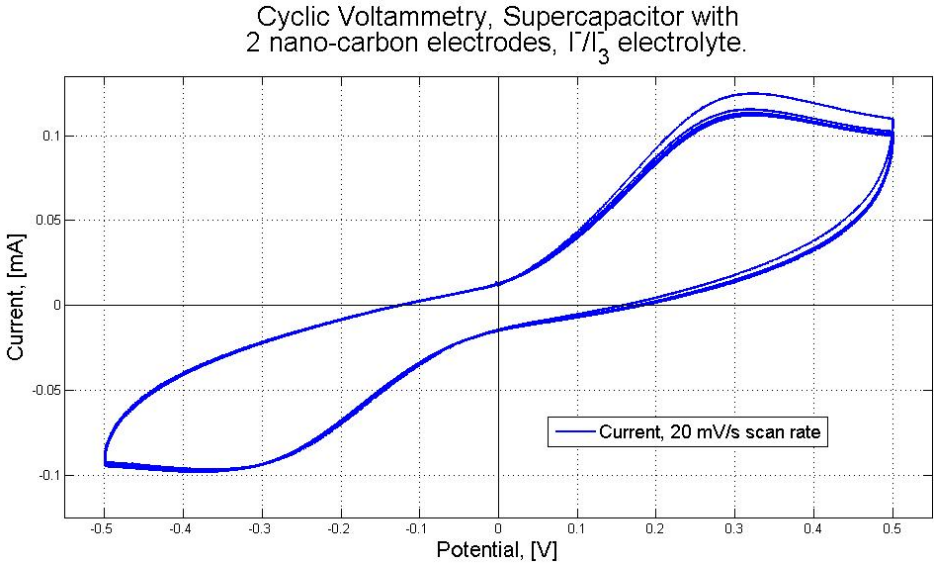

Figure 4.5: CV-graph of nano-carbon v nano-carbon supercapacitor, I^-/I_3^--electrolyte. 20 mV/s scan rate.

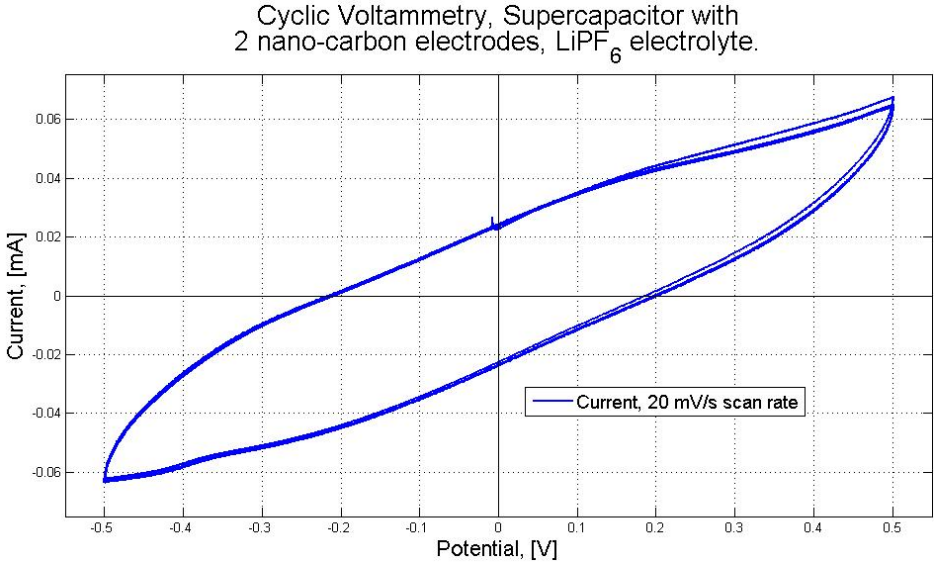

Figure 4.6: CV-graph of nano-carbon v nano-carbon supercapacitor, $LiPF_6$-electrolyte. 20 mV/s scan rate.

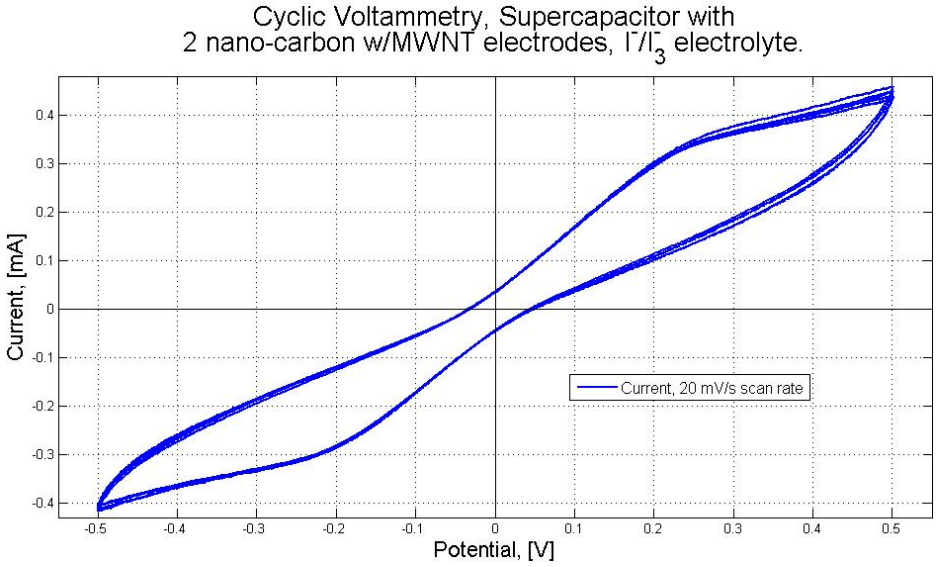

Figure 4.7: CV-graph of nano-carbon w/MWNTs v nano-carbon w/MWNTs supercapacitor, I^-/I_3^--electrolyte. 20 mV/s scan rate.

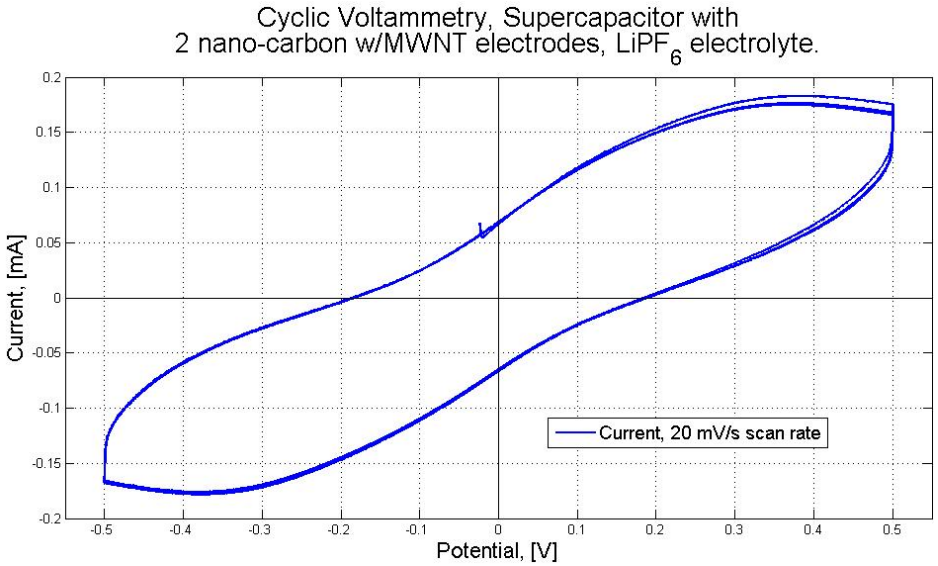

Figure 4.8: CV-graph of nano-carbon w/MWNTs v nano-carbon w/MWNTs supercapacitor, $LiPF_6$-electrolyte. 20 mV/s scan rate.

Comparing these figures to figure 4.1 in the previous section, a significant difference can be seen. The most noticeable is the presence of non-ideal behaviour. The first of these are that all of the figures are slanted, clearly indicating the presence of ohmic resistances. The second non-ideal behaviour are the small peaks in the curves for the SCs that use the I^-/I_3^--electrolyte. These occur at about ± 0.3 V. These peaks are most prominent in the SCs with electrodes of just nano-carbon. The SCs that use $LiPF_6$ as electrolyte have curves that are more even, with only slight indications of peaks at the ends of the scan range. These may better be described as flattening of the otherwise slanted curve, and could be a function of the ohmic resistance, and not necessarily from a redox reaction. A third observation to make is the peak-to-peak current of the different cells. Generally, the SCs that use the nano-carbon w/ MWNTs electrodes have noticeable higher currents than the ones that only have nano-carbon electrodes.

The effective capacitance of all the fabricated supercapacitors were calculated using the same method that was used for the commercial supercapacitor. The calculated values are listed below in tables 4.2-4.5.

Table 4.2: Effective capacitance of fabricated supercapacitor. Nano-carbon electrodes, I^-/I_3^--electrolyte.

Nano-carbon, I^-/I_3^-	**Scan Rates, [mV/s]**					
	5	**10**	**20**	**30**	**50**	**100**
Effective Capacitance, [mF]	2.9 ± 0.2	2.23 ± 0.04	1.56 ± 0.03	1.24 ± 0.02	0.95 ± 0.01	0.656 ± 0.007

Table 4.3: Effective capacitance of fabricated supercapacitor. Nano-carbon electrodes, $LiPF_6$-electrolyte.

Nano-carbon, $LiPF_6$	**Scan Rates,[mV/s]**					
	5	**10**	**20**	**30**	**50**	**100**
Effective Capacitance, [mF]	1.96 ± 0.09	1.28 ± 0.02	0.7969 ± 0.0006	0.5995 ± 0.0003	0.4206 ± 0.0004	0.2656 ± 0.0003

Table 4.4: Effective capacitance of fabricated supercapacitor. Nano-carbon w/MWNTs electrodes, I^-/I_3^--electrolyte.

Nano-carbon, w/MWNTs, I^-/I_3^-	**Scan Rates, [mV/s]**					
	5	**10**	**20**	**30**	**50**	**100**
Effective Capacitance, [mF]	5.1 ± 0.3	4.14 ± 0.08	3.10 ± 0.07	2.45 ± 0.03	1.714 ±0.009	0.878 ± 0.008

Table 4.5: Effective capacitance of fabricated supercapacitor. Nano-carbon w/MWNTs electrodes, $LiPF_6$-electrolyte.

Nano-carbon, w/MWNTs, $LiPF_6$	**Scan Rates, [mV/s]**					
	5	**10**	**20**	**30**	**50**	**100**
Effective Capacitance, [mF]	4.0 ± 0.6	3.97 ± 0.02	2.946 ± 0.009	2.437 ± 0.006	1.958 ± 0.005	1.526 ± 0.003

A few of the observations seen in the graphs are reflected in the values in the tables. One of these are the effect of MWNTs in the electrodes. For the lowest scan rates, the SC with MWNTs have a capacitance of about 2 mF higher than their pure nano-carbon counterpart. Another of these observations are that the SCs with I^-/I_3^- have a capacitance that is higher than the ones with $LiPF_6$, for low scan rates. This could come from the increased hysteresis in the graphs caused by potential redox reactions. Consequently, it can also be seen the the capacitance from the I^-/I_3^- SCs drop more rapidly than the $LiPF_6$ SCs with increasing scan rates.

To check the effect of the nano-structuring of the supercapacitor electrodes, a quick estimation can be done. In this estimation, equation (2.5) from chapter 2 is used, rearranged with regard to surface area;

$$A = \frac{C \cdot d}{\epsilon} \tag{4.1}$$

In this ϵ is the relative permittivity of water, and the distance d can be set as the Debye length, given by equation (2.11). With an ion concentration of 0.05 M,

and temperature of 300 K, the Debye length is found to be;

$$d = \sqrt{\frac{80 \cdot 8.854 \cdot 10^{-12} Fm^{-1} \cdot 1.380 \cdot 10^{-23} JK^{-1} \cdot 300K}{(1.602 \cdot 10^{-19})^2 \cdot 3.0 \cdot 10^{25} m^{-3}}} = 1.95 \cdot 10^{-9} m \quad (4.2)$$

Here the ion concentration was converted to number density, $n = N_A \cdot c$, where N_A is Avogadros constant, and c the ion consentration in mol/m^3. [16,30] Choosing the fabricated supercapacitor with the highest calculated effective capacitance, nano-carbon w/MWNTs electrodes and I^-/I_3^--electrolyte, the effective surface area is calculated;

$$A = \frac{2 \cdot 5 \cdot 10^{-3} F \cdot 1.95 \cdot 10^{-9} m}{80 \cdot 8.854 \cdot 10^{-12} Fm^{-1}} = 2.8 \cdot 10^{-2} m^2 \quad (4.3)$$

In the calculation the effective capacitance is doubled. This is because of the relation between the total capacitance in a symmetric supercapacitor, and the capacitance at each of the electrodes, given by equation (2.13). The chambered coverslips that were used as separators had an internal area of 1.77 cm^2. The ratio between the effective surface area of the electrode and this is as follows;

$$Ratio = \frac{A_{electrode}}{A_{coverslip}} = \frac{2.8 \cdot 10^{-2} m^2}{1.77 \cdot 10^{-4} m^2} = 155.7 \quad (4.4)$$

From this we can see that the nano-texturing of the electron surface has increased the effective surface area about 156 times.

4.2 Photovoltaic measurements

The characterization of the photovoltaic cells on their own was done with the same motivation as the characterization of the supercapacitors; To find their specific individual performance, that would similarly give an indication on the upper bound of performance.

In the testing of the photovoltaic cells, the approach for the commercial solar cell was straight forward. For the fabricated photovoltaic cells, however, this was a bit more tricky.

4.2.1 Commercial solar cell

The commercial solar cell used was a poly-crystalline silicon cell, measuring 2 cm x 2.5 cm. The characterization was to a large degree straight forward, with only a minor issue with the position of the illumination on the cell. Though a small cell, it still had two cells in series. This effected the V_{oc} some, but the I_{sc} in particular. With just slight variations in the position of the illumination, with the same illumination area and light intensity, the I_{sc} was observed to shift considerably. To account for this, the solar cell was fixed firmly on the sample stage, and all the measurements were taken in quick succession. Though perhaps not ideal measurements, this at least assured consistency for further calculations.

The solar cell was characterized at several different illumination intensities. Initially, the illumination intensities were set at 100, 80, 60, 40, and 20 mW/cm^2, but due to a calibration error discovered later on, they were recalculated to being 88, 70, 53, 35 and 18 mW/cm^2, respectively. For consistency these recalculated intensities were used for the reminder of the testing. The cell was also characterized at no illumination.

Below in figure 4.9 the I-V measurements for all the different illuminations intensities are shown, for the 20 mV/s scan rate. Also, in figure 4.10 the I-V measurement for no illumination is given, at 20 mV/s scan rate.

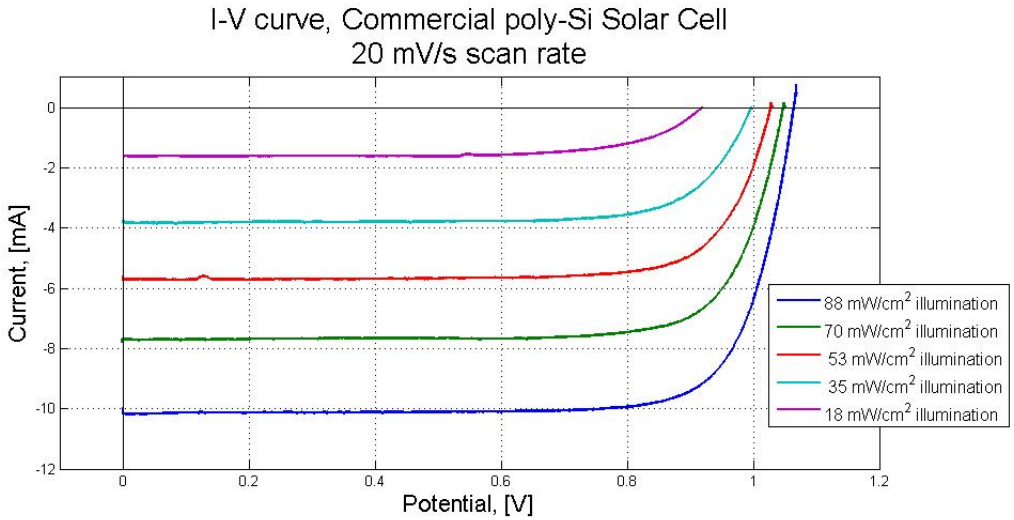

Figure 4.9: Commercial solar cell, 5 different illumination intensities, 20 mV/s scan rate

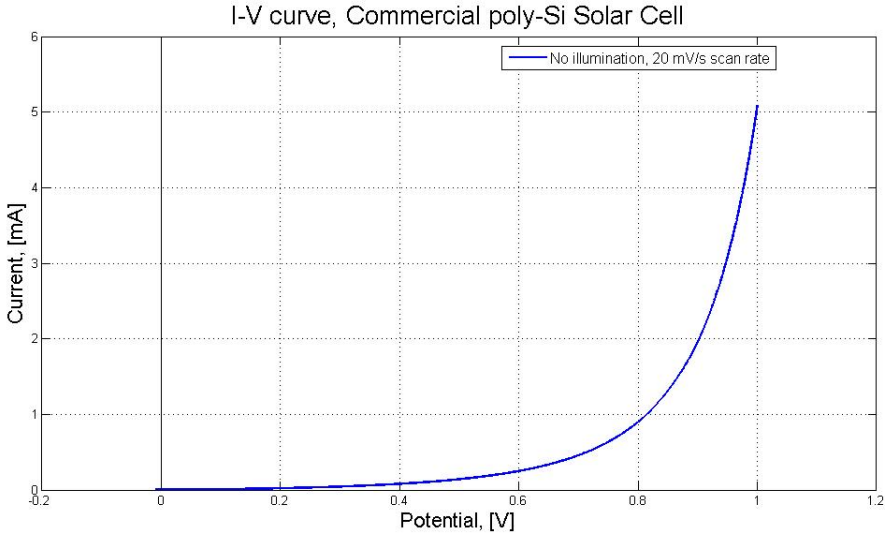

Figure 4.10: Commercial solar cell, no illumination, 20 mV/s scan rate

From the figure above it can be seen that the I-V curves from the commercial solar cell are close approximations to the curve of an ideal photovoltaic cell. The current remains stable throughout most of the scan range, with a favourable exponential rise when approaching the V_{oc}. It can also seen how both V_{oc} and I_{sc} decrease with decreasing illumination intensity.

The photovoltaic cell parameters for all the different scan rates and illumination intensities were calculated. These calculations were done using a self-written program in MATLab. In this program the voltage and current measurement where imported, and processed. The short-circuit current and open-circuit voltage was estimated by finding the data points closest to the I- and V-axis, respectively, and the values noted. The fill factor was found by first finding the max power point. This was found by taking the product of the current and voltage at each data point, and then finding the maximum value. The efficiency was calculated by dividing the power at the maximum power point with the power of the incident light. The power of the incident light was calculated from the illumination intensity per cm^2, times the aperture opening of 1.06 cm^2. In table 4.6 below the parameters for the 88 mW/cm^2 illumination measurement are shown.

Table 4.6: Photovoltaic cell parameters, Commercial Solar Cell, $88mW/cm^2$ illumination.

Photovoltaic cell parameters	**Scan Rates, mV/s**					
	5	**10**	**20**	**30**	**50**	**100**
Short-Circuit Current, [mA]	-10.22	-10.11	-10.17	-10.08	-10.25	-10.13
Open-Circuit Voltage, [V]	1.06	1.06	1.06	1.07	1.06	1.06
Fill Factor	0.79	0.79	0.78	0.80	0.79	0.80
Efficiency, [%]	9.66	9.51	9.52	9.60	9.66	9.66

Form the table the commercial solar cell can be seen to have a fill factor of about 0.80, and an efficiency of about 9.5-9.6%. These values reflect the more ideal IV-curves seen in the above figures. The fill factor also matches the listed parameters for poly-crystalline silicon in table 2.1, with the efficiency being somewhat lower. The lower efficiency is most likely a cause of the positioning of the illumination.

4.2.2 Fabricated photovoltaic electrodes

The challenges in characterizing the fabricated photovoltaic electrodes on their own lay in the need for a counter-electrode. These are a necessity in electrochemical photovoltaic cells, to reduce/oxidize the oxidized/reduced ions in the electrolyte back to their initial state, completing the circuit. For dye-sensitized solar cells, the proposed type of CE is often a conductive polymer or oxide, coated with a carbon species to catalyse the process. Since the supercapacitor electrodes already consisted of Indium-Tin Oxide slides coated with nano-porous carbon spheres, a different form of carbon was chosen. The choice fell on an ITO-slide with a layer of soot added, partly because of its simplicity in making. The soot was applied by simply holding the slide over an open flame from a lighter, until completely covered. A small area was left clear for cable connection. [45]

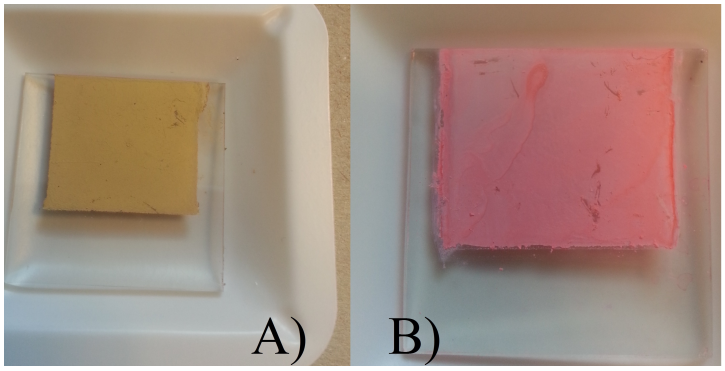

Figure 4.11: Pictures of the various photocapacitor electrodes. A) Nano-silicon electrode B)Dye-Sensitized Solar cell

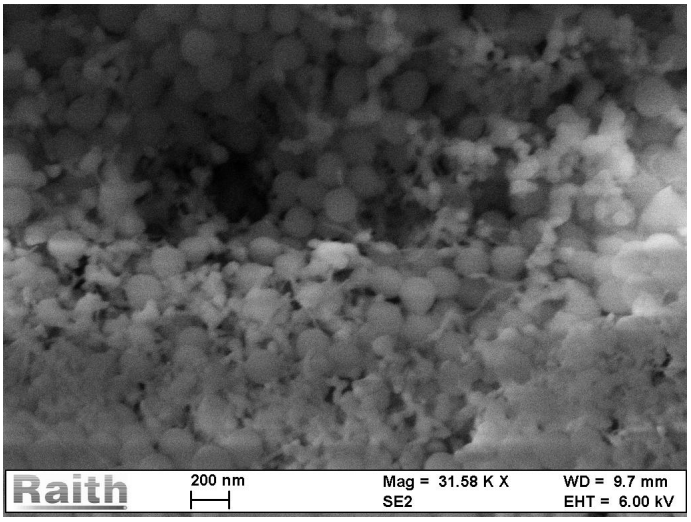

Figure 4.12: SEM image of the nano-silicon electrode.

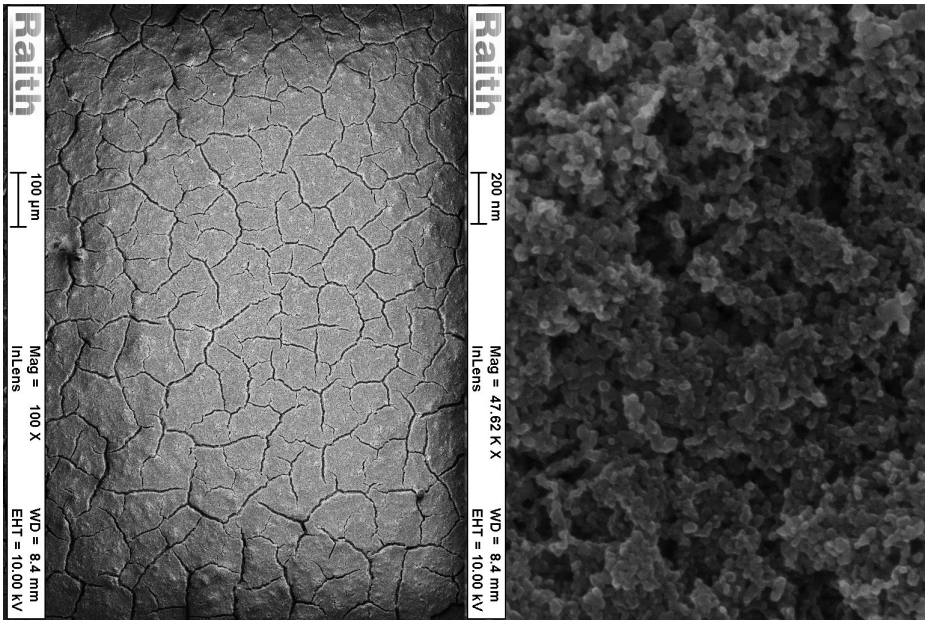

Figure 4.13: SEM images of the DSSC electrode.

In figures 4.11-4.13 above, camera pictures and SEM images of the two types of photovoltaic electrodes are shown, respectively. The initial intent was to test both DSSC electrodes and photovoltaic electrodes made of nano-silicon particles in the photocapacitor systems. However, when testing the nano-silicon cells for photovoltaic characteristics, no significant response was observed. This was the same with both nano-carbon CE and with a platinum on ITO CE, using $LiPF_6$ as an electrolyte. As a consequence, the further photovoltaic characterizations are only focused on the DSSCs.

The characterization of the DSSC was done with the IVC technique in EC-lab, with an I^-/I_3^- electrolyte, at $88mW/cm^2$ illumination. The cell was scanned at 5, 10, 20, 30, 50 and 100 mV/s scan rates. The graph of the 20 mV/s measurement is shown below in figure 4.14.

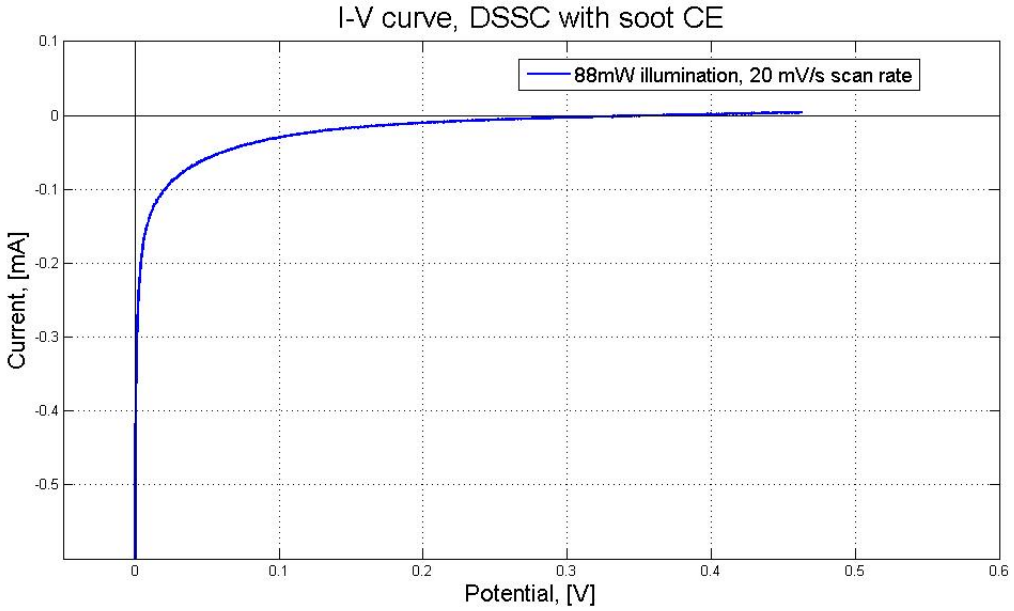

Figure 4.14: Dye-Sensitized Solar Cell w/ soot CE, $88mW/cm^2$ illumination, 20 mV/s scan rate

In this graph, a few observations can be made that needs to be commented on. The most noticeable feature, is the deviation from the ideal IV-curve of a photovoltaic cell. The current in the graph starts at a low value for the I_{sc}. When the voltage starts increasing and the curve moves into the fourth quadrant, the current increases extremely fast. After the rise the current then levels off somewhat, before rising slowly towards the V_{oc}. What may cause this type of shape in an IV-curve is discussed in the next chapter.

In table 4.7 below the calculated photovoltaic parameters are presented. These parameters were calculated in the same way as was done for the commercial solar cell.

Table 4.7: Photovoltaic cell parameters, Dye-Sensitized Solar Cell w/ soot CE, $88mW/cm^2$ illumination.

Photovoltaic cell parameters	**Scan Rates, mV/s**					
	5	**10**	**20**	**30**	**50**	**100**
Short-Circuit Current, [mA]	-0.55	-0.60	-0.50	-0.57	-0.71	-0.79
Open-Circuit Voltage, [V]	0.55	0.46	0.36	0.31	0.25	0.21
Fill Factor	0.01	0.01	0.02	0.02	0.02	0.02
Efficiency, [%]	0.0045	0.0035	0.0035	0.0033	0.0034	0.0039

From the table it can be seen that both the fill factor and the efficiency of the cell is very low. By first seeing the extremely non-ideal IV-curve, this is not that surprising. It can also be seen that the V_{oc} and the I_{sc} varies greatly with scan rate.

4.3 Photocapacitor measurement

After the individual components had been tested and characterized, they were combined to form a complete photocapacitor system. For the commercial components this meant connecting the solar cell and the supercapacitor in series. For the fabricated photocapacitors, this meant combining the various types of photovoltaic electrodes, supercapacitor electrodes, and electrolytes.

The commercial component system are presented first. This is done to first give a better understanding of how such a system might perform, separated from non-ideal behaviour. The measurements for the fabricated photocapacitors are presented afterwards.

4.3.1 Commercial components system

For characterizing the commercial components systems both of the previous techniques were used, in addition to one other. This other technique was a potential difference technique, that measured the potential between two points in the circuit. This was done with a differential voltage module, and the 'Logger Pro' program.

In the setup, the anode of the supercapacitor was connected to the cathode of the solar cell. Before each measurement the supercapacitor was emptied of charge by shorting its two leads. The CV measurements were done with no illumination, while the IVC measurements where done with the same illumination intensities as the commercial solar cell. The potential difference technique was used to observe how the voltage over the capacitor changed with charging and discharging, as well as how the voltage over the complete system changed in various situation like fully charged under illumination, fully charged in darkness, and during a short-circuit discharge. A circuit connection diagram for the photovoltaic system and the measuring instruments are given in figure 3.4 in chapter 3.

In figure 4.15 below all the measurements done at 88 mW/cm^2 illumination with different scan rates are shown. The supercapacitor was discharged between each measurement.

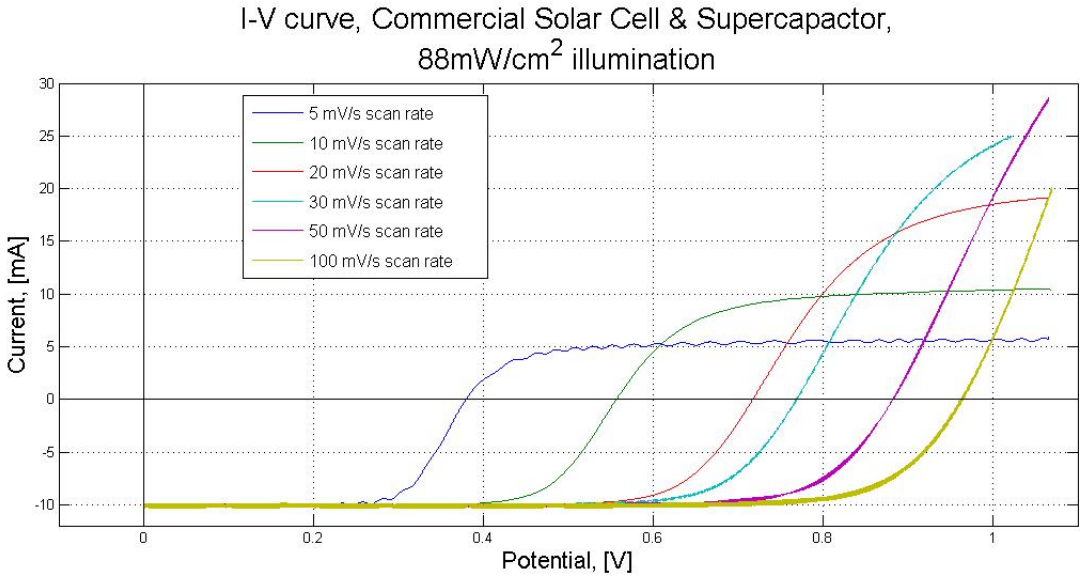

Figure 4.15: Commercial solar cell & supercapacitor system, 88mW/cm^2 illumination, 6 different scan rates

One interesting thing that can be observed with these measurement is that depending on the scan rates, the V_{oc} will change significantly. While measuring, the current would suddenly start to increase exponentially, before the V_{oc} value

that was estimated by the program, and continue with a positive current until the estimated V_{oc} voltage was reached. The slower the scan rate, the earlier this rise occurred. With the change in V_{oc} as an exception, the I_{sc} and shape of the curve remained about the same as for the solar cell on its own.

In table 4.8 the calculated photovoltaic parameters from the $88mW/cm^2$ illumination measurements are presented.

Table 4.8: Photovoltaic cell parameters, Commercial Solar Cell & Supercapacitor system, $88mW/cm^2$ illumination.

Photocapacitor cell parameters	**Scan Rates, mV/s**					
	5	**10**	**20**	**30**	**50**	**100**
Short-Circuit Current, [mA]	-10.13	-10.12	-10.11	-10.06	-10.02	-10.66
Open-Circuit Voltage, [V]	0.38	0.56	0.72	0.77	0.88	0.96
Fill Factor	0.72	0.74	0.76	0.77	0.79	0.75
Efficiency, [%]	3.12	4.66	6.16	6.66	7.81	8.67

In the table above a interesting change in the efficiency can be observed. While the fill factors remain about the same for all the scan rates, the efficiency gets significantly reduced with lower scan rates. This reflects what is seen in the graphs, with the shape of the curve remaining the same, but with decreasing V_{oc} for decreasing scan rates. Considering the strange behaviour of these graph, dissimilar to the normal I-V curve seen for photovoltaic cells, the accuracy of calculated parameters should to be questioned.

To further investigate the shifting of the V_{oc}, an additional set of IVC measurements were performed. In this test the IVC technique would be run 10 consecutive times, at 88 mW/cm^2 illumination, and with a scan rate of $20mV/s$. In the first measurement the supercapacitor leads where short-circuited with a switch, effectively giving the IV-curve of the solar cell on its on. For the second measurement the switch was turned off, and remained off for the remaining 9 measurements. Simultaneous with these measurements, the differential voltage over the supercapacitor was measured. The anode and the cathode of the differential voltage module was connected to the anode and the cathode of the supercapacitor, respectively. The complete connection diagram is the one given in figure 3.4. These two sets of measurements can be seen below in figures 4.16 and 4.17.

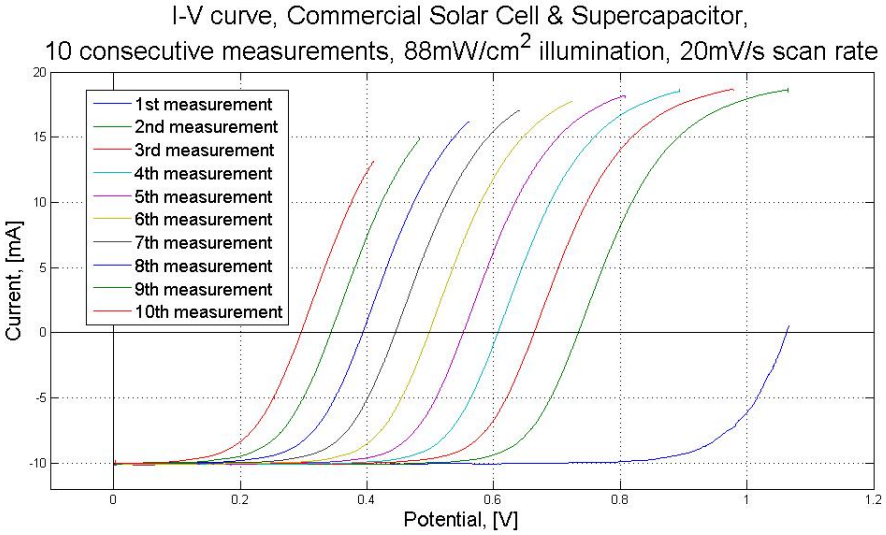

Figure 4.16: Commercial solar cell & supercapacitor system, $88mW/cm^2$ illumination, 20 mV/s scan rate, 10 consecutive IVC measurements. The graph shows the IV-curves of the 10 measurements done.

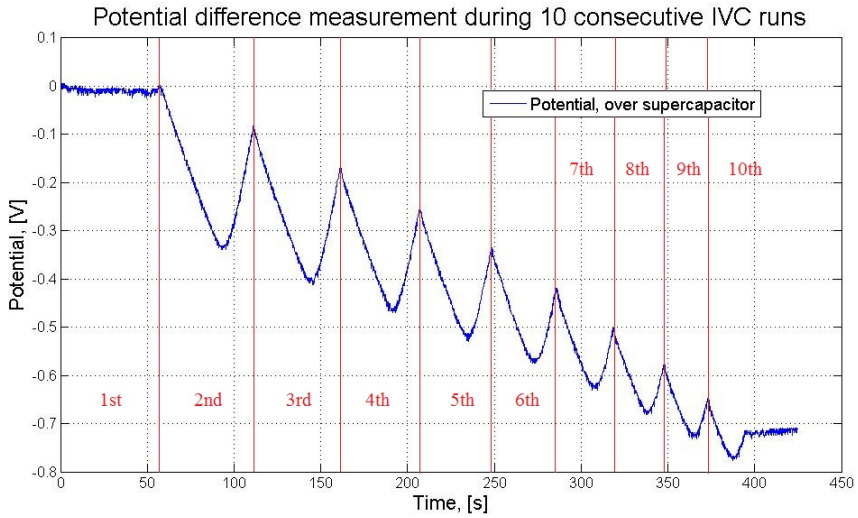

Figure 4.17: Commercial solar cell & supercapacitor system, $88mW/cm^2$ illumination, 20 mV/s scan rate, 10 consecutive measurements. The graph shows the differential voltage measured done over the supercapacitor, in parallel with the measurements in figure 4.16. The red lines and lettering marks the time intervals corresponding to the measurement number.

These figures and the probable cause for the shifting of the V_{oc} is discussed further in the next chapter.

In addition to the IVC measurements, a set of CV measurements at no illumination were done, at the same scan rates. The graph for the 20 mV/s measurement is shown below in figure 4.18

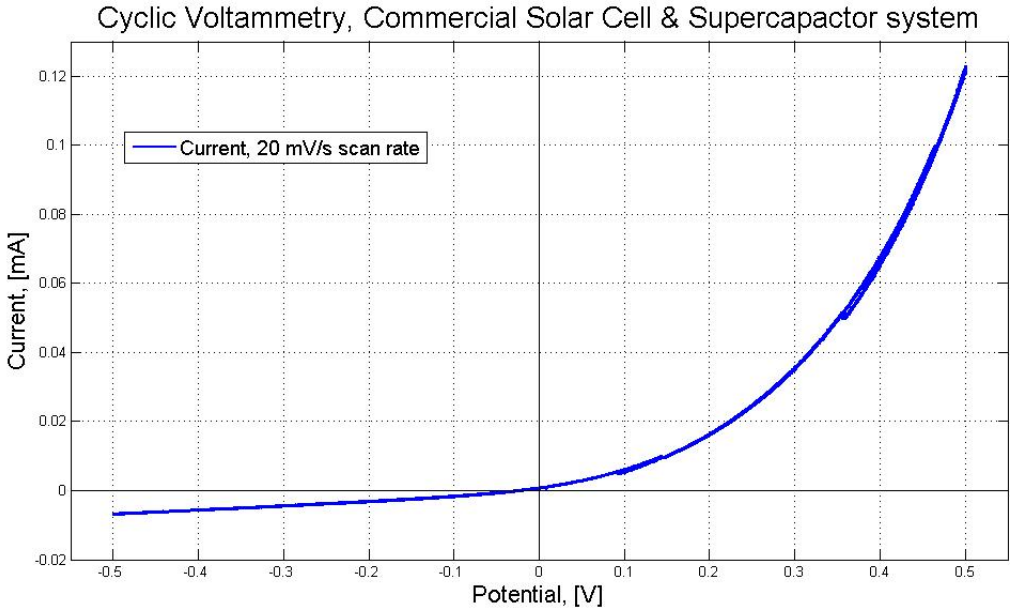

Figure 4.18: Commercial solar cell & supercapacitor system, no illumination, 20 mV/s scan rate. Cyclic Voltammetry measurement, 5 cycles.

The most interesting features in the figure above is the complete lack of a hysteresis, as would normally be observed for a CV measurement of a supercapacitor. The curve closely resembles the curve seen for the individual solar cell in figure 4.10. A capacitance value could be calculated from this curve using the method as previously used. However, the calculated value would most certainly by unrelated to the actual capacitance of the system. What may be the probable cause for this shape of the curve is covered in the next chapter.

The last test that was performed on the commercial component system was the charging and discharging of the supercapacitor, over the complete system. Discharging of the supercapacitor was done previously, but then by always shorting the two leads directly from the supercapacitor. These direct connections would not be accessible in a fabricated photocapacitor system, and this method of discharging would be unavailable.

To charge the system, the anode from the solar cell and the cathode from the supercapacitor had to be connected to each other, short-circuiting the system. This was done during 88 mW/cm^2 illumination. The supercapacitor was completely filled when the potential over the supercapacitor was equal, but with opposite sign, to the V_{oc} of the solar cell. The open-circuit voltage over the total system was zero. The charging mechanics of the system is discussed in more detail in the next chapter. To measure the charging and discharging, the voltage was measured over the supercapacitors. This measured charging is shown in figure 4.19 below.

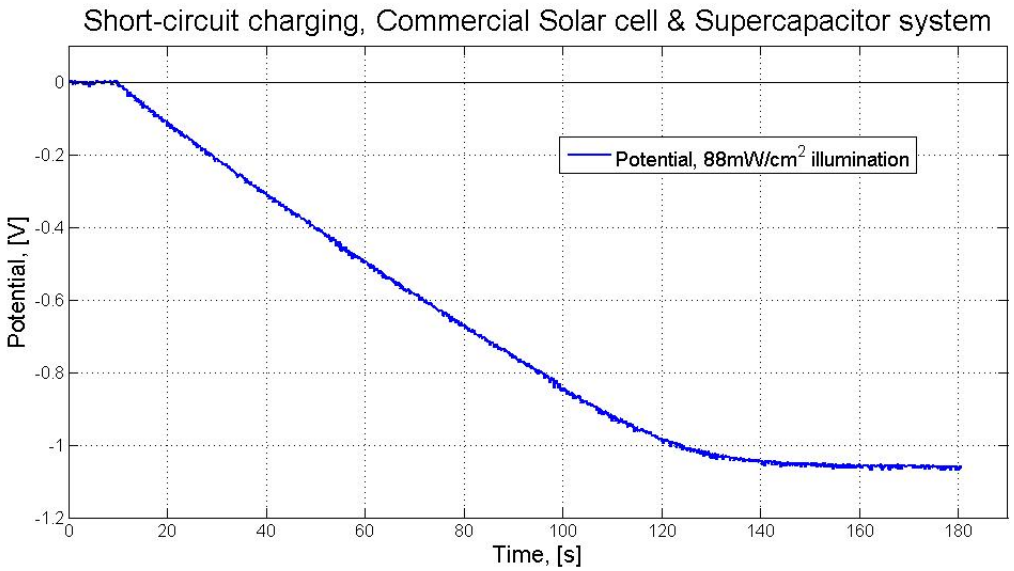

Figure 4.19: Commercial solar cell & supercapacitor system, charging curve, 88 mW/cm^2 illumination.

The curve was seen to stabilize at around -1.06 V, after about 140 seconds. Using equation (2.21) for the total energy stored in the supercapacitor, and dividing

by the charging time, the power of the charging could be calculated. Assuming a capacitance of 1 F, the power was calculated to be about 4mW. With a $88mW/cm^2$ illumination, the total efficiency of the system was calculated to be 4.3%.

The discharging was initiated by turning off the light source, so there were no illumination of the solar cell, and then short-circuiting the complete system again. The discharge curve is shown below in figure 4.20

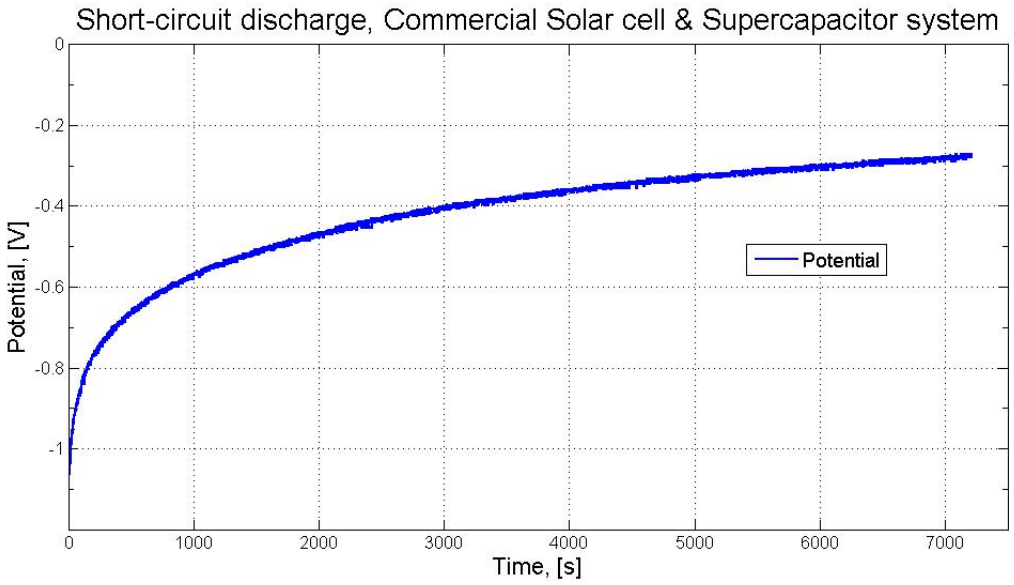

Figure 4.20: Commercial solar cell & supercapacitor system, SC discharge curve.

Looking at the time scale on the discharge, it can be seen that the discharging of the cell was extremely slow. Starting at around -1.06 V, the voltage was still at around -0.3 V after 2 hours.

4.3.2 Fabricated photocapacitor

As was mentioned in section 4.2.2, the photovoltaic electrodes made of nano-silicon did not show any significant photovoltaic properties. As for the $LiPF_6$-electrolyte, this was primarily intended to be used with this electrode. The electrolyte was

tested in use with the DSSCs, but though photovoltaic properties were seen, the dye molecules in the cell quickly deteriorated, bleaching the cell completely.

As a result of these observations, the final characterizations were done a bit asymmetric. There were two final types of DSSCs that were characterized. These were cells with DSSC photovoltaic electrodes, I^-/I_3^--electrolyte, and nano-carbon or nano-carbon w/ MWNTs supercapacitor electrodes, respectively. These were tested for both photovoltaic and capacitive properties. There were also two types of photocapacitor devices with nano-silicon photovoltaic electrode, $LiPF_6$-electrolyte, and nano-carbon or nano-carbon w/ MWNTs supercapacitor electrodes, respectively. These were only tested for capacitive properties. Figure 4.21 below shows a diagram of the complete fabricated photocapacitors.

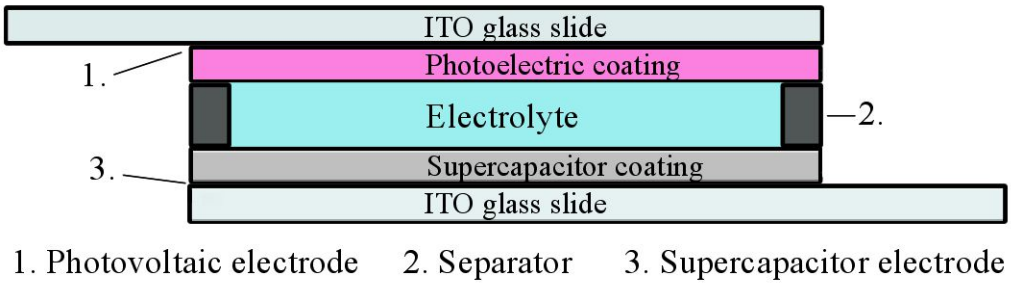

Figure 4.21: Diagram of a complete fabricated photocapacitor.

For the testing of photovoltaic and capacitive properties on the fabricated cells, the same techniques as for the commercial components system were used. For some of the tests, however, there were a difference in how the measurements were taken. Unlike in the commercial components system, all the measurements had to be taken over the complete system. Among others, this cause the discharging curves to look a bit different. There was also a difference in the stability of the cells. With the DSSCs, a noticeable degradation could be observed after a relatively short amount of time. The degradation was most prominent during the time the cells were illuminated. Consequently, to try to minimize the effect of this degrading, the cells were only tested at 88 mW/cm^2 illumination for the IVC and discharging measurements, and with no illumination for the CV measurements.

In the next three sections the photocapacitor cell with the nano-carbon supercapacitor electrode is presented first, followed by the cell with the nano-carbon w/ MWNTs electrode, and lastly the photocapacitors with nano-silicon electrodes.

4.3.2.1 Photocapacitor with DSSC & nano-carbon electrodes

From the IVC measurements of the photocapacitor with nano-carbon electrode, at 88 mW/cm^2 illumination, the 20 mV/s scan rate measurement is presented below in figure 4.22.

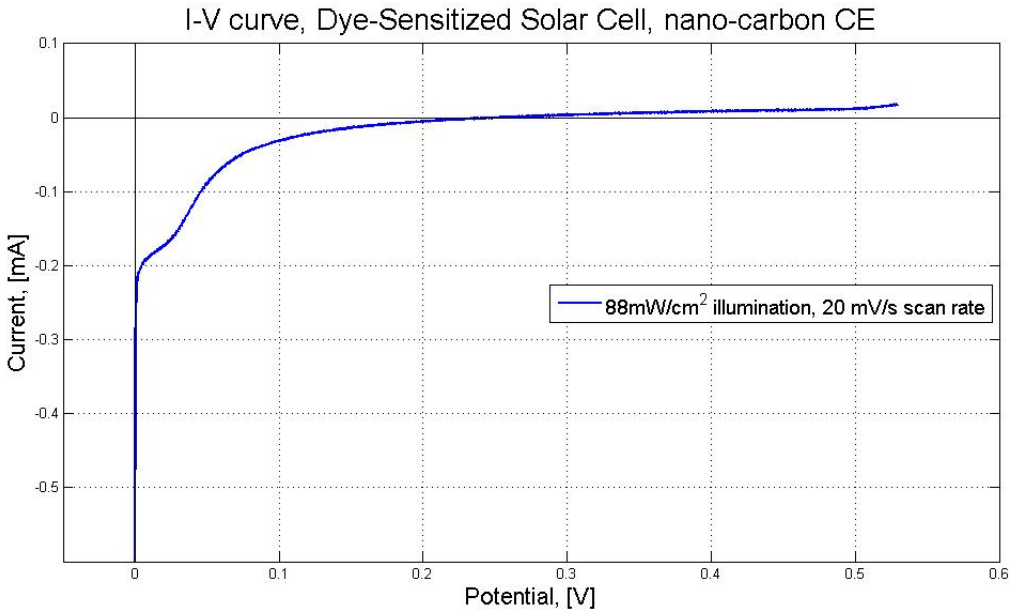

Figure 4.22

Comparing this graph to the one in figure 4.14, many of the same observations can be seen. The curve quickly rises when entering the fourth quadrant, before levelling off somewhat. One difference between the two, is that instead of a steady rise towards the V_{oc} as is seen in figure 4.14, the curve makes a second, seemingly exponential rise at around 0.03-0.05 V, before leveling off again. This second rise was observed for all the scan rates.

The calculated photovoltaic parameters for these IVC measurements are presented below in table 4.9

Table 4.9: Photovoltaic cell
parameters, Dye-Sensitized Solar Cell with nano-carbon CE, $88mW/cm^2$ illumination.

Photocapacitor cell parameters	**Scan Rates, mV/s**					
	5	**10**	**20**	**30**	**50**	**100**
Short-Circuit Current, [mA]	-0.32	-0.42	-0.35	-0.43	-0.44	-0.60
Open-Circuit Voltage, [V]	0.53	0.43	0.25	0.20	0.17	0.19
Fill Factor	0.03	0.02	0.05	0.07	0.11	0.11
Efficiency, [%]	0.0056	0.0038	0.0054	0.0066	0.0090	0.0133

In figure 4.23 below the CV-measurement at 20 mV/s is shown.

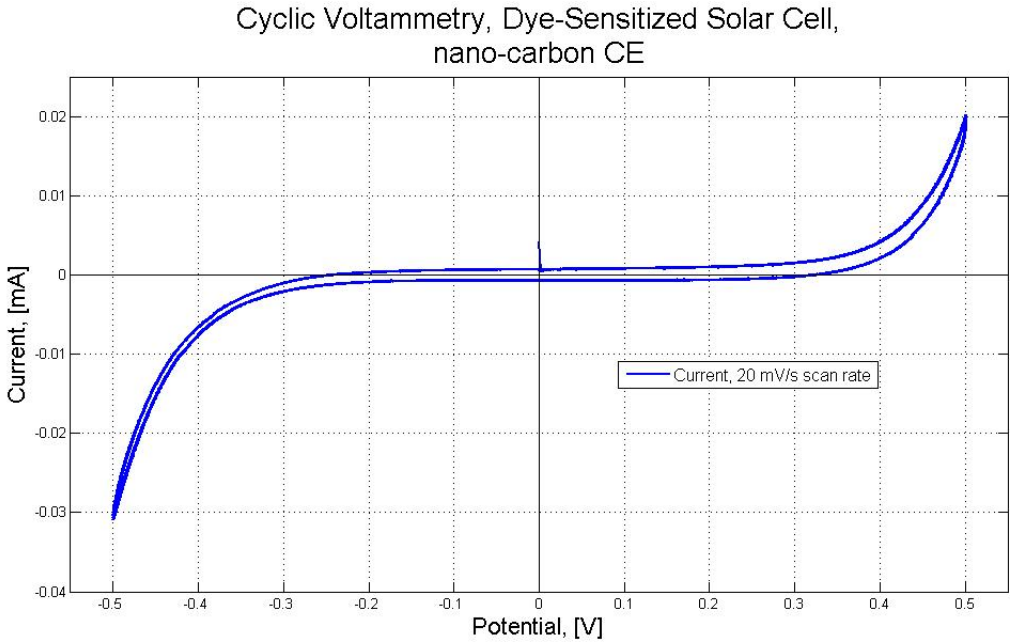

Figure 4.23: CV-graph of DSSC with nano-carbon CE, I^-/I_3^--electrolyte. 20 mV/s scan rate, 5 cycles.

The curve in this graph has a similar shape to the the curve in figure 4.18. One difference is that there is an observable hysteresis. Also, the curve is odd in relation to the I-axis, instead of there only being an exponential rise in the area of positive voltage. However, despite the hysteresis, a calculation of the effective capacitance for this curve would still not likely give an accurate reference to the actual capacitance of the device.

The cell was charged in a similar matter as the commercial component setup. The two terminals of the cell was shorted, during illumination, and left till the supercapacitor was completely charged. This was observed by disconnecting the two terminals, and measuring the potential to be zero. The discharge however, was done a bit differently. Instead of turning of the light, the cell was left in open-circuit condition, with illumination. The discharge curve can be seen below in figure 4.24.

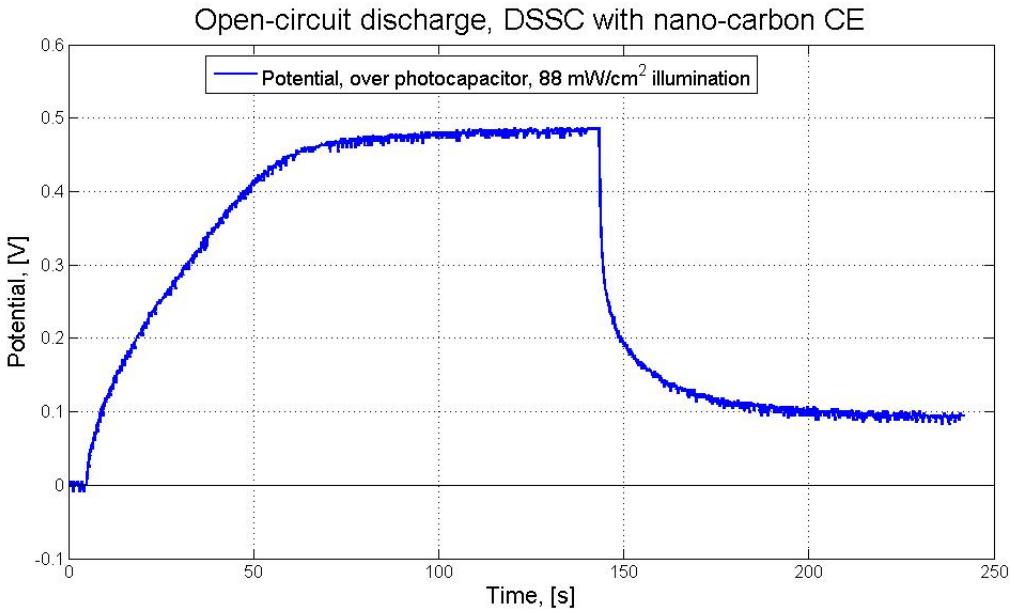

Figure 4.24: Potential voltage, over a DSSC with nano-carbon CE, I^-/I_3^--electrolyte, 88 mW/cm^2 illumination.

The curve can be observed to slowly rise from zero voltage, towards the V_{oc} of the solar cell. When the voltage plateaus, the light was shut off, and the drop in voltage measured. The suspected reason for the discharging during the open-circuit, illuminated period, is most likely due to a high leakage current caused by low shunt resistance. An accurate discharge measurement under short-circuited condition, or with a known external resistance, became difficult because of this high leakage current.

4.3.2.2 Photocapacitor with DSSC & nano-carbon w/ MWNTs electrode

For the photocapacitor with nano-carbon w/ MWNTs electrode, the same sets of tests as in the previous section were performed. The IVC measurement at 88 mW/cm^2 illumination and 20 mV/s scan rate is presented below in figure 4.25.

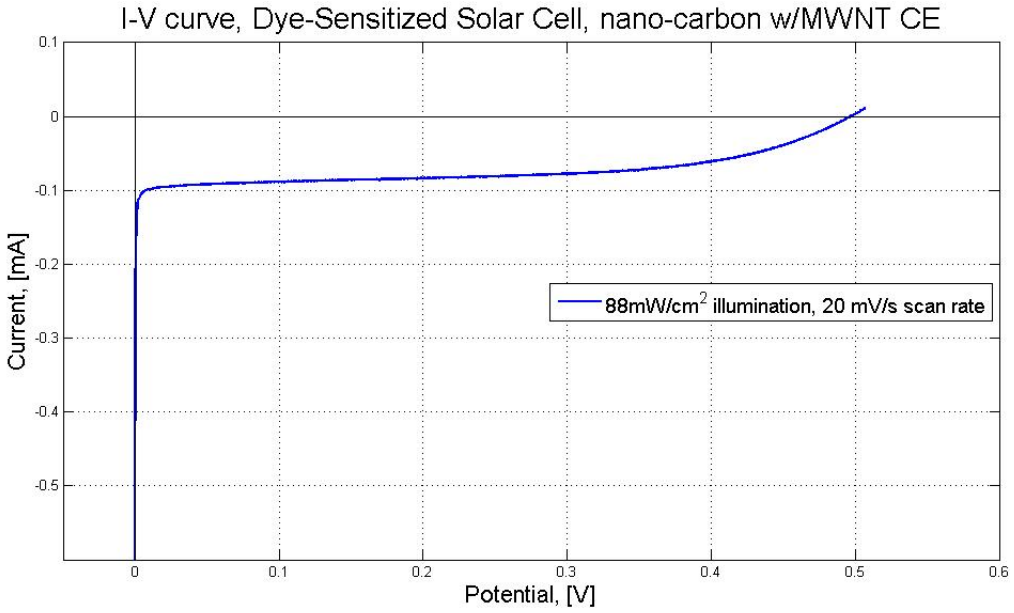

Figure 4.25

The curve in this graph is a bit different from the curves in figures 4.14 and 4.22. It has the same sudden rise as soon as the curve enters the fourth quadrant. The difference in this curve is observed after this point. The curve levels off sharply,

and remains quite stable for some time, before a clear exponential rise occur when the voltage approaches the V_{oc}. In table 4.10 below the calculated photovoltaic parameters are presented.

Table 4.10: Photovoltaic cell parameters, Dye-Sensitized Solar Cell with nano-carbon w/ MWNTs CE, $88mW/cm^2$ illumination.

Photocapacitor cell parameters	**Scan Rates, mV/s**					
	5	**10**	**20**	**30**	**50**	**100**
Short-Circuit Current, [mA]	-0.22	-0.45	-0.32	-0.52	-0.54	-0.67
Open-Circuit Voltage, [V]	0.51	0.50	0.50	0.49	0.49	0.49
Fill Factor	0.21	0.11	0.16	0.10	0.10	0.08
Efficiency, [%]	0.0272	0.0278	0.0287	0.0287	0.0291	0.0291

Though still low, the fill factor and efficiency of this cell can be seen to be much higher than the ones calculated for the other other two DSSCs.

In figure 4.26 below the CV-curve for the 20 mV/s scan rate measurement is shown.

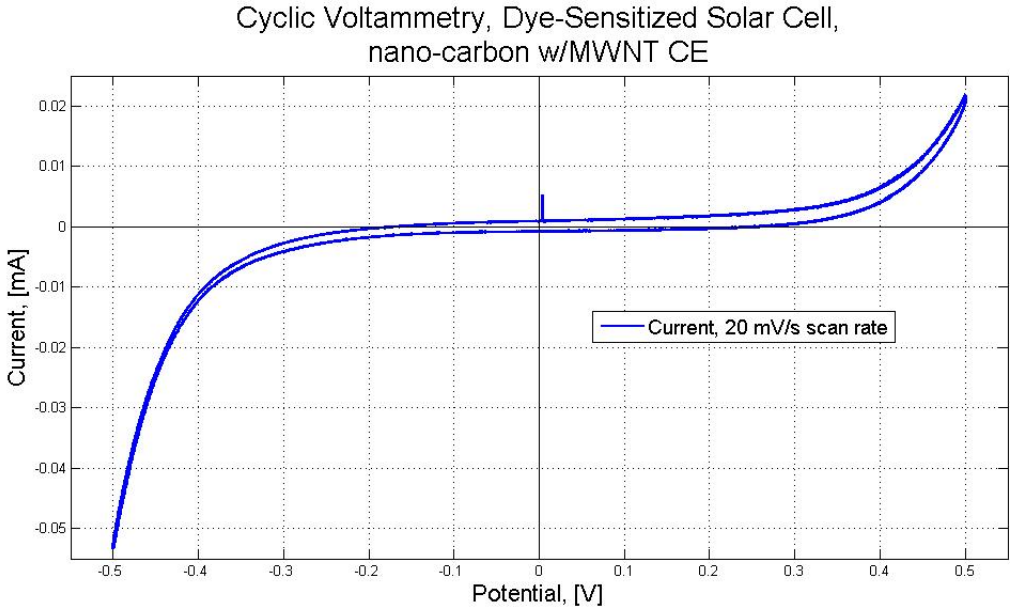

Figure 4.26: CV-graph of DSSC with nano-carbon w/MWNTs CE, I^-/I_3^--electrolyte. 20 mV/s scan rate, 5 cycles.

This curve is very similar to the curve in figure 4.23 for the other type of fabricated photocapacitor. The curve is odd around the I-axis, and there is a small but clear hysteresis between the forward and backward cycles. The argument regarding calculated effective capacitances still holds true here, and the calculation is withheld.

The charging, and discharging of this type of cell was done in the same fashion as for the other fabricated cell. The discharge curve is shown below in figure 4.27.

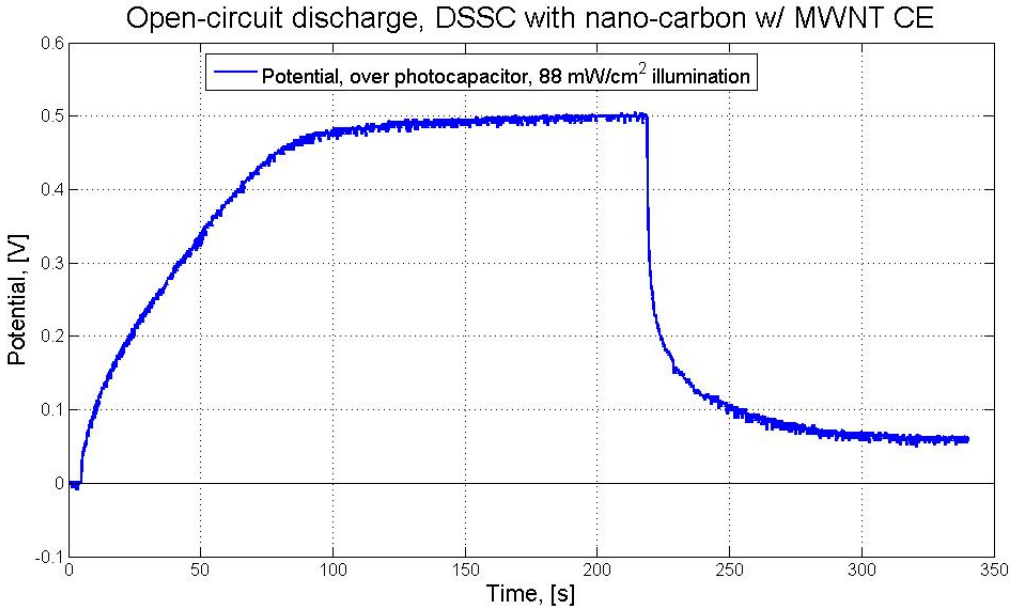

Figure 4.27: Potential voltage, over a DSSC with nano-carbon w/ MWNTs CE, I^-/I_3^--electrolyte, 88 mW/cm^2 illumination.

This curve is very similar in shape to the discharge curve of the other fabricated photocapacitor, figure 4.24. The discharging of this device is also most likely caused by a low shunt resistance.

4.3.2.3 Photocapacitors with nano-silicon electrode

For the two types of photocapacitors with nano-silicon photovoltaic electrodes, only CV measurements were performed. The effective capacitance was also calculated for these devices. In figures 4.28-4.29 below the CV-curve for the 20 mV/s scan rate measurements are shown, as well as the calculations in tables 4.11-4.12.

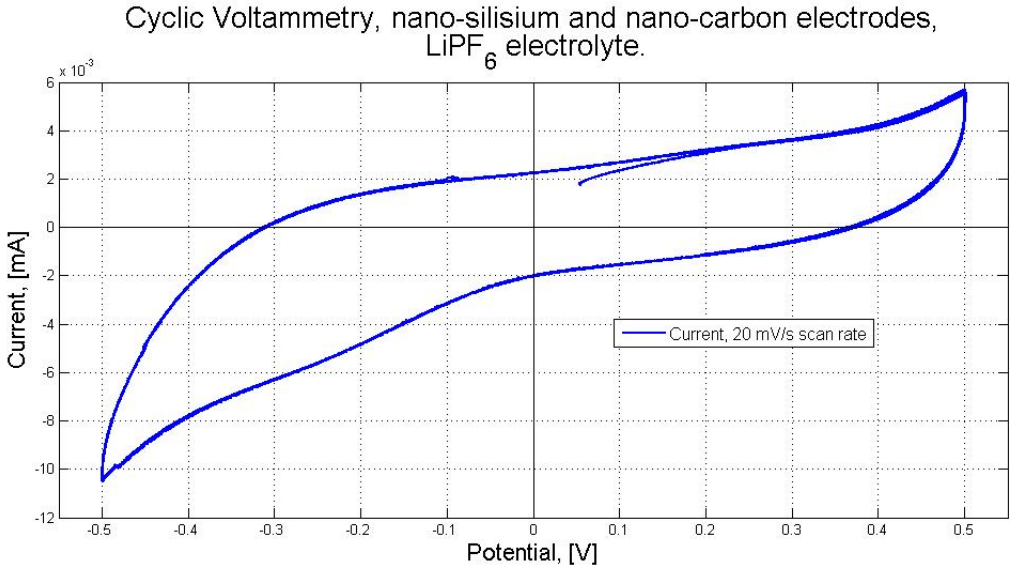

Figure 4.28: CV-graph of nano-silicon with nano-carbon CE, $LiPF_6$-electrolyte. 20 mV/s scan rate, 5 cycles.

Table 4.11: Effective capacitance of fabricated photocapacitor. Nano-silicon and nano-carbon electrodes, $LiPF_6$-electrolyte.

Nano-silicon, nano-carbon	**Scan Rates, [mV/s]**					
	5	**10**	**20**	**30**	**50**	**100**
Effective Capacitance, [mF]	0.18 ± 0.02	0.141 ± 0.002	0.1116 ± 0.0003	0.0997 ± 0.0003	0.0832 ± 0.0001	0.0666 ± 0.0001

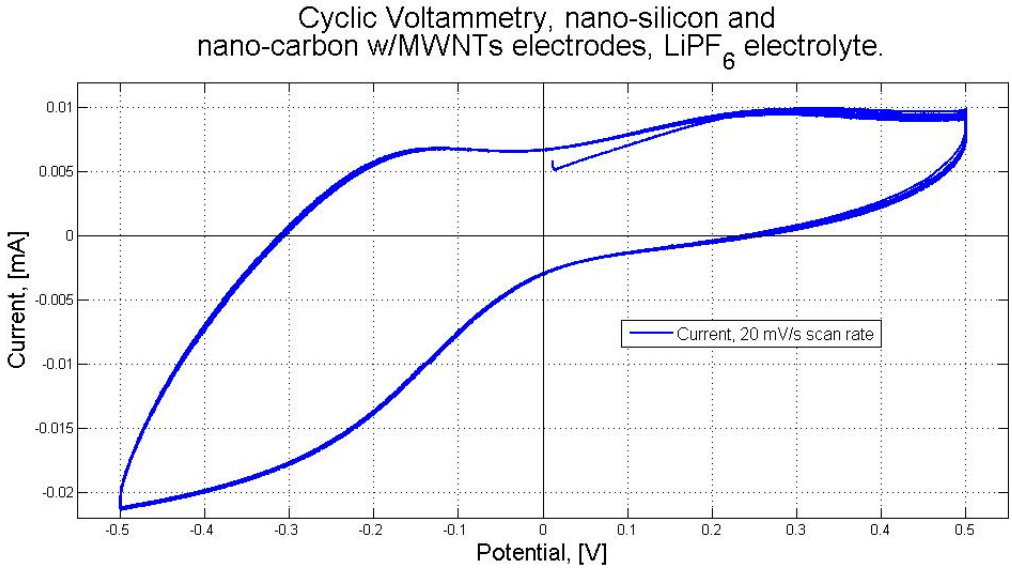

Figure 4.29: CV-graph of nano-silicon with nano-carbon w/MWNTs CE, $LiPF_6$-electrolyte. 20 mV/s scan rate, 5 cycles.

Table 4.12: Effective capacitance of fabricated photocapacitor. Nano-silicon and nano-carbon w/MWNTs electrodes, $LiPF_6$-electrolyte.

Nano-silicon, ano-carbon w/MWNTs	**Scan Rates, [mV/s]**					
	5	**10**	**20**	**30**	**50**	**100**
Effective Capacitance, [mF]	0.47 ± 0.05	0.361 ± 0.002	0.264 ± 0.002	0.2212 ± 0.0002	0.1785 ± 0.0002	0.1341 ± 0.0005

Chapter 5

Discussion

In a discussion regarding photocapacitor systems, there are several elements of the system that are of particular importance, and needs to be looked upon. Some of these include the general quality of the components, the characterization of their performance parameters, and the synergy between their specific working principles. Also of interest is how the charging and discharging mechanisms of an actual photocapacitor system would happen. All of these will be looked upon. To starting off, the performance of the commercial component system is evaluated.

5.1 Commercial components photocapacitor system

The commercial components system was comprised of a 1 F supercapacitor, and a poly-crystalline silicon solar cell. From the testing of the individual components, the capacitance of the supercapacitor was indeed found to be 1 F, for low scan rates, and the efficiency of the solar cell was estimated to around 9.7 %. The components where then connected together, and a number of the same tests were performed. Some of these tests were inconclusive, because the measurement data no longer resembled the expected curves or values. The system was also tested during charging and discharging.

For the charging, the maximum voltage over the supercapacitor and the charging time was approximated to be -1.06 V and 140 second, respectively. The power of the charging current was found to be 4 mW, which with a illumination intensity of 88 mW/cm^2, and solar cell light-to-electricity conversion efficiency of 9.7 %, gave a total light-to-stored-energy efficiency of 4.3 %. Comparing this efficiency to

the efficiency of the solar cell, the electricity-to-stored-energy efficiency was found to be 44.3%. These efficiency gives a measure on how well a photocapacitor system might perform.

The validity of the charging and discharging mechanisms presented in section 2.3.2 is strengthened by look at the discharge curve in figure 4.20. For this discharge the two terminals of the photocapacitor system was short-circuited. The total series resistance is therefore only the sum of the series resistance of the solar cell in the dark, and of the supercapacitor. In the figure we see the initial fast discharge, as the voltage over the supercapacitor is still large enough to drive a sufficiently large current. However, as the voltage get lower and lower, the drop in voltage slows down. After two whole hours at short-circuited discharge, the voltage is only reduced to around 0.3 V, with a drop of only around 0.1 V in the last hour. In a resistance measurement taken over the complete system, the resistance was found to be between 1.0-1.4 kΩ, fluxuating greatly. Comparing this relatively high resistance for a short-circuit discharge to equation (2.36), the long discharge time could be understood. Since the current that runs through the diode is inversely proportional to the series resistance, the high resistance measured could give a very small discharge current, especially when the voltage over the supercapacitor, V_C, gets low.

In the described mechanisms for the charging and discharging of a photocapacitor system in 2.3.2, there is an important point to remember. This point is that in the described system the solar cell is a solid-state device. This will be different to an electrochemical photocapacitor system, where an electrolyte is involved. How this difference will affect the charging and discharging of the system is an important and necessary point to consider. Next, with the charging and discharging mechanisms of an electrochemical photocapacitor system in focus, we look at the synergy between the various parts that makes up such a system.

5.2 Synergy between components in an electrochemical photocapacitor system

To talk about the synergy, it is useful to first quickly summarize how the various parts are meant to function.

For the photovoltaic part, its function is to generate an electrical current. This is done by generating electron-hole pairs through absorption of light. These charges then needs to be separated by a potential barrier to produce a steady

electrical current. In electrochemical photovoltaic cells, this barrier comes from the difference in the Fermi level of the semiconductor material, and the redox potential of the electrolyte. In a DSSC, this is specificity achieved by oxidizing the dye, which then injects electrons into the TiO_2, and then further into an external circuit. The oxidized dye needs to be reduced back again to its initial state by the I^-/I_3^--electrolyte. The oxidized species in the electrolyte then needs to be reduced at the CE, which is connected to the external circuit. A break in any of these parts of the system, and the current will stop running. [10, 20]

For the supercapacitor part, its function is to store the produced electrical current. This is done by attraction between the ions in the electrolyte, and the free charge carriers in the electrode. For the current to be stored, however, the attracted charges do not get to meet, and needs to remain spatially and conductively separated. For this to remain true, the electrodes needs to be as inert as possible.

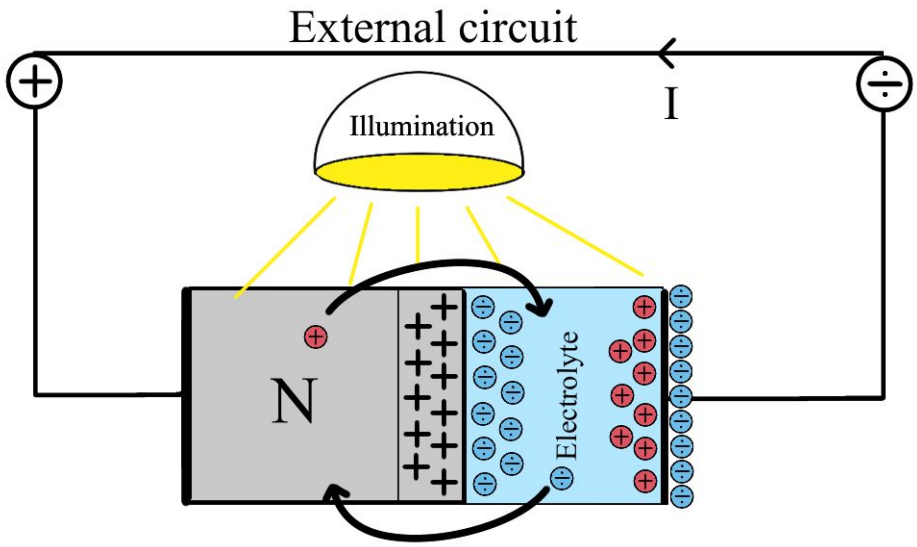

Figure 5.1: Diagram of an electrochemical photocapacitor system.

In figure 5.1 above an idealized circuit diagram of an electrochemical photocapacitor system is shown. The system is being charged under short-circuit

condition, and all the parts are functioning properly. In a real electrochemical photocapacitor, however, this is most likely not the case.

5.2.1 Reactivity between the electrodes and the electrolyte

From the quick summaries, two of the important requirements for proper functionality are contradictory to each other. These requirements are the ones regarding the reactions between the electrodes and the electrolyte. For a electrochemical photovoltaic cell, like the DSSC, to function properly, there should be as much reactivity between free charge carriers in the electrodes and the ions in the electrolyte as possible. For a supercapacitor, the opposite is true. As little reactivity as possible is desired. How these different requirements affect a photocapacitor system, are of crucial importance.

In this project there were primarily two different setups for photocapacitor systems that were looked at. One was the system with a DSSC photovoltaic electrode, with nano-textured carbon counter electrodes. The other was the system with a nano-textured silicon photovoltaic electrode, with nano-textured carbon counter electrodes. The last setup was based on the work presented by Lo et al. in their 2010 paper. [33].

In testing the different types of system, a few things were observed. For the DSSC system, a clear photovoltaic response was seen. When the cell was illuminated, a light-generated current could clearly be measured. For the charging of the photocapacitor system, however, the results were less than ideal. When the cells were short-circuit charged in the same manner as the commercial component system were, a certain build up of charge could be observed, by the shift in the voltage over the cell. This shift was very slight, however, and if the short-circuit connection was broken, the voltage quickly increased back to the open-circuit voltage of the DSSC. This would most likely indicate that the small amount of charge stored at the electrodes quickly reacted with each other, and recombined. For the nano-silicon system, no photovoltaic respond was observed.

That the stored charge on the DSSC system quickly recombined is perhaps not that surprising. In DSSC reported in the literature, both of the electrodes are usually optimized for reactivity. The TiO_2 electrode is dyed with a dye molecule that is highly reactive with the chosen electrolyte [20]. The CE used are often current collectors with high conductivity, like gold or platinum [40, 43]. In the few articles that report the creation of photocapacitor-like devices, devices that can both generate and store the electric charge, a slight detail can be noted. This is

that non of the devices use both an electrochemical photovoltaic electrode, and a supercapacitor electrode, in a 2-electrode setup. In the Lo et al. paper, the charge separation seems to be achieved by a solid-state junction between the nano-silicon and the ITO-current collector [33]. In a later paper by the same group, they had created a device with a DSSC, but with the a traditional parallel plate capacitor with a PVDF film as a dielectric [24]. They also used a third "quasi"-electrode to keep a current running in the circuit. In a third system, like the one presented by Yang et al., both a DSSC electrode was used, and a supercapacitor [49]. In this device, however, the photovoltaic part and the supercapacitor parts were separated, and a three-electrode setup was used. To charge and discharge the system, different leads had to be switched. This in turns limits the potential benefits from a two-electrode photocapacitor, in terms of efficiency in size and resistive loss.

From the results, and the literature, a clear indication on the conflicts for reactivity - non-reactivity between electrochemical photovoltaic cells and supercapacitors is seen. This conflict is a very probable cause for the poor energy storing results seen.

5.2.2 Total capacitance in an electrochemical photocapacitor

Another topic regarding the synergy between components is the total capacitance of the device. As was shown in section 2.1.3, the total capacitance for a supercapacitor is a function of the capacitance for each of the two electrodes. It was also shown that when the two capacitances are dissimilar, it is the lowest of the two that has the greatest impact on the total capacitance. What this could mean is that the contribution to the total capacitance from an optimally constructed supercapacitor electrode could be negligible. The total capacitance would still largely be dependent on the capacitance of the photovoltaic electrode.

For the DSSCs, the specific surface area of these electrodes would likely be quite large, as they are constructed from nano-structured TiO_2. However, the other important factors for a high capacitance pose big problems. The perhaps biggest of these problems is the requirement for the ions in the electrolyte and the free-charge carriers in the electrodes to be non-reactive. In DSSCs, the TiO_2 are coated in dye molecules that serves the exact opposite purpose, as they are highly reactive with the electrolyte. Because of this no electrochemical double layer will form, and despite the large surface area of TiO_2, no significant capacitance. This in turn makes the total capacitance negligibly small. The DSSC electrode will not be available for energy storage, and consequently, neither will the photocapacitor

device.

This is different for the nano-silicon photovoltaic electrode. This electrode is also nano-structured, as can be seen in figure 4.12, which will give a large surface area. Unlike the DSSC, the surface will not be highly reactive with the electrolyte, meaning an electrochemical double layer could form. From the photocapacitors that were fabricated in this project, two types with nano-silicon and nano-carbon electrodes were tested using the CV technique. The measurement curves for these devices showed a noticeable hysteresis, indicating a decent capacitance value. An estimation on the capacitance value for the nano-silicon electrode can be made, using equation (2.12), and the effective capacitances of the nano-carbon supercapacitors in section 4.1.2;

$$\frac{1}{C_{total}} = \frac{1}{C_{carbon}} + \frac{1}{C_{silicon}} \tag{5.1}$$

Using the capacitances for the 5 mV/s measurements from tables 4.5 and 4.12, the calculation is as follows. For the supercapacitor, the electrodes are identical, and assumed to have the same capacitance. Their capacitance is then given as

$$C_{carbon} = 2 \cdot C_{total} = 2 \cdot 4.0mF = 8.0mF \tag{5.2}$$

This value is one of the two capacitances in equation (5.1), with the capacitance of the nano-silicon electrode being the other. The total capacitance is the value given in table 4.12. Rearranging with regard to the nano-silicon capacitance, we get

$$C_{silicon} = \frac{C_{carbon} \cdot C_{total}}{C_{carbon} - C_{total}} = \frac{8.0mF \cdot 0.47mF}{8.0mF - 0.47mF} = 5.0mF \tag{5.3}$$

From this, we can see that the surface of the nano-silicon electrode can hold a decent amount of charge. This would also mean that this type of photovoltaic electrode could be used in photocapacitor device, unlike the DSSC electrode.

5.2.3 The power of the energy in an electrochemical photocapacitor

A third topic regarding the synergy between the components is the power of the stored energy, when discharging the system. As was seen in the first section of this

chapter, the discharge current of the supercapacitor will be strongly influenced by the voltage over the solar cell diode, and the equivalent series resistance of the circuit. To get a fast discharge, the voltage over the diode must be over a certain value, known as the turn-on-voltage. When the voltage over the diode starts to decrease, the rest of the energy is only accessible at a lower power. Also, if the equivalent series resistance is high, the voltage over the diode will be significantly lowered, further lowering the power. [12]

From this, we can see that to have a photocapacitor system with a high discharge power, the voltage over the supercapacitor part should also be high. In a real photocapacitor system, however, there are some immediate limitations. The first of these are the voltage over the system. The voltage over a self-charging system is limited to the height of the open-circuit voltage of the photovoltaic part. For the tested commercial solar cell this value was 1.06 V, and for the fabricated DSSC cells, around 0.5 volt.

The second limitation, is the turn-on-voltage of the diode. This voltage will vary some, depending on parameters like the equivalent series resistance of the circuit, and the temperature. It will, however, typically be at a voltage near the open-circuit voltage of the solar cell under illumination. The more ideal the solar cell, the closer the turn-on-voltage will lie. This could mean that with an ideal solar cell, only the energy stored past the turn-on-voltage could be utilized at a decent rate.

In this regard, there is another relation to remember. This is the relation between the total energy stored in a supercapacitor, and the voltage over it, as seen in equation (2.21) in chapter 2;

$$E_{total} = \frac{1}{2}CV^2 \tag{5.4}$$

From the equation, it can be seen that the total energy stored increases with the square of the voltage. This means that a major part of the stored energy in a supercapacitor will be stored at the higher voltages. This also means that during a discharge of a photocapacitor system, the initial discharge with high power, will also count for most of the stored energy. This can be shown by looking at figure 4.20, the short-circuit discharge curve for the commercial components system. In this curve, the voltage starts at -1.06 V, and drops down to around -0.55 V after the first 1000 seconds of the 2 hour discharge. Using equation (5.4), and assuming a capacitance of 1 F for the supercapacitor, the energy in this voltage interval can

be calculated

$$E_{[-0.55,-1.06]} = \frac{1F}{2} \cdot \{(-1.06V)^2 - (-0.55V)^2\} = 0.41J \tag{5.5}$$

This energy can then be compared to the total energy stored in the supercapacitor

$$\frac{E_{[-0.55,-1.06]}}{E_{total}} = \frac{0.41J}{0.5F \cdot (-1.06V)^2} = 0.73 \tag{5.6}$$

From this calculation it can be seen that though the discharge power of the photocapacitor system drops significantly with decreasing voltage, a major portion of the stored energy will still be available at a high power.

5.3 The photocapacitor systems' respond to typical characterization techniques

In the testing there were primarily two techniques used, namely the cyclic voltammetry (CV) technique and the I-V curve (IVC) technique. Both of these are extremely useful for characterizing supercapacitors and photovoltaic devices on their own. However, when they were used on a photocapacitor system, they both started exhibiting some strange behaviour.

5.3.1 Cyclic voltammetry measurements on photocapacitor system

For the CV, this took the form of cycling curves with little or no hysteresis, even though a functioning supercapacitor was known to be connected in the system. Instead of the square curve that is seen in an ideal supercapacitor, the curve resembled the I-V curve of a diode with only a very low current running until a turn-on-voltage is reached. These curves are shown in figures 4.18, 4.23 and 4.26, which are the CV measurements done on three of the types of photocapacitor systems that were tested. The curves for the fabricated solar cells can also be seen acting like an odd function, as the turn-on-voltage happen at both positive and negative voltages, with positive and negative currents, respectively. With the

characteristic I-V curve for a diode as a clue, the reason for this behaviour is probably not too hard to deduce.

Most likely, the diode behaviour of the photovoltaic component in the system, that was not illuminated, restricted the availability for the current to run through the circuit, and fill up the supercapacitor. In a CV measurement on just a supercapacitor, the voltage over the component is controlled, and the current that is generated when electrical charge builds up on the electrodes is free to move. It is this current response that is crucial in determining the capacitance of the photocapacitor. However, when the flow of charge is restricted, this current response is mostly lost. This means that though effective on individual supercapacitors, the CV-measurement technique is no longer a viable method for determining the capacitance of the photocapacitor system.

5.3.2 I-V curve measurements on photocapacitor system

For the IVC technique, the strange behaviour was observed when the open-circuit voltage of the photovoltaic component was measured to be lower than the predicted value. How far off the measured value was from the predicted one was also observed to be heavily influenced by the scan rate, as was shown in figure 4.15. The most likely reason for the change in the measured V_{oc} is that while the IVC measurement is running, the supercapacitor gradually charges up. As this charging occur an electrical potential starts building up, with opposite direction to the V_{oc}. Then, at some point during the IVC measurement, the applied voltage over the system is equal to the actual V_{oc} of the photovoltaic component, minus the built-up voltage over the supercapacitor, V_C :

$$V_{oc,measured} = V_{oc,actual} - V_C.$$

The program will then register this as the V_{oc}, but will continue until the estimated V_{oc} is reached. The value of estimated, actual V_{oc} is done at the very start of the program, and will therefore be higher than the measured value. As for the shifts dependence on the scan rate, this is easily explained. With a slower scan rate, the time one measurement takes will be longer. This also means that the current that runs through the circuit will run for a longer time. With the relation between current and charge, $I = \frac{dq}{dt}$, this means that more charge will have flowed into the supercapacitor, charging it more, and subsequently building up a higher V_C. When several IVC measurements are taken in a row, without discharging the supercapacitor between each measurement, the voltage will just keep building up

until the supercapacitor is full. This gradual charging is seen in figures 4.16-4.17. In these figures it can also be seen that during the periods where the controlled voltage is over the measured V_{oc}, the current is positive, and the supercapacitor starts discharging.

5.4 The effect of non-ideal behaviour

In this last section, the effect of non-ideal behaviours in the various parts of the photocapacitor system will be discussed. Many of these behaviours were observed during the characterization of the fabricated cells, and their quality will also be discussed.

In photovoltaic and supercapacitor circuits there are two parameters in particular that have a great influence on the quality of the cell. These are the shunt and series resistances of the circuits, R_{sh} and R_s, respectively. Ideally, R_{sh} should be as large as possible, while R_s should be as small as possible. If these parameters do not have ideal values, the whole system will quickly exhibit non-ideal behaviour.

The reason for the R_s to be as low as possible is easily shown. The R_s is a resistance in the circuit the current have to pass through. By relating R_s to the current in the system, the loss in power over the resistance can be expressed [28];

$$P = R_s \cdot I^2 \tag{5.7}$$

From this equation it is seen that to have as little loss of efficiency as possible, the R_s in the system should be as low as possible. The reason for the R_{sh} to be as high as possible follows directly from Kirchhoff's circuit laws. R_{sh} is the electrical resistance of an alternative pathway in the circuit, bypassing the preferred route. By making sure that R_{sh} is as large as possible, only a small fraction of the total current will run through this circuit. If R_{sh} becomes to small, an increasing percentage of the current will run through this pathway, and there will be a loss in efficiency, same as for the series resistance. The consequences of both a high R_s and a low R_{sh} were seen in the measurements of both of the fabricated photocapacitor systems, but also in the individual components on their own. Since it is clear that there are both shunt and series resistances in both of the components on their own, an equivalent circuit diagram can be made to display these, in the complete photocapacitor system:

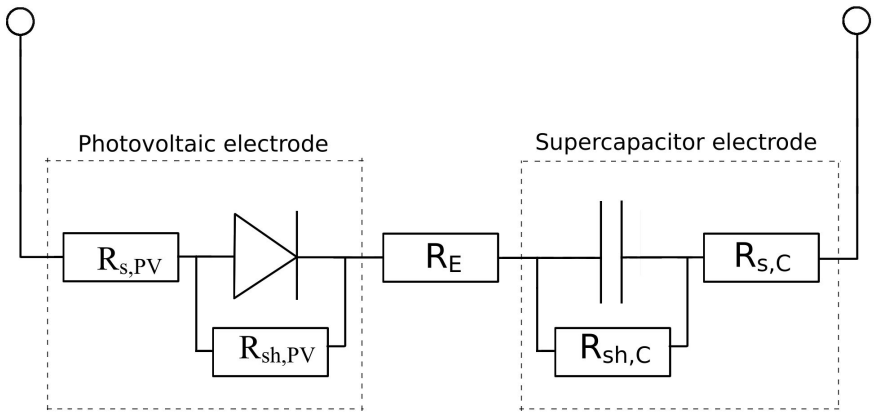

Figure 5.2: Equivalent circuit diagram of the photocapacitor system.

In this figure, there are two sets of shunt and series resistances, one for the photovoltaic electrode, and one for the supercapacitor electrode. These are labelled $R_{sh,PV}$ and $R_{s,PV}$, and $R_{sh,C}$ and $R_{s,C}$, respectively. Between these two sets there is another series resistance, R_E, which is the electrical resistance of the electrolyte. In the next two sections, each of the two sets of shunt and series resistances will be looked at, starting with the ones for the photovoltaic electrode.

5.4.0.1 Shunt and series resistance in the photovoltaic electrode

To get a proper understanding of how the shunt and series resistances influence the photovoltaic electrode, it is useful to look at the equation for a photovoltaic cell where these are included, equation (2.33);

$$I = I_0\Big[exp\frac{q(V - R_s \cdot I)}{mk_BT} - 1\Big] - I_{ph} + \frac{V - R_s \cdot I}{R_{sh}}$$

For the shunt resistance, its effect on the system can be seen in the last term on the right side of the equation. In this term, the shunt resistance is the denominator, and when the voltage over the cell is zero the term will have little impact on the total current. This changes as soon as the voltage starts to increase, and the term will have an increasing positive value. The positive value means that

its contribution to the total current goes in the opposite direction to the light-generating current. As the voltage increases further, the total current will get even lower, partially because the part that lowers the effect of the increasing voltage, $R_s \cdot I$, will get smaller as well. If the shunt resistance of the cell is very large, the denominator of this term will be very large, and the effect of increasing voltage will be reduced. If the shunt resistance is very small, however, the denominator will be very small, and an increasing voltage will have a great impact on the total current.

While the effect of the shunt resistance is most prominent around the I_{sc}, the series resistance will mostly affect the IV-curve close to the V_{oc}. As seen from the equation, its contribution is in the exponential term. If the series resistance is very low, the slope of this term will be very steep as the voltage approaches V_{oc}. If the series resistance is very large, however, the slope will be much flatter. This will cause the photovoltaic cell to deviate further from the ideal, square curve, and the efficiency will be reduced. In addition to the effect on the slope of the exponential expression, the series resistance will also affect the impact of the shunt resistance in the system. This is seen in the same term of the equation. From this term it is seen that a higher series resistance will actually counteract the effect of a low shunt resistance.

From knowing how the shunt and series resistance affect the photovoltaic system, the quality of the fabricated photovoltaic components can be evaluated. As was commented in chapter 4, the curves for the IVC measurements of the fabricated cells starts off at a higher short-circuit current, which then drop down extremely fast once the voltage over the cell starts increasing. This sudden drop is a clear indication that the shunt resistance is much lower than it ideally should be. This view is reinforced by looking at the SEM-image of the DSSC electrode, figure 4.13. In this image it can be seen that there are a considerable amount of cracking in the TiO_2 film. In these cracks the electrolyte can make direct contact with the underlying ITO-slide, causing a low shunt resistance. To increase the shunt resistance, the fabrication procedure should be revised to find a method that gives a more uniform film with fewer cracks. In this regard, an interesting observation was made during the fabrication of the DSSC electrode. The degree of macroscopic cracking and flaking of the TiO_2-film was related to the thickness of the masking tape. A thinner tape gave a film with fewer visible cracks. For the series resistance, a difference can be observed between the ones with MWNTs added, and the ones without. One of the reasons for adding the MWNTs was to increase the conductivity of the film, which is proposed several times in the literature [44]. From the IV-curves, this addition seems to have contributed to a lower series resistance. From the IVC measurement of the cell with MWNTs,

the curve have a steep exponential rise when the voltage approaches V_{oc}. This same steep rise is not observed in the cell without MWNTs. In this curve, after the current levels off, it simply rises steadily towards the V_{oc}. A difference in the second relation for the series resistance is also observed in these curves. For the cell with MWNTs, the current increases extremely fast from the I_{sc} value, and settles almost immediately at around -0,1 mA. For the cell without MWNTs, this initial rise from the I_{sc} value happens slower.

5.4.0.2 Shunt and series resistance in supercapacitors

In supercapacitor systems, the effect of non-ideal shunt and series resistances become apparent in slightly different areas.

For the series resistance, this area is the CV curve. When there is a considerable amount of series resistance in a supercapacitor the CV curve will become slanted, and deviate from the ideal, square curve with constant currents. The series resistance will probably not reduce the capacitance of the supercapacitor much, in and of itself, but there will be a loss in efficiency, equation (5.7). The energy lost over the resistance would be transformed into thermal energy, which if not dissipated fast enough would raise the temperature of the cell. A raise in temperature would increase the Debye length of the electrochemical double-layers, and that would in turn reduce the capacitance.

For the shunt resistance, the height of this parameter become apparent when looking at the stability of the charge retention. Looking at figure 5.2 for the supercapacitor part, the capacitor and the shunt resistance form a closed circuit. If the shunt resistance is very large, little or no charge will move through this circuit. This will enable the supercapacitor to retain the stored charge for a long period of time, when under open-circuit condition. If the shunt resistance is very small, however, there will be a large leakage current through the shunt resistance, and the stored energy will quickly be lost as heat. It will also reduce the charging efficiency of the device, as a lesser percentage of the total current is actually stored.

In the supercapacitor parts of the fabricated cells, the shunt and series resistances are most likely too small and too large, respectively. From the CV curves of the devices, a significant slant of the curves are observed, indicating a large series resistance. A large portion of this resistance probably comes from the ITO-slide. This is observed by doing resistance measurements over the complete devices. The resistance typically lies between 60-100 Ω, which is about the listed resistance of the ITO-slides. A too small shunt resistance is observed in how fast the fabri-

cated cells discharge during open-circuit conditions. Right after the cells are fully charged and disconnected from short-circuit condition, a large voltage change is observed, as shown in figures 4.24 and 4.27. After a time period of just around 2 minutes, the voltage over the cells is about equal to the open-circuit voltage of the photovoltaic component, indicating that the supercapacitor is almost completely discharged. Because of this fast self-discharge, measuring the discharging of the photocapacitor over an external circuit became difficult. This also made it difficult to determine the effective capacitance, considering that the CV measurements also gave inaccurate results.

5.4.1 Lifetime of the devices

One last thing regarding non-ideal behaviour, is the lifetime of the fabricated devices. Ideally, all chemical reactions that occur should be as reversible as possible, to promote a long lifetime.

In the supercapacitor parts, no chemical reactions should occur, yielding an even longer lifetime. When fabricating the supercapacitor electrodes, one alternative to the ITO-slide that was tested was steel foil. As a current collector it would have had a much smaller series resistance, giving a higher efficiency. There were a few major problems, however. The first problem was the uneven surface area. This made it difficult to apply an even film. The second and much bigger problem was that the electrolyte made contact with the steel through the shunt pathways. The electrolytes proved to be very corrosive, almost immediately corroding the steel. This corrosion also showed up as redox peaks in the CV measurements. Because of this, these types of cells had a very limited lifetime. This is also the reason the ITO-slides were ultimately used. Though having a much higher series resistance, they were much more resilient against the corrosive properties of the electrolyte.

In the DSSC parts, the chemical reactions are a necessity for proper functionality. This means that to ensure a long lifetime, the dye molecules in particular should remain stable through consecutive cycles of oxidation and reduction. In the fabricated cells, a noticeable degree of bleaching of the DSSC was unfortunately observed after just a short period of time. With this bleaching a noticeable drop in V_{oc} and I_{sc} followed. What might be the cause of this bleaching, is hard to tell. One possibility is that the dye molecules were not properly bonded to the surface of the TiO_2. Another possibility is that the presence of impurities promoted irreversible reactions with the dye molecules.

Chapter 6

Conclusion

For the commercial component supercapacitor system, a proposed charging and discharging mechanism was found to fit with experimental data. Because of the diode nature of the solar cell, the drop in voltage over the device during SC discharge happened very slowly. A large portion of the stored energy could be accessed at a decent power, however. The system was able to both generate and store electrical energy from light. It showed efficiencies of 4.3% and 44.3% for light-to-stored-energy and electricity-to-stored-energy conversion, respectively.

From the testing of the fabricated photocapacitor devices, poor photocapacitive properties was observed for both of the two main types tested. For the DSSC type photocapacitor, photovoltaic properties where observed, and measured to have a V_{oc} of about 0.5 V, and a I_{sc} of around -0.5 to -0.2 A. It showed little promise in energy storage, however, because of the highly reactive electrodes. Because of this, it failed on one half of a photocapacitor systems properties. For the silicon type photocapacitor, a significant capacitance could be measured. With both nano-carbon and nano-carbon w/MWNTs added as CE, an effective capacitance for the device was calculated to 0.18 mF and 0.47 mF, respectively. It did not show photovoltaic properties, however, and therefore failed the other half of a photococapacitor systems properties.

Some typical characterization techniques gave inconclusive data when being used on the photocapacitor system. The CV measurement failed when there was a significant photovoltaic response in the system. The IVC measurement give inaccurate measurement of the photovoltaic properties of the system, because of a partial filling of the supercapacitor component during the measurement. This lowered the measured open-circuit voltage.

Bibliography

[1] tonne of oil equivalent (toe). BusinessDictionary.com, http://www.businessdictionary.com/definition/tonne-of-oil-equivalent-TOE.html. Retrieved 29-09-2014.

[2] Key world energy statistics 2014. International Energy Agency, http://www.iea.org/publications/freepublications/publication/KeyWorld2014.pdf, 2014. Retrieved 29-09-2014.

[3] Battery performance characteristics. http://www.mpoweruk.com/performance.htm, 7. April 2015.

[4] Dictionary.com unabridged. http://dictionary.reference.com/browse/viscosity, 24. Mar 2015.

[5] Dynamic, absolute and kinematic viscosity. http://www.engineeringtoolbox.com/dynamic-absolute-kinematic-viscosity-d_412.html, 24. Mar 2015.

[6] Dynamic modelling and control design of advanced energy storage for power system applications. http://www.intechopen.com/books/dynamic-modelling/dynamic-modelling-and-control-design-of-advanced-energy-storage-for-power-system-applications, 7. April 2015.

[7] Equilibrium of diffusion and field currents. http://www.tf.uni-kiel.de/matwis/amat/elmat_en/kap_2/backbone/r2_4_2.html, 24. Mar 2015.

[8] High-intensity halogen lamp light source. https://www.thorlabs.de/catalogpages/V21/1366.PDF, 1. June 2015.

[9] http://www.kemet.com/lists/technicalarticles/attachments/113/2010 http://www.kemet.com/Lists/TechnicalArticles/Attachments/113/

2010%20CARTS%20Europe%20-%20Power%20Film%20Capacitors%20for%20Industrial%20Applications.pdf, 8. April 2015.

[10] Pn and metal–semiconductor junctions. http://www.eecs.berkeley.edu/~hu/Chenming-Hu_ch4.pdf, 8. April 2015.

[11] Pn junction. http://pveducation.org/pvcdrom/pn-junction, 22. April 2015.

[12] Solar cell operation. http://pveducation.org/pvcdrom/solar-cell-operation, 22. April 2015.

[13] Solar cell operational principles. http://www.slideshare.net/DelftOpenEr/solar-cell-operational-principles, 23. April 2015.

[14] Zeta potential, short tutorial. http://www.dispersion.com/zeta-potential-short-tutorial, 24. Mar 2015.

[15] Francois Beguin and Elzbieta Frackowiak. Carbon for electrochemical energy storage and conversion systems. chapter 8, pages 329–375. CRC Press, 2010.

[16] Raymond Chang. Redox reactions and electrochemistry. In *General Chemistry. The Essential Concepts*, chapter 19, pages 657–667. McGraw-Hill, 5th edition, 2008.

[17] Raymond Chang. Redox reactions and electrochemistry. In *General Chemistry. The Essential Concepts*, chapter 19, pages 642–683. McGraw-Hill, 5th edition, 2008.

[18] Rajesh Davé1, Ram Gupta, Robert Pfeffer, Sankaran Sundaresan, and Maria Silvina Tomassone. Deagglomeration and mixing of nanoparticles. http://www.nseresearch.org/2006/NewFiles/41Dave%2005006722%20NIRT%202005%20overview.pdf. Retrived 30. april 2015.

[19] Amal K. Ghosh, Charles Fishman, and Tom Feng. Theory of the electrical and photovoltaic properties of polycrystalline silicon. *Journal of Applied Physics*, 51(1):446–454, 1980.

[20] Michael Gratzel. Photoelectrochemical cells. *Nature*, 414(6861):338–344, Nov 2001.

[21] Øivin Holter, Finn Ingebretsen, and Hugo Parr. *Fysikk og energiressurser*. Universitetsforlaget, 1998.

[22] Øivin Holter, Finn Ingebretsen, and Hugo Parr. Energiressurser. In *Fysikk og energiressurser*, chapter 9, pages 257–272. Universitetsforlaget, 3 edition, 2010.

[23] Øivin Holter, Finn Ingebretsen, and Hugo Parr. Energiressurser. In *Fysikk og energiressurser*, chapter 2, pages 31–58. Universitetsforlaget, 3 edition, 2010.

[24] Xuezhen Huang, Xi Zhang, and Hongrui Jiang. Energy storage via polyvinylidene fluoride dielectric on the counterelectrode of dye-sensitized solar cells. *Journal of Power Sources*, 248(0):434 – 438, 2014.

[25] M. Jayalakshmi and K. Balasubramanian. Simple capacitors to supercapacitors - an overview. *Int. J. Electrochem. Sci.*, 3:1196–1217, October 2008.

[26] Jill Johnsen and Stephanie Chasteen. Solar cells: Juice from juice. `https://d-ccmr.hosting.cornell.edu/sites/default/files/Solar%20Cells%20Unit.pdf`. Retrived 04. may 2015.

[27] Joyce Laird. Pv's falling costs: In the u.s., the doe is pioneering research in order to reduce the cost of installed pv to below a dollar-per-watt by 2017. *Renewable Energy Focus*, 12(2):52,54,56, 2011.

[28] Egil Lillestøl, Ola Hunderi, and Jan R. Lien. Generell fysikk for universiteter of høgskoler - bind 2 varmelære og elektromagnetisme. chapter 27, pages 403–420. Universitetsforlaget, 2 edition, 2006.

[29] Egil Lillestøl, Ola Hunderi, and Jan R. Lien. Generell fysikk for universiteter of høgskoler - bind 2 varmelære og elektromagnetisme. chapter 22, pages 305–320. Universitetsforlaget, 2 edition, 2006.

[30] Egil Lillestøl, Ola Hunderi, and Jan R. Lien. Kondensatorer og kapasitanser. In *Generell Fysikk for universiteter of høgskoler - BIND 2 Varmelære og Elektromagnetisme*, chapter 20, pages 255–277. Universitetsforlaget, 2 edition, 2006.

[31] Egil Lillestøl, Ola Hunderi, and Jan R. Lien. Kondensatorer og kapasitanser. In *Generell Fysikk for universiteter of høgskoler - BIND 2 Varmelære og Elektromagnetisme*, chapter 19, pages 203–254. Universitetsforlaget, 2 edition, 2006.

[32] Egil Lillestøl, Ola Hunderi, and Jan R. Lien. Kondensatorer og kapasitanser. In *Generell Fysikk for universiteter of høgskoler - BIND 2 Varmelære og Elektromagnetisme*, chapter 18, pages 165–202. Universitetsforlaget, 2 edition, 2006.

[33] Chi-Wei Lo, Chensha Li, and Hongrui Jiang. A photoelectrophysical capacitor with direct solar energy harvesting and storage capability. In *Optical MEMS and Nanophotonics (OPT MEMS), 2010 International Conference on*, pages 65–66, Sapporo, Aug. 2010. IEEE.

[34] Pierre Mars. Using a small solar cell and a supercapacitor in a wireless sensor. `http://www.sensorsmag.com/networking-communications/energy-harvesting/using-a-small-solar-cell-and-a-supercapacitor-a-wireless-sen-7310`, 2010. Retrived 23. april 2015.

[35] Iván Mora-Seró and Juan Bisquert. Breakthroughs in the development of semiconductor-sensitized solar cells. *The Journal of Physical Chemistry Letters*, 1(20):3046–3052, 2010.

[36] Adam Marcus Namisnyk. A survey of electrochemical supercapacitor technology. Master's thesis, University of Technology, Sydney, 2003.

[37] Jenny Nelson. *The Physics of Solar Cells*. Imperial College Press, 2003.

[38] Krishnan Rajeshwar. *Fundamentals of Semiconductor Electrochemistry and Photoelectrochemistry*. Wiley-VCH Verlag GmbH & Co. KGaA, 2007.

[39] Muzeyyen Saritas and Harry D. McKell. Comparison of minority-carrier diffusion length measurements in silicon by the photoconductive decay and surface photovoltage methods. *Journal of Applied Physics*, 63(9):4561–4567, 1988.

[40] Subrata Sarker, Hyun Woo Seo, and Dong Min Kim. Calculating current density–voltage curves of dye-sensitized solar cells: A straight-forward approach. *Journal of Power Sources*, 248(0):739 – 744, 2014.

[41] Maheshwar Sharon and Madhuri Sharon. chapter Electric Double-Layer Capacitors and Carbon Nanomaterials. McGraw Hill Professional, Access Engineering, 2010.

[42] Dean Sigler. battery capacity comparison. `http://blog.cafefoundation.org/are-ultracapacitors-ready-for-prime-time/battery-capacity-comparison/`, 2011. Retrieved 25-10-2014.

[43] Magdalena Skunik-Nuckowska, Katarzyna Grzejszczyk, Pawel J. Kulesza, Lei Yang, Nick Vlachopoulos, Leif Häggman, Erik Johansson, and Anders Hagfeldt. Integration of solid-state dye-sensitized solar cell with metal oxide charge storage material into photoelectrochemical capacitor. *Journal of Power Sources*, 234(0):91 – 99, 2013.

[44] L.G.H. Staaf, P. Lundgren, and P. Enoksson. Present and future supercapacitor carbon electrode materials for improved energy storage used in intelligent wireless sensor systems. *Nano Energy*, 9(0):128 – 141, 2014.

[45] K. Takechi, R. Muszynski, and P.V. Kamat. Fabrication procedure of dye-sensitized solar cells. `http://www3.nd.edu/~pkamat/pdf/solarcell.pdf`. Retrived 30. april 2015.

[46] Paul A. Tipler and Ralph A. Llewellyn. *Modern Physics*. W. H. Freeman and Company, 6th edition, 2012.

[47] Orville Wright. Telegram from orville wright in kitty hawk, north carolina, to his father announcing four successful flights, 1903 december 17. World Digital Library, 1903. Retrieved 29-09-2014.

[48] Peihua Yang and Wenjie Mai. Flexible solid-state electrochemical supercapacitors. *Nano Energy*, 8(0):274 – 290, 2014.

[49] Zhibin Yang, Jue Deng, Hao Sun, Jing Ren, Shaowu Pan, and Huisheng Peng. Self-powered energy fiber: Energy conversion in the sheath and storage in the core. *Adv. Mater.*, 2014. Online publication, doi: 10.1002/adma.201401972.

Appendix 1 - Summary Tables

Instruments, chemicals and computer programs - Summary tables

A variety of instruments, chemicals and computer programs were used in the fabrication and testing of the photocapacitor cells. These are given in summary tables below.

Table 1: Computer programs

Program name	**Version**
EC-Lab	10.19
Logger Pro	3.8.6
MATLab	R2015a
LibreOffice Calc	4.2.8.2
Texmaker	4.1
MS Paint	6.1
GIMP	2.8.10
MS Windows OS	7 - Home Premium

Table 2: Instruments

Instrument name	**Manufacturer**
OSL1-EC - High Intensity Fiber Light Source with CE-Mark	Thorlabs, Inc.
ABT 220-4M	Kern
CPA Analytical Balance CPA324S	Sartorius
CB160 Hotplate	Stuart
KC3 Ultrasonic Cleaning Bath	Kerry, Guyson
B3510 Ultrasonic Cleaner	Branson
OPTIPLEX 990 w/ MS Windows	DELL
SP-50 Potentiostat	Bio-Logic
LabQuest Mini	Vernier
Differential Voltage Probe	Vernier
HM8118 LCR Bridge/Meter	Rohde & Schwarz
Raith eLine	Raith

Table 3: Chemicals

Name and description	**Manufactorer**
Carbon, nanopowder, $<$ 50 nm particle size	Aldrich
Carbon nanotube, multi-walled	Aldrich
Silicon, nanopowder, $<$ 100 nm particle size	Aldrich
Titanium(IV) oxide, nanopowder, 21 nm particle size	Aldrich
Titanium(IV) isopropoxide, 97%	Aldrich
Poly(vinylidene fluoride)	Aldrich
Tetrahydrofuran, anhydrous, $\geq$ 99.9%, inhibitor free	Sigma-Aldrich
Eosin Y, Dye content 99%	Sigma-Aldrich
Iodine solution, volumetric, 0.05M I_2	Fluka
Potassium iodide, ACS reagent, $\geq$ 99.0%	Sigma-Aldrich
Ethylene glycol, 99+%, spectrophotometric grade	Sigma-Aldrich
Lithium hexafluorophosphate, battery grade, $\geq$ 99.99% trace metals basis	Aldrich
Indium tin oxide coated glass slides, 8-12Ω/sq surface resistivity	Aldrich
Indium tin oxide coated glass slide, square, surface resistivity 30-60Ω/sq	Aldrich
Ethanol	Sigma-Aldrich
Deionized water	

Appendix 2 - MATLab programs

Calculate effective capacitance

```
function cv_out=find_capacitance(cv_in,scan_rate,cycles_in)
num_cycles = cycles_in;
voltage = cv_in(1:end,3);
current = cv_in(1:end,4);
cycle = cv_in(1:end,5);
power = voltage.*current;

hysteresis_area_pos = zeros(cycles_in,1);
hysteresis_area_neg = zeros(cycles_in,1);

for i = (1:(length(voltage)-1))
    for j = (1:cycles_in)
        if j == cycle(i)
            if voltage(i) > 0
                hysteresis_area_pos(j) = (hysteresis_area_pos(j)
                                          + trapz(voltage(i:(i+1)),power(i:(i+1))));
            end
            if 0 > voltage(i)
                hysteresis_area_neg(j) = (hysteresis_area_neg(j)
                                          + trapz(voltage(i:(i+1)),power(i:(i+1))));
            end
        end
    end
end

energy_total = zeros(cycles_in,1);
capacitance_effective = zeros(cycles_in,1);

for i = (1:cycles_in)
    energy_total(i)=(hysteresis_area_pos(i)-hysteresis_area_neg(i))/scan_rate;
    capacitance_effective(i) = ((energy_total(i)*2)/(0.5).^2)/4;
end

capacitance_out = [mean(capacitance_effective), std(capacitance_effective)];

cv_out = capacitance_out;
```

Calculate photovoltaic parameters

```
function [out_params] = find_photovoltaic_params(in_matrix, in_radiation_power)
    V_vec = in_matrix(1:end,1);
    I_vec = in_matrix(1:end,2);

    max_out_loc = max_point_function(V_vec,I_vec);
    V_max = V_vec(max_out_loc);
    I_max = I_vec(max_out_loc);
    P_max = abs(V_max*I_max);

    I_sc_loc = intersect_point(V_vec);
    I_sc = I_vec(I_sc_loc);

    V_oc_loc = intersect_point(I_vec);
    V_oc = V_vec(V_oc_loc);

    FF = abs((P_max)/(I_sc*V_oc));

    efficiency = (P_max)/(in_radiation_power *1.05);
    out_params = [I_sc, V_oc, P_max, I_max, V_max, FF, efficiency];

end

function [max_loc] = max_point_function(v_in_1,v_in_2)
    n = length(v_in_1);
    max_value = -inf;
    for i = 1:n;
        if v_in_1(i)>0 & v_in_2(i)<0
            if abs(v_in_1(i)*v_in_2(i)) > max_value
            max_value = abs(v_in_1(i)*v_in_2(i));
            max_loc = i;
            end
        end
    end
end
```